MODAL TESTING AND ANALYSIS OF UNCRACKED AND CRACKED PLATES IN AIR AND IN WATER

AGUNG BUDIPRIYANTO

MODAL TESTING AND ANALYSIS

OF UNCRACKED AND CRACKED PLATES

IN AIR AND IN WATER

By

©AGUNG BUDIPRIYANTO

A Thesis Submitted to the School of Graduate Studies

in Partial Fulfilment of the Requirements for

the Degree of Master of Engineering

FACULTY OF ENGINEERING AND APPLIED SCIENCE

MEMORIAL UNIVERSITY OF NEWFOUNDLAND

JANUARY, 1993

ST JOHN'S   NEWFOUNDLAND   CANADA

Canadä

A b s t r a c t

This thesis has investigated the analytical and experimental changes that occur in modal parameters (i.e., natural frequency, damping and peak response magnitude) of a vibrating horizontal cantilever plate due to the presence of a crack and due to immersion in two fluids having different densities. Three plates were investigated, viz., an uncracked plate and two cracked plates with 1/32" and 3/32" crack depths, machined on both sides of the plates.

From the analycal study, it was found that cracks caused the natural frequencies of plates in air to reduce by a maximum of 3% and also changed the modal vectors slightly. The modal vector changes were mainly around the region of the cracks. It was also observed that the modal vectors changed from "in vacuum" to "in air" condition.

Experiments were carried out in air and at two levels of water submergence. For the experiment in air, it was observed that due to the presence of a 2x1/32" crack, the natural frequencies of the plate were lowered by a maximum of 0.75% than the uncracked one. When the water level was just about the middle of the plate thickness, the natural frequencies reduced by as high as 26.8% and the damping increased by 5 times. For full submergence (where the water level was about 23 cm above the upper surface of the plate), a maximum natural frequency reduction of 40% and damping increase of about 6 times were observed.

Experimental and analytical results were compared for plates tested in air. The maximum difference between the measured and the predicted natural frequencies were found to be within 8.6%. The correlation of normalized peak strain response magnitudes were good for modes one, two and four.

Acknowledgements

Contents

List of Figures

List of Tables

List of Symbols

A	The amplitude of forcing function
A_{gr}	Residue of multi degrees of freedom system
A^*_{ar}	Complex conjugate of A^*_{ar}
A_n	The averaging after n ensembles
A_{n-1}	The previous average after n-1 ensembles
A_r	Residue at pole p_r
A_r^*	The complex conjugate of A_r
B_n	The nth ensemble
B(s)	The inverse of system transfer function
c	System damping of a single degree of freedom system
c_1	The proportionality factor between pressure and the velocity of the surface in the normal direction
C_r	The generalized damping
C_0	Residual function coefficient of frequency response function
C_1	Residual function coefficient of frequency response function
C_2	Residual function coefficient of frequency response function
d	A distance measured from the fixed-end of the plate to the crack location
D^{el}	The material elasticity matrix
f	Forcing function
F(s)	Forcing function in Laplace domain
$FR_{0.420}$	The relative frequency reduction in precent for water depth to plate length ratio is equal to 0.420 (partially submerged condition)
$FR_{0.767}$	The relative frequency reduction in precent for water depth to plate length ratio is equal to 0.767 (fully submerged condition)
G_{yy}	The output auto spectrum
G_{yx}	The cross spectrum
G_{xy}	The cross spectrum
G_{xx}	The input auto spectrum
H	The true response function of system
h	Crack depth
H(s)	System transfer function which relates system input to system response in Laplace domain
H_1	System transfer function assumes that noise exists in the output and the input is free of noise
H_2	System transfer function considers the noise to be present in the input and to be absent in the output
H^P	The interpolation function for pressure in the fluid at node P^{th} or DOF

H_v	System transfer function assumes the noise to exist both in the input and output signals
$H(\omega)$	System frequency response function
k	System stiffness of a single degree of freedom system
k_1	The proportionality factor between pressure and displacement of the surface in the normal component of surface displacement
K_f	The Bulk Modulus of the fluid
K_r	The generalized stiffness
L	Plate length
m	System mass of a single degree of freedom system
M_r	The generalized mass
n	The outward normal to the structure
n	Number of eigenvalues (modal frequencies) in displacement frequency response formulation
N^N	The interpolation function at N^{th} degrees of freedom
p	The pressure on the fluid structure interface
p_s^Q	The steady state values of p^Q
p_r	The pole of the underdamped system
p_r^*	Complex conjugate of p_r
Q_r	Modal scaling factor
r	Volumetric drag (force per unit volume per velocity)
r	Number of the eigenvector (modal vector) in displacement frequency response function formulation
s	Laplace variable
$S_{jk}(\omega)$	Strain frequency response function
t	Surface traction in the structure
t	Time variable
t	Plate thickness
T_d	Sweep duration
U_{ir}	Modal coefficient at measured degrees of freedom i and mode r
u^m	The nodal variables in the structure
$\dot{u}$	The fluid particle velocity
$\dot{u}_n$	Normal fluid velocity component with positive direction into the fluid
$\dot{u}^m$	The velocity of a point in the structure
$\ddot{u}$	The particle acceleration
$\ddot{u}^m$	A point acceleration in the structure
w	Crack width
x	Spatial position of the fluid particle
X	System input
$X(s)$	System response in Laplace domain
Y	System output
$\Re(p^N)$	The real part of forcing applied to the structure
$\Re(p^Q)$	The real part of the response amplitude of the fluid
$\Re(v^{hM})$	The real part of the response amplitude of the structure

$\Im\,(p^N)$	The imaginary part of the forcing applied to the structure
$\Im\,(p^0)$	The imaginary part of the response amplitude of the fluid
$\Im\,(v^M)$	The imaginary part of the response amplitude of the structure
α_c	The mass proportional damping factor (Rayleigh damping)
β_c	The stiffness proportional damping factor (Rayleigh damping)
γ^2_{yx}	The coherence function
δu^m	Variational displacement field
$\delta\epsilon$	The strain variation which is compatible with δu^m
ϵ_{jr}	Component of rth strain modal vector in a known direction at point j
ϵ_{xr}	The rth strain mode shape in x direction
η	Noise presents in the output of a system
ν	Noise presents in the input of a system
v_s^M	The steady state values of v^M
ξ_r	Modal damping ratio
ρ	Material density
ρ_f	The fluid density
σ	The stress in the structure
σ_r	Damping factor
υ	Generalized variable in the structure in the fluid-structure interaction
ϕ	The phase of forcing function
ϕ_{kr}	Component of mass normalized displacement mode shape in a known direction at point k
ϕ_{zr}	The rth displacement mode shape in z direction
Ω	System natural frequency
ω	Frequency variable
ω	Complex circular frequency in fluid-structure interaction formulation
ω_a	The natural frequencies of the plate in air
ω_f	The natural frequencies of the plate in full submergence condition
$\omega(t)$	The frequency range of interest in a frequency sweep
ω_h	The highest frequency in the sweep range
ω_l	The lowest frequency in the sweep range
ω_p	The natural frequencies of the plate in partial submergence condition
ω_r	Damped natural frequency
ε_1	The relative amount of noise at input
ε_2	The relative amount of noise at output

Chapter 1

Introduction

Due to wave, wind, current and other environmental forces acting on them, fixed or floating structures in the sea experience reversal of loads. Consequent stresses of various amplitudes can result in fatigue damage to the structures. Statistical studies performed by Wheeler (1980), Almar-Naess (1985) and Parfitt (1986), on the hot spot regions of welded tubular joints of offshore and onshore structures, showed that large stress concentrations occur around these regions resulting in fatigue cracks due to the repeated load cycling. Akita (1983) reported that large fatigue cracks of lengths, more than 200 mm, were observed around the ends of (welded) stiffeners fitted on the floor plates or bulkheads in the peak tanks of ships registered with Nippon Kaiji Kyokai, Japan.

In order to determine whether the cracks will affect the integrity of structures, these cracked regions have to be detected early so that detailed studies can be carried out on the sizing of cracks. Many procedures and techniques for detecting and measuring cracks are available today, such as Magnetic Particle Inspection (MPI), Alternating Current Field Measurement

(ACFM), Eddy Current (EC) and Ultrasonic Technique (UT). In all these techniques, the sensors have to be located very close to the cracked regions and measurements made at a small distance away from the damaged zones, may not indicate the presence of cracks.

In the last few years, the experimental and analytical modal analysis method has been utilized to detect cracking of structures through observations made on the change of modal parameters, i.e., mode shapes, damping, natural frequencies and transfer functions. Due to the existence of cracks, natural frequencies reduce, mode shapes get altered depending on the damage magnitude, unit response amplitudes may increase or decrease depending on the position of crack and damping also changes. By comparing the modal parameter changes that occur in structures due to cracking, a researcher may be able to detect and localize the damage area.

1.1   Scope of the thesis

The purpose of the present study is to carry out analytical and experimental studies on uncracked and cracked steel plates with the intent of :

    a. Identifying the modal changes that occur in structures, in air and water, due the presence of cracking in structures;

    b. Making some observations on the sizing of cracks from these modal changes;

    c. Carrying out experiments on uncracked and cracked structures in order to verify the results of the theoretical prediction;

    d. Determining whether the presence of cracks cause any change of modal properties of structures vibrating in water, due to the changed mode of fluid-structure interaction.

2

The organization of the topic introduced above is made in the following manner. The second chapter reviews the relevant research carried out on fluid-structure interaction, strain gage application to modal analysis studies and other studies on crack identification. The theoretical background of analytical/numerical and experimental modal analysis is given in Chapter 3. Numerical results on modal behaviour obtained using ABAQUS computer program are given in Chapter 4, and results of experimental studies are presented in Chapter 5. Analytical and experimental results are compared and correlated in Chapter 6. The final chapter summarizes the salient findings of the work carried out in this thesis and gives relevant topics for further research.

Chapter 2

Literature Review

Studies on the dynamic behaviour of structures, interacting with air or water, have been carried out extensively to determine the effect of fluid on the structural response in terms of added masses, hydrodynamic damping and natural frequencies. In the last few years, modal analysis approach has been used to identify the change of modal parameters due to apparent added mass contribution. In addition, along with extensive research on integrity assessment of structures using various experimental techniques the modal analysis methodology has also been used to determine the existence of cracks/damages in structures. Recently, investigators have proposed procedures, not only to detect cracks/damages but also to localize them. The possibility of using strain gages as transducers in modal analysis allows the approach to be used in the fatigue life prediction of structures. Strain gages are believed to be more reliable in the fatigue experiment since the transducers show directly regions where the highest strain/stress magnitudes occur; this is not given by other transducers.

This chapter is broken into three sections. The first section contains a review of work on

fluid-structure interaction. The second section discusses work carried out on modal analysis using the strain gage as a transducer. The last section is a review of recent studies on crack identification.

2.1   Experimental and Analytical Studies on Fluid - Structure Interaction

Components of structures, such as plates and cylinders, have been used as test specimens either to understand the phenomenon studied or to gain an accurate computational procedure before tests on large and more complicated structures are carried out. Examples of research investigations carried out using these kinds of specimens, can be found elsewhere; for instance in Leibowitz (1975) who carried out extensive analytical and experimental studies to investigate the response of turbulence excited structures in fluids. In the rest of this section, a few of the recent studies on vibration of plates or cylinders in fluid are reviewed.

Vibration response of steel plates of various sizes interacting with air and water was examined by Lindholm *et al.* (1965). Frequencies of the first five modes of plates, in air and in water, with several levels of submergence, were measured. As an numerical comparison, "beam in vacuum" natural frequencies were calculated using the thin plate theory. To get a better agreement to measured values the added mass factors were derived and used to correct the frequencies computed using the theory. For the ratio of plate width to plate length equal to 3 and the ratio of plate thickness to plate width equal to 0.0611, which is nearly the same as the ratio used in this thesis, the difference in resonant frequencies between analytical and experimental values ranged from 5.0% to 6.2% for plates in air; and the analytical values were

5

higher up to 39% than the experimental values for plates deeply submerged in water. Compared to plates in air, the experimental resonant frequencies of plates, deeply immersed in water, reduced by about 35%. No pattern was found in the frequency variation of the fluid structure system. Experimental results of plates vibrating in water, at various levels of submergence showed that natural frequency variation between various levels of submergence was relatively small when water level above the plate surface exceeded approximately a half of the plate length. Damping variation was not investigated in this study. Almost a similar study was carried out by Muthuveerappan et al. (1979). They employed fluid-beam finite element models to investigate the change of the natural frequencies of a cantilever steel beam due to different levels of submergence in water. An important observation that could be made from their study was that by increasing the water depth above the beam surface, the relative variation in the natural frequency became less and less. They stated that mode shapes changed slightly in water compared to those in air. They also observed that the submergence effect was larger in the higher modes than in the lower ones. These results agreed well with the earlier ones given by Lindholm et al. (1965). They extended their study to different plate materials, i.e., aluminum and copper, fluid densities and plate boundaries (Muthuveerappan et al., 1980). Like Lindholm et al. they found that natural frequencies reduced significantly until a certain level of submergence. And after that level, the changes in resonant frequencies were not substantial; also the modes shapes, in general, altered slightly for different fluid densities.

Added mass and hydrodynamic damping of perforated and unperforated circular plates were determined by De Santo (1981). Three different plates were investigated both in air and in water; two perforated plates were of the same in diameter and hole patterns but the second

6

one was three times thicker than the first one; and the third plate was unperforated, same thickness as the first one and one cm smaller in diameter. Semi-empirical formulae, for computing added mass and hydrodynamic damping of perforated plates, were given. These formulae were obtained by correlating derived analytical formula with experimental values. It was found that the natural frequency shifts of the plates ranged from 10.89% to 16.03%. Added mass for the third plate was the highest; and for the first plate, the perforated one, it was the lowest. Damping of the first plate was found to be less than the second plate but slightly higher than the third plate. Jezequel (1983) proposed a method to compute the hydrodynamic added mass based on measured mode shapes in air and in water. By a mass modification procedure, the computed added mass was used to predict the change in dynamic behaviour of structures immersed in fluids. To validate the method, test on a steel rectangular plate partially immersed in water, to about two third of the plate height, was carried out. The plate was hung vertically by two wires which were fastened to the corners of the specimen; and the first six modes were measured. Because of the influence of immersion, the reduction in measured natural frequencies varied from 18.34%, in the fifth mode, to 40.7%, in the sixth mode; the other frequencies reduced between those two values. Comparison was also made between the measured and predicted natural frequencies of the structure. The computed values were close to the experimental values when the apparent added mass was taken into consideration.

Randall (1985) reported his work on the identification of natural frequencies and mode shapes of a cylindrical structure in air and totally immersed in water, using the modal analysis method. Using accelerometers, mounted both around and along the cylinder height, he compared the response of the cylinder in air and in water. He found that the experimentally measured first

frequency decreased by 50.5%; and the higher frequencies reduced by less than 50%. They noted that a problem was encountered in distinguishing the cylinder modes since the frequencies were closely spaced. Formulas for computing the natural frequency of a cylinder interacting with fluid medium were derived by assuming the cylindrical shell to be infinitely long. There was a good correlation between the measured values and calculated values.

Added mass of circular plates which were partially submerged in water were experimentally investigated by Lieb *et al*. (1989). The plates were with and without perforations. The plates were vertical; and to measure the natural frequencies three accelerometers were mounted on top, mid-height and bottom of the plate with their direction normal to plane of the plate. Natural frequencies were measured for seven different levels of submergence. Using the measured natural frequencies and the mass of the plate specimen or known additional masses attached on the specimen, when the plate mass data was not available, added masses of the plates were calculated. As in the previous studies, the natural frequencies reduced from air to water. For an unperforated plate with 99% submergence, i.e., when 99% of the area of the plates were covered with water, the first resonant frequency reduced by 55.5% from that in air; and for the perforated plates a frequency reduction as high as 25.9% was observed. It is quite understandable that the unperforated plate reduction in the natural frequency was larger than the perforated one, since the added mass contribution is greater in the case of unperforated plate. They also found that there was a good agreement between the added masses obtained experimentally and those calculated using formulae given by De Santo (1981); the values given by Lieb *et al*. (1989) are higher than those given by De Santo.

2.2   Studies on Modal Analysis using Strain Gages

In the last few years, strain gages have become a popular tool in studying dynamic response of structural elements using the modal analysis method. Due to several reasons, many researchers prefer to use strain gages than accelerometers. One of the reasons is that strain gage transducers give more reliable information in stress/strain fields of vibrating structures than other transducers. In parallel with experimental studies, a number of theoretical developments on strain frequency response function determination have been proposed and developed. It is possible that in the near future, strain gages may play an important role, especially in the fatigue life prediction and failure analysis of structures, using the modal analysis or modal testing approach. Some of the pertinent studies carried out on the same are reviewed here.

Young and Joanides (1982) investigated the use of strain gages in fatigue life certification of a space shuttle orbiter component. Experimentally derived modal strain response functions were developed. According to them, the use of the strain response function in any experiment has at least two advantages. First, unlike in a pure analytical model, in experimental modal testing using strain gages boundary condition assumptions are not needed. Second, strain and stress concentration can be predicted with relatively lower measurement cost. One of the disadvantages is that the strain gages can only measure strains at the local area. Another disadvantage is that the strain may not be spatially continuous as that of displacement. This implies that smooth strain mode shapes perhaps cannot be determined. For verification of the theory, tests on the body flap of the space shuttle orbiter was carried out to obtain the frequency response function data. Then the frequency response function was synthesized using proposed

theory. The synthesized result was next compared to the original data. Furthermore, during the acoustic data analysis, measured and predicted response spectra were also compared. The conclusion of this study was not given out because of the sensitive nature of their studies. But, it was stated ·   the combination of the results of analytical model with the experimentally measured model was important and desirable since it combined the strengths of experimental measurements and analytical prediction.

Hillary and Ewins (1984) developed a numerical model for predicting the strain transfer function and determining the force acting on the system. Tests on a uniform cantilever beam and a compressor blade were carried out. Both accelerometers and strain gages were used to monitor the behaviour of structures; they were subjected to two forces, applied simultaneously. It was observed that the strain model was more reliable in estimating the force and the strain frequency response function than the accelerometer one. Staker (1985) highlighted the advantages of implementing strain frequency response functions in production problems and in design evaluation. Two advantages were mentioned, viz., the ability to estimate the fatigue life of a structure and the ability to identify the structural area where high stresses could occur and zoom on the area to get more reliable results. Based on the solid elastodynamic theory, Bernasconi and Ewins (1989a) derived mass normalized modal strain and strain frequency response functions. A sample application to a beam with an abrupt change of section was given. Three methods, FEM, displacement modal testing applied by use of accelerometer and strain modal testing using strain gages were compared to verify their theory. A good agreement was found among those methods. Similar to Staker's paper (1985), implementation of strain modal testing in fatigue life evaluation was suggested. Based on the theory given in their previous paper, Bernasconi and

10

Ewins (1989b) carried out experimental studies on a discontinuous beam, a curved plate and a steam turbine blade. They suggested further evaluation, development and improvement of the strain modal testing theory, especially in simulating a real case where modal strains are complex.

Strain gage transducers were used in modal testing to identify the causes of failure in a finned-tube heat exchanger (Powell and Goldberger, 1989). The reason for using the strain gages was that they showed the failure region more reliably since at resonance high strain amplitudes are observed around these regions; this was not the case in the measurements using accelerometer. They reported that strain gages could be employed successfully as a tool to identify the vortex induced vibration problems. Debao *et al.* (1989) derived strain transfer functions on the basis of strain-displacement relationships. They found that the shapes of modes, measured by accelerometers and strain gages, for a plate and a beam were similar for the first three modes. It was also found that the strain gages gave a little bit higher values of natural frequencies and damping than the accelerometers.

2.3 Recent Studies on Crack Identification

Change of modal parameters due to changes in structures, from a "virgin" to cracked/damaged condition, can be utilized as a tool to detect and localize the existence of damages in structures. Using an aluminum rectangular plate and a carbon reinforced plastic trapezoidal plate as test pieces, Cawley and Adams (1979) performed transient tests on these plates. A hole, a number of saw cuts and a crushed damage were introduced in the specimens after measurements were completed on undamaged specimens. To find out the effect of defects on the natural

11

frequencies of plates, saw cuts and crush damages were applied sequentially to the plastic plate. Analytically, they used eight-noded isoparametric elements to predict the frequency shifts and the damage location. The natural frequency shifts were computed by sensitivity analysis while damage locations were predicted through the use of an error function which gave a minimum value at the damaged position. They observed that the resonant frequencies reduced when damages existed. But the location and magnitude of the damages could not be detected successfully. Damage detection of a real offshore structure located in the North sea was performed by Kenley and Dodds (1980). They measured the natural frequencies of the platform, before and after the platform members were cut, using accelerometers which were placed both above the water line and under water. Accelerometers mounted above the water line were intended to measure the so called overall mode of vibration while those placed underwater were used to obtain local mode of the platform. They stated that only the former could be utilized to detect severe damages while the latter could be used to observe the less severe damages.

Nataraja (1983) reported his investigations on the integrity monitoring of three jacket type platforms in the North sea. Accelerometers were used constantly to measure the response of the structures over a period of time; strain gages were used for only one of the platforms which was considered to be a complex structure. In order to simulate the damage possibility of the structures, dynamic behaviour of the "damaged" structures was analyzed using the finite element approach. The analytical results showed that the resonant frequencies of the lowest five modes reduced considerably and in the other modes the frequency changes were negligible. According to Nataraja, only the first three natural frequencies were stable during the time of investigation. From the stability characteristics of the resonant frequencies, he concluded that there was no

12

considerable damage in the structure when the investigations were carried out.

Chinese researchers (Feng *et al.*, 1989) investigated the change of natural frequencies and strain mode shapes of a 410x30x5 mm thick slotted beam. Fifteen strain gages, mounted along the longitudinal axis of the beam, were used as sensors to acquire the responses of the vibrating beam; additional seven strain gages were placed in an area near the slot to study the strain mode shapes in the region. The beam was clamped at one end and free at other end. From the study, they found that around the area of the slot, the strain mode shape vector magnitudes increased significantly; in areas far away from the slot there were no significant changes.

Mannan and Richardson (1990) examined the methodology to detect and localize damage in a free-free aluminium plate via frequency response function. The plate response data was acquired before and after a saw cut was made. It was found that the natural frequencies changed. By computing the stiffness difference between the undamaged and damaged plates, they examined the procedure of localizing the damage. However, it was found that the damage localization effort was not successful, since there were large stiffness differences not only in the near DOFs where the damage existed but also in some of the other DOFs. Investigations on crack identification and localization of free-free beams, in which simulated cracks with various depths and locations were introduced, was carried out by Gomes and Silva (1990). Analytically, they used a torsional spring element to model the cracked part of the beam. But comparison of analytical and experimental results were not given in this paper. Natural frequency variations of experimental results of cracked and slotted beams with different depths of crack or slot were plotted against the simulated damage locations. The plots showed that, although those variations were similar, the resonance frequency variations of cracked beams are a little higher than the

13

damper was added to the system. Using the formulation derived by Mannan and Richardson (1990), Chowdhury analyzed a three DOF mass, spring, damper model with various mass and stiffness values. He found that a stiffness reduction did not influence the mass matrix, while mass changes affected both mass and stiffness matrices; it was also found that a damping change did not influence either the mass or the stiffness matrix of the system.

2.4   Summary

Modal analysis has been used to study phenomena in fluid structure interaction, crack identification and fatigue life prediction. In the last few years, strain gages have been used as complementary transducers in experimental studies. To facilitate the experimental results, analytical strain modal testing theories have been developed. It has been found that the use of strain gages as response sensors gives better accuracy of measurements and also assists in the location of the cracked/damaged regions.

This thesis examines the change of modal parameters of a simple cantilever plate, with and without the existence of cracks, immersed in water/air for the first five resonant frequencies of the structure. Analytical and experimental studies are carried out. The experimental study primarily relies on the data acquired using strain gages; only one accelerometer was mounted in the plate and used in modal testing. To predict the dynamic response of the plates, both in vacuum and in air, the ABAQUS computer package was employed.

slotted ones. They mentioned that the discrepancies may be because of the fact that the crack propagation line is not parallel to the axis toward which it propagates. Consequently, the crack area is larger than the equivalent slot area.

By assuming a small damage in a structure, Richardson and Mannan (1991) derived the so called sensitivity equations for the changes in mass, damping and stiffness of structures. The inherent assumption was that mode shapes do not alter substantially due to the existence of damage. A three DOF system was used to validate the equations. Up to a maximum of 10 % change in structural properties, i.e., mass, stiffness and damping could be predicted accurately. According to Mannan and Richardson, unlike small change case in which modal parameters of undamaged structures, i.e, mode shapes, mass, damping of damaged structures are needed, the "large" change case requires additional data on mode shapes of damaged structures. Chowdhury (1991) carried out experimental and analytical studies to investigate the variation of modal parameters due to changes in mass, damping and stiffness properties of a simply supported beam system. Experimentally two steel plates, with and without damages (cracks), were tested. To examine the effect of stiffness reduction on the dynamic behaviour of the system, the first plate specimen was tested under two conditions, i.e., before and after a saw cut was introduced. Two more cases were also investigated for the second specimen when external mass and damping were introduced. First, an additional mass was mounted on the plate. Second, a damper was fastened to the plate. By comparing the plate with and without a cut, Chowdhury found that most of modal frequencies decreased after the saw cut was introduced; the modes whose modal patterns were not influenced by the defect did not undergo any changes. The additional mass resulted in the reduction of lower frequency modes and the modal damping increased when a

14

Chapter 3

Modal Analysis Theory

Modal analysis is defined as the process of characterizing modal parameters of a system either through analytical or experimental approach. Analytically, modal analysis is accomplished by the use of finite element method. The general finite element procedure includes the assemblage of local structural element characteristics and its transformation to global coordinates; thereafter the elemental mass, stiffness and damping matrices and load vector are assembled for the whole structural system and solved to determine the pertinent variables of these system equations. In order to economize computationally, all the degrees of freedom of structures need not be included in the analysis; consequently, substructuring and condensation techniques are often needed.

Experimentally, modal analysis is performed by monitoring the input and the output of an oscillating structure at salient points of measurement. The measured data are, then, analyzed to get the desired modal parameters. Experimental modal analysis is needed to verify the results obtained by analytical techniques or to determine the condition of a prototype structure during

16

its operational life. Due to assumptions made in solving the analytical modal problems, analytical modal parameter values may differ from those acquired experimentally. Usually comparison between analytical and experimental modal analyses is made in order to refine or to validate the finite element model. In this chapter, the theoretical background of analytical and experimental modal analysis techniques are briefly reviewed.

3.1   Analytical Modal Analysis

As mentioned earlier, finite element method is an analytical tool which is being increasingly used to predict the dynamic behaviour of structures. In the present study, the general purpose finite element program ABAQUS, version 4.9-1, developed by Hibbitt, Karlsson and Sorensen, Inc. is used for analyzing the dynamic response of an uncracked/cracked cantilever plate in vacuum and in air. Two types of modelling have been considered in the discretization of the structure for analysis. When the plate was considered to be immersed in a fluid (air), a plane strain modelling of the fluid-structure medium using three-noded beam element for the structure and eight-noded plane strain element for the fluid was utilized along with a three-noded interface element between the structure and the fluid. When the discretization of the plate in vacuum was carried out for eigenvalues, eight-noded shell (otherwise called plate) elements were used to model the plate with condensation of unwanted degrees of freedom to achieve computational economy. Node ordering of the shell and beam element are shown in Figure 3.1 and 3.2.

17
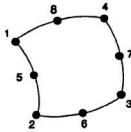
Figure 3.1 Eight-noded shell element : node numbering
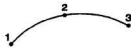
Figure 3.2 Three-noded beam element : node numbering
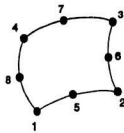
Figure 3.3 Eight-noded acoustic element : node numbering

3.1.1 Analysis of Fluid Structure Interaction

The vibrating plate in air, was modeled by using three-noded beam element and eight-noded acoustics element. Figure 3.3 shows the acoustic element used in the study. The interface element, shown in Figure 3.4, was used to couple the fluid elements to structural elements so that compatibility with the structural model as well as acoustic model were achieved. It is assumed that the fluid is compressible, inviscid and undergoes small motion. Two types of boundary conditions are available for implementation, namely, (i) the general boundary conditions which could be used by giving kinematic values for the boundary degrees of freedom and (ii) fluid absorbing boundary conditions which could be obtained by relating the boundary surface normal velocity to the pressure at the point and the time rate of change of pressures. Using the condition given in (ii) above the normal velocity of fluid at the boundary can be written as,

$$\dot{u}_n = -\left(\frac{1}{k_1}\dot{p} + \frac{1}{c_1}p\right) \tag{3.1}$$

where:

$\dot{u}_n$ = normal fluid velocity component with positive direction into the fluid,

k_1 = the proportionality factor between pressure and displacement of the surface in the normal component of surface displacement,

c_1 = the proportionality factor between pressure and the velocity of the surface in the normal direction,

p = pressure in fluid.
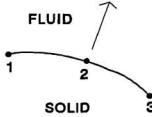
Figure 3.4 Interface element : node numbering

By giving specific values to k_1 and c_1 at desired regions, normal fluid velocity can be specified for the problem.

Full derivation of the fluid structure interaction equation taken from ABAQUS Manual (Hibbitt, Karlsson and Sorensen, 1989), can be found in Appendix A.

The equations of motion for fluid-structure interaction is,

$$
\begin{bmatrix}
\Re[A_f^{PQ}] & \Im[A_f^{PQ}] & S_{fs}^{PM} & 0 \\
\Im[A_f^{PQ}] & -\Re[A_f^{PQ}] & 0 & -S_{fs}^{PQ} \\
[S_{fs}^{QN}]^T & 0 & \Re[A_s^{NM}] & \Im[A_s^{NM}] \\
0 & -[S_{fs}^{QN}]^T & \Im[A_s^{NM}] & -\Re[A_s^{NM}]
\end{bmatrix}
\begin{Bmatrix}
\Re(p^Q) \\
\Im(p^Q) \\
\Re(v^M) \\
\Im(v^M)
\end{Bmatrix}
=
\begin{Bmatrix}
0 \\
0 \\
\Re(P^N) \\
-\Im(P^N)
\end{Bmatrix}
\tag{3.2}
$$

where:

$$
\Re[A_f^{PQ}] = \frac{1}{\omega^2}(K_f^{PQ} + K_{fr}^{PQ}) - (M_f^{PQ} + M_{fr}^{PQ})
$$

$$
\Im[A_f^{PQ}] = -\frac{1}{\omega}(C_f^{PQ} + C_{fr}^{PQ})
$$

20

$$\Re[A_z^{NM}] = K^{NM} - \omega^2 M^{NM}$$

$$\Im[A_z^{NM}] = -\omega \left(C_{(m)}^{NM} + C_{(\beta)}^{NM} \right)$$

$$S_{fs}^{PM} = \int_{S_{fs}} H^P n . N^M \, dS$$

$$S_{fs}^{PQ} = \int_{S_{fs}} N^P n . N^Q \, dS$$

$$S_{fs}^{QN} = \int_{S_{fs}} H^Q n . N^N \, dS$$

$$K_f^{PQ} = \int_{V_f} \frac{1}{\rho_f} \frac{\partial H^P}{\partial x} \frac{\partial H^Q}{\partial x} \, dV$$

$$K_{fr}^{PQ} = \int_{S_{fr}} \frac{r}{\rho_f} \frac{1}{c_1} H^P H^Q \, dS$$

$$M_f^{PQ} = \int_{V_f} \frac{1}{K_f} H^P H^Q \, dV$$

$$M_{fr}^{PQ} = \int_{S_{fr}} \frac{1}{k_1} H^P H^Q \, dS$$

$$C_f^{PQ} = \int_{V_f} \frac{r}{\rho_f} \frac{1}{K_f} H^P H^Q \, dV$$

$$C_{fr}^{PQ} = \int_{S_{fr}} \left(\frac{r}{\rho_f} \frac{1}{k_1} + \frac{1}{c_1} \right) H^P H^Q \, dS$$

$$M^{NM} = \int_V \rho N^N N^M \, dV$$

$$C_{(k)}^{NM} = \int_V \left[\beta_c \beta^N : D^d : \beta^M \right] dV$$

$$K^{NM} = \int_V \left[\frac{\partial \beta^N}{\partial u^M} : \sigma + \beta^N : D^d : \beta^M \right] dV$$

$$I^N = I_0^N + K^{NM} \Delta \upsilon^M + C_{(k)}^{NM} \dot{\upsilon}^M$$

$$I_0^N = \int_V \beta^N : \sigma_0 \, dV$$

$$\upsilon^M = \upsilon_0^M + \left(\Re(\upsilon^M) + i\Im(\upsilon^M) \right) e^{i\omega t}$$

$$P^N = \left(\Re(P^N) + i\Im(P^N) \right) e^{i\omega t}$$

in which:

p^r is the pressure on the fluid structure interface,

$$= H^P p^P$$

H^P is the interpolation function for pressure in the fluid at node P^{th},

p^r is the generalized pressure at node P^{th},

u^m is the nodal variables in the structure,

$$= N^M v^M$$

N^M is the interpolation function at M^{th} degree of freedom,

v^M is the generalized variable in the structure at M^{th} degree of freedom,

x is spatial position of the fluid particle,

ρ is material density,

ρ_f is the fluid density,

r is volumetric drag (force per unit volume per velocity),

K_f is the Bulk Modulus of the fluid,

n is the outward normal to the structure,

σ is the stress in the structure,

D^d is the material elasticity matrix,

α_c is the mass proportional damping factor (Rayleigh damping),

β_c is the stiffness proportional damping factor (Rayleigh damping),

p_s^Q and v_s^M are the steady state values of p^Q and v^M,

$\Re$ (p^Q), $\Im$ (p^Q) and $\Re$ (v^M), $\Im$ (v^M) are the real and imaginary part of the amplitude of the response,

$\Re$ (P^N) and $\Im$ (P^N) are the real and imaginary part of the forcing applied to the structure,

ω is complex circular frequency,

and

t is time variable,

Superscripts P and Q refer to pressure DOF in fluid and superscripts N and M refer to displacement DOF in the structure.

The response of the system can be obtained through the so called steady state dynamics procedure over the frequency range of interest.

In ABAQUS, the above equations of motion are solved using either eigenvalue based solution or direct integration techniques. The eigenvalue based solution technique is used in the linear system. In the non-linear system case or in the case of coupled fluid-structure where the matrix in Equation (3.2) may not symmetric, ABAQUS integrates the equation using a direct integration procedure. These two techniques are summarized in Appendix A.

3.2   Experimental Modal Analysis / Modal testing

Modal Testing is usually done by following a procedure that consists of several phases, i.e., modal analysis theory, experimental modal analysis methodology, modal data acquisition, modal parameter estimation and modal data presentation (Allemang and Brown, 1988 and

24

Allemang, 1990). The first phase, modal analysis theory, deals with the part of vibration theory that discusses concepts of natural frequency, mode shape and damping. The next phase, experimental modal analysis methodology, discusses theoretically, the relationships that exist between the measured data and the conventional modal analysis theory. In the modal data acquisition phase, the requirements for modal data acquisition are characterized. The data are analyzed in the next phase (modal parameter estimation) to estimate the modal parameters. Since processing errors may be involved in the analysis of the acquired data, this phase should be carried out carefully to minimize the contribution from extraneous sources of noise. The quality of the estimated modal parameters are judged on the basis of the mathematical model used in the experimental modal analysis methods. Error in this phase is defined as the difference between the measured data and the result of the mathematical model. Since it is assumed that the results of experimental data analysis are correct, the mathematical model employed is sometimes forced or modified to fit the experimental data. The last phase, modal data presentation, deals with the mode of tabulation and graphical presentation of data for modal frequency, modal damping and modal vectors so as to elicit the maximum information available from the analytical/experimental results. Comparison of measured and predicted values are often carried out. This leads to the validation of finite element model used in the study.

In the subsequent sections the various phases involved in experimental modal analysis are briefly discussed.

25

3.2.1 Modal Analysis Theory

Modal Analysis theory utilizes three basic assumptions. The first assumption is that the structure is considered to behave in a linear manner and that its dynamic response can be represented by a series of second order differential equations. Secondly, during the test the structure is time invariant. And the third one is that the structure follows Maxwell-Betti's reciprocal relationships.

Based on the domain of analysis, the results of the theoretical modal analysis can be grouped into three categories, viz., (i) transfer function in Laplace domain; (ii) frequency response function in frequency domain; and (iii) impulse response function in time domain (Allemang *et al.*, 1988). Modal parameter estimation is carried out in this thesis through the frequency domain; in other words, frequency response function approach is used to obtain those parameters.

In understanding modal analysis theory, a sound understanding of the basic theoretical vibration becomes prerequisite. Since multi-degrees of freedom systems (MDOF) can be generally represented as the linear superposition of a number of single degree of freedom systems (SDOF), the SDOF system is briefly discussed first before the multi-degree of freedom systems. Discussion also includes the concept of transfer function, frequency response function (for displacement and acceleration) as well as strain response function.

3.2.1.1 Single Degree of Freedom System

Considering a single degree of freedom system, shown in Figure 3.5, the governing equation of the system is given by,

$$m\ddot{x}(t) + c\dot{x}(t) + kx = f(t) \tag{3.3}$$

where:

    m   = system mass,

    c   = system damping,

    k   = system stiffness, and

    f   = forcing function.
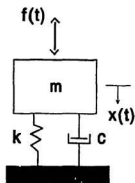
Figure 3.5 A single degree of freedom system

For underdamped single degree of freedom systems, i.e., damping ratio $\xi < 1$ (since most of real structures behave in an underdamped manner) the characteristic roots are a pair complex conjugate ones (see Figure 3.6). For convenience the pole locations in mode r are denoted by p_r and p_r^*; thus

$$
\begin{aligned}
p_r &= -\xi\,\Omega \pm i\left(\sqrt{1-\xi^2}\right)\Omega \\
&= -\sigma_r + i\omega_r \\
p_r^* &= -\xi\,\Omega \pm i\left(\sqrt{1-\xi^2}\right)\Omega \\
&= -\sigma_r - i\omega_r
\end{aligned}
\tag{3.4}
$$

where:

Ω = system natural frequency,

σ_r = damping factor,

ω_r = damped natural frequency.
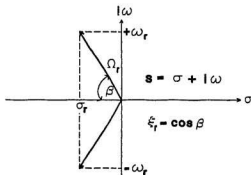
Figure 3.6 Pole locations

The particular solution, i.e., the steady state condition, depends on the forcing function and is obtained using Laplace transform. With zero initial displacement and velocity, the solution for displacement X(s) is obtained as

$$X(s) = H(s) \ F(s) \tag{3.5}$$

where:

s $= \sigma_r + i\omega_r$

$F(s)$ = forcing function in Laplace domain,

$X(s)$ = system response in Laplace domain,

$H(s)$ = system transfer function which relates system input to system response in Laplace domain which can be written as,

$$= \frac{1/m}{(s-p_r)(s-p_r^*)}$$

For a SDOF system, the transfer function $H(s)$ can be written in a simpler form as,

$$H(s) = \frac{A_r}{(s-p_r)} + \frac{A_r^*}{(s-p_r^*)} \tag{3.6}$$

where A_r^* (a complex conjugate of A_r) is the residue at the pole p_r^* (a complex conjugate of p_r).

The displacement frequency response function (DFRF) can be derived by evaluating the transfer function along the imaginary axis, i.e., $s = i\omega$, as

$$H(\omega) = \frac{A_r}{(i\omega - p_r)} + \frac{A_r^*}{(i\omega - p_r^*)} \tag{3.7}$$

29

3.2.1.2 Multi-Degrees of Freedom System

Assuming that the input-output relationship of multi-degrees of freedom system (MDOF) can be represented as a linear superposition of a number of single degree of freedom systems, the system transfer function and displacement frequency response function (of underdamped systems) can be written in partial fraction expansion form as,

Transfer Function :

$$H(s) = \sum_{r=1}^{n} \left[\frac{A_{ikr}}{(s - p_r)} + \frac{A_{ikr}^*}{(s - p_r^*)} \right] \tag{3.8}$$

Displacement Frequency Response Function :

$$H(\omega) = \sum_{r=1}^{n} \left[\frac{A_{ikr}}{(i\omega - p_r)} + \frac{A_{ikr}^*}{(i\omega - p_r^*)} \right] \tag{3.9}$$

where:

    s = Laplace variable,

    ω = angular frequency,

    r = number of the eigenvector (modal vector),

    n = number of eigenvalues (modal frequencies),

    subscripts i   = response at i^{th} degrees of freedom,

    subscripts k   = input at k^{th} degrees of freedom,

$A_{kr} = A^*_{kr}$ = residue,

$\quad = Q_r \, U_{ir} \, U_{kr}$

Q_r = modal scaling factor,

U_{ir} = modal coefficient at measured degrees of freedom i and mode r.

Further details of the experimental procedure for obtaining the modal parameters of the displacement multi-degree of freedom system are given in subsequent sections.

Strain Frequency Response Function :

Several strain frequency response function theories have been proposed; two of them, developed by Ewin and Bernasconi (1989a) and Debao et al., (1989), are summarized here.

Ewins and Bernasconi (1989a) have developed the strain frequency response function (SFRF) using elastodynamic theory. Full derivation is not reviewed here; but the strain frequency response function is rewritten as,

$$S_{jk}(\omega) = \sum_r \frac{\epsilon_{jr} \, \phi_{kr}}{(\omega_r^2 - \omega^2 + 2i\xi_r \omega_r \omega)} \qquad (3.10)$$

where:

ω = frequency variable,

ω_r = damped natural frequency,

ξ_r = modal damping ratio,

ϕ_{kr} = component of mass normalized displacement mode shape in a known direction at

point k, and

ϵ_{jr} = component of rth strain modal vector in a known direction at point j.

Debao *et al.*, (1989) derived strain frequency response function for plate and beam which is written as,

$$S_{jk}(\omega) = \sum_{r=1}^{n} \frac{\{\epsilon_{xr}\}\{\phi_{zr}\}^T}{[K_r - \omega^2 M_r + i\omega C_r]} \qquad (3.11)$$

where :

$K_r = \{\phi_{zr}\}^T [K] \{\phi_{zr}\}$

is generalized stiffness,

$M_r = \{\phi_{zr}\}^T [M] \{\phi_{zr}\}$

is generalized mass,

$C_r = \{\phi_{zr}\}^T [C] \{\phi_{zr}\}$

is generalized damping,

ϵ_{xr} = the rth strain mode shape in x direction,

ϕ_{zr} = the rth displacement mode shape in z direction.

Equation (3.10) and (3.11) are not used in this thesis, because the strain frequency response function needs both displacement mode shapes and strain mode shapes while in the experimental

32

part of this thesis only one accelerometer was used to monitor the displacements; hence the displacement mode shapes could not be obtained from the results. Obviously it is possible to get the responses for several points on the specimen by moving an accelerometer to several different locations. But that method is time consuming and as such is not used in the experimental modal analysis carried out in this study.

3.2.2 Experimental Modal Analysis Procedure

In performing experimental modal analysis or modal testing, the system is assumed to be linear, time invariant, observable and is considered to follow Betti-Maxwell's reciprocal theorem. The linear assumption on the system implies that the response of the system, due to any combination of inputs which applied simultaneously, is equal to the sum of the individual responses to the each input, acting individually. The second assumption means that the measured parameters are constant during the duration of the test. Observable assumption implies that the measured data contains sufficient information to model the dynamic behaviour of the system. This assumption is needed because measurements are generally done in a limited frequency range and resolution. In addition the measured data are limited only to strains, accelerations or displacements; other data such as rotation or curvature cannot be obtained because no rotation or curvature measuring transducer is available in the market today. Betti-Maxwell's reciprocal theorem states that the deformation at point j due to a force applied at point k is equal to the deformation at point k due to a force at point j. Assuming the system to obey the theorem, it is required to measure only a column or a row of the system transfer function matrix as well as

the system frequency response function.

Input and output relationship for the displacement frequency response function procedure for a multi-degrees freedom system can be expressed as,

$$[[m]s^2 + [c]s + [k]]\{X(s)\} = \{F(s)\} \tag{3.12}$$

where [m], [c], [k] are system mass, damping and stiffness in matrices.

If B(s) is defined as,

$$[B(s)] = [[m]s^2 + [c]s + [k]] \tag{3.13}$$

Equation (3.12) can rewritten as,

$$[B(s)]\{X(s)\} = \{F(s)\} \tag{3.14}$$

and,

$$\{X(s)\} = [H(s)]\{F(s)\} \tag{3.15}$$

where:

$$H(s) = \frac{adj\,[B(s)]}{det\,[B(s)]} \tag{3.16}$$

The modal vector can be extracted from the adjoint of matrix B(s), using

$$[B(s)]\,[B(s)]^{-1} = [I]$$

$$[D(s)] = adj\,[B(s)]$$

$$[B(s)]\,[D(s)] = det\,[B(s)]\,[I]$$

34

Evaluating the above equation at the location of poles, i.e., **det [B(s)] = 0**, leads to

$$[B(p_r)] \ [D(p_r)] = 0 \qquad (3.17)$$

Evaluating Equation (3.17) for an arbitrary column of adjoint matrix **B**(s) at the pole locations,

$$[B(p_r)] \ \{D(p_r)\} = 0 \qquad (3.18)$$

gives the modal vectors of the Equation (3.15).

Thus by evaluating an arbitrary column of adjoint matrix **B**(s) to **D**(s), modal vectors of a system can be obtained. When the real part of the pole becomes zero, the transfer functions become frequency response functions. Since it is assumed that the Betti-Maxwell theorem applies to the system, as stated before, modal vectors can be estimated by measuring either a column or a row of system frequency response function.

3.2.3 Digital Signal Processing

Digital signal processing deals with the transformation of a continuous analog data into a vector of discrete digital data for system input and output. In this phase of the experimental modal analysis, errors due to extraneous noise and due to limitations in measurement are taken into account and eliminated from the data before analysis. Digital signal processing methods are used to minimize noise in measurement. Elimination of three types of noise present in the data, viz., (i) a noncoherent noise resulting from stray electrical signals or unmeasured excitation sources, (ii) signal processing noise produced during analysis due to the use of discrete fourier

35

transform to convert time into frequency domain or vice versa, and (iii) nonlinear noise due to non-linear system behaviour need to be considered in the signal processing methods. These noises are eliminated by utilizing a signal averaging procedure (for noncoherent noise) and sufficient length of data with proper windows and frequency resolution (for signal processing noise). The possibility for the presence of nonlinear noise due nonlinear system behaviour must be eliminated.

Five error reduction techniques used to minimize errors in frequency response function measurements are : (i) Choice of the appropriate frequency response function estimator, (ii) Use of signal averaging methods, (iii) Selection of an optimal excitation signal, (iv) Choice of proper frequency resolution, and (v) Use of a suitable weighting function or window.

Based on the assumed noise input into the system, the frequency response function estimating procedure can be grouped into three different methods, viz., H_1, H_2 and H_v.

H_1 assumes that noise exists in the output and the input is free of noise. Hence

$$[H_1]\{X\} = \{Y\} - \{\eta\} \qquad (3.19)$$

H_2 estimator considers the noise to be present in the input and to be absent in the output,

$$[H_2]\{\{X\} - \{v\}\} = \{Y\} \qquad (3.20)$$

H_v assumes the noise to exist both in the input and output signals, consequently

$$[H_v]\{\{X\} - \{v\}\} = \{Y\} - \{\eta\} \qquad (3.21)$$

36

The most common frequency response function estimation approaches are the least square techniques and auto power and cross power spectra based techniques. For the system shown in Figure 3.7, the 2034 B&K signal analyzer used in the experimental part of this thesis utilizes the spectral approach.
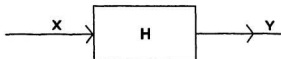
Figure 3.7 System with no noise

While the excitation could be single or multiple, equation derived for a single excitation is given as,

$$H_1 = \frac{G_{xy}}{G_{xx}} \tag{3.22}$$

$$H_2 = \frac{G_{yy}}{G_{yx}} \tag{3.23}$$

where:

G_{xx} is the input auto spectrum,

$$= \sum_{i=1}^{n} X_i \, X_i^*$$

G_{yy} is the output auto spectrum,

$$= \sum_{i=1}^{n} Y_i \, Y_i^*$$

$G_{xy} = G_{yx}$ is the cross spectrum,

$$= \sum_{i=1}^{n} X_i Y_i^*$$

$$= \sum_{i=1}^{n} Y_i X_i^*$$

In any actual situation, the noise occurs both in output and input as shown in Figure 3.8 in which apostrophe denotes the true measured input/output.
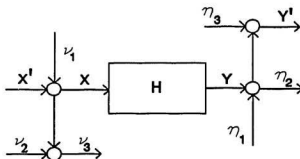
Figure 3.8 System with noise

Therefore, H_1 and H_2 are further defined as,

$$H_1 = \frac{H}{(1+\varepsilon_1)} \tag{3.24}$$

$$H_2 = H(1+\varepsilon_2) \tag{3.25}$$

where:

H is the true response function of system

ε_1 is the relative amount of noise at input

$$= \frac{G_{vv}}{G_{xx}}$$

$$v = v_1 + v_2$$

ε_2 is the relative amount of noise at output

$$= \frac{G_{\eta\eta}}{G_{yy}}$$

$$\eta = \eta_1 + \eta_2$$

It can be seen that H_1 is the lower bound and H_2 is the upper bound of H.

The level of confidence in frequency response function estimation can be identified by the ordinary coherence function which is defined as,

$$\gamma_{yx}^2 = \frac{|G_{yx}|^2}{G_{xx} \, G_{yy}} = \frac{G_{xy} \, G_{yx}}{G_{xx} \, G_{yy}} \tag{3.26}$$

γ_{yx}^2 is real valued and varies from 0 to 1. The coherence function is used to measure the degree of noise in measurement. Zero value of coherence function means the response is generated by the noise or a source other than measured input. When the coherence function is one, however, the measurement is perfect, i.e., the output is caused by the measured input. Error such as leakage can cause the coherent function to be less than one. By increasing the number of averages, the variance of the coherence will be less.

Signal averaging process can be viewed as " the weighted running average process giving

at any time the average value over the previous averaging time". Several time averaging methods are available such as linear, exponential and peak averaging (B&K 2034 analyzer manual, 1987). For linear averaging,

$$A_n = \left[1 - \frac{1}{n}\right] A_{n-1} + B_n \tag{3.27}$$

where:

A_n is the averaging after n ensembles,

A_{n-1} is the previous average after n-1 ensembles,

B_n is the nth ensemble.

Signal averaging can be performed with or without the overlapping of the time record. The overlap process is intended to enhance the measured data by including consecutive history data before the previous data is completed. In the analyzer the degree of overlap could be 50%, 75% or a maximum of 85%. In the maximum overlap, spectra are calculated as fast as possible and all of them are averaged.

Choice of a proper excitation function can reduce the bias error. Signals which have been used in experimental modal analysis are slow sine sweep, fast sine sweep (or periodic chirp), impact, and random signals. In the experimental study reported in this thesis, fast sine sweep signal was applied to specimens. The fast sine sweep signal is a sine wave signal in which the frequency is gradually increased as a function of time over the frequency range of interest while the amplitude and phase are held constant; in mathematical form (De Silva, 1987),

$$f(t) = A \sin[\omega(t)t + \phi] \tag{3.28}$$

40

where:

A = the amplitude,

ϕ = the phase,

$\omega(t)$= the frequency range of interest,

$$= \omega_l + \left(\omega_h - \omega_l \right) \frac{t}{T_d}$$

ω_l = the lowest frequency in the sweep range,

ω_h = the highest frequency in the sweep range,

T_d = sweep duration,

t   = time variable.

The advantages of using the sine signal are the relatively short measurement time, the possibility of reducing leakage error and the high signal to noise ratio.

Increase of the frequency resolution minimizes the leakage error. Increasing frequency resolution would mean the reduction of frequency measurement band or the zooming in of smaller frequency range of interest which would automatically require a longer time record. When the frequency response function peak is narrower than the frequency resolution measurement, error occurs. In this case the frequency response function will "leak" or be wider around the region of interest. Resonant and anti-resonant peaks of the frequency response function are susceptible to this type of error.

By applying a weighting function or a window, error in frequency response function can be reduced. There are several type of windows such as Rectangular, Hanning, Flat Top and

And frequency response function of Equation (3.29) is,

$$H(\omega) = \frac{A_r}{2i(i\omega + p_r)} + \frac{A_r^*}{2i(i\omega - p_r^*)} \qquad (3.30)$$

Equation (3.30) is symmetric about σ_r axis. One side describes the motion in the negative frequencies and the other side characterizes the motion in the positive frequencies. Usually the FFT analyzer evaluates the data only for the positive frequencies; hence the above equation can be rewritten as,

$$H(\omega) = \frac{A_r}{2i(i\omega - p_r)} \qquad (3.31)$$

This can also be thought that the contribution of negative frequencies are neglected. Substitution of the residue and the characteristic poles into the above equation, yields

$$H(\omega) = \frac{A_{r1} + A_{r2}i}{2\{-(\omega - \omega_r) - \sigma_r i\}} \qquad (3.32)$$

Real and imaginary parts of Equation (3.32) are,

$$\Re\,[H(\omega)] = -\frac{\{A_{r1}(\omega - \omega_r) + A_{r2}\sigma_r\}}{2\{(\omega - \omega_r)^2 + \sigma_r^2\}} \qquad (3.33)$$

$$\Im\,[H(\omega)] = +\frac{\{A_{r1}\sigma_r - A_{r2}(\omega - \omega_r)\}}{2\{(\omega - \omega_r)^2 + \sigma_r^2\}} \qquad (3.34)$$

43

Kaiser Bessel (Windows to FFT Analysis, 1987). Randal (1988) suggests the use of Hanning window for stationary signals; in this study Hanning window is used in the signal analysis.

3.2.4 Modal Parameter Estimation

The STAR computer programme from SMS provides five modal parameter estimators based on curve fitting techniques. These techniques are quadrature, coincident, peak, polynomial and global methods. The first three methods estimate modal parameters only in single degree of freedom systems; the other two are applicable for identifying these parameters in heavily damped and multi-degrees of freedom systems. The essential theory of these modal parameter estimation methods are reviewed here.

STAR SMS formulates the frequency response function as,

$$H(s) = \frac{A_r}{2i(s-p_r)} + \frac{A_r^*}{2i(s-p_r^*)} \tag{3.29}$$

where:

A$_r$ is the residue,

$= A_{r1} + A_{r2} i$

A$_r^*$ is the complex conjugate of A$_r$,

$s = \sigma_r + i \omega_r$,

p$_r$ is the pole of the underdamped system, and

p$_r^*$ is complex conjugate of p$_r$.

Evaluating these values at the peak $\omega = \omega_1$ gives,

$$\Re\,[H(\omega)] = -\frac{A_{r1}}{2\,\sigma_r} \qquad (3.35)$$

$$\Im\,[H(\omega)] = +\frac{A_{r1}}{2\,\sigma_r} \qquad (3.36)$$

Real part of the residue refers to the coincident response or the in-phase response and the imaginary part of the residue refers to the quadrature response or the out-of-phase response. It can be seen that the real part of the residue is proportional to the imaginary part of frequency response function while imaginary part of the residue is proportional to real part of frequency response function.

In lightly damped system, where the contribution of the adjacent mode in the vicinity of the identified resonant frequency can be ignored, the residue is always real. Therefore the modal vectors (modal residues or mode shapes) can be identified by only employing the imaginary part of the frequency response function.

Complex peak method fits, in the least squared error sense, the complex value of frequency response function data to estimate the modal frequency and the peak magnitude of the frequency response function. Modal damping is not identified in this method.

By use of the rational fraction least square method, polynomial curve fitting method estimates the modal frequencies, damping and the residues. This method can be applied to both single degree of freedom and multi-degrees of freedom systems. For lightly damped single degree of freedom model, the frequency response function is written as,

44

$$H(\omega) = \frac{A_{r1}\,\omega_r + A_{r2}\,\sigma_r + iA_{r2}\,\omega}{\sigma_r^2 + \omega_r^2 - \omega^2 + 2i\,\sigma_r\,\omega} + C_0 + C_1(i\omega) + C_2(-\omega^2)$$ (3.37)

in which C_0, C_1 and C_2 are residual function coefficients.

The extension of rational fraction least square method, which is called the global curve fitting method, is provided by STAR SMS to get better accuracy and to accommodate the heavy modally coupled system in which resonant frequencies are closely spaced. Global curve fitting method is performed in two steps. First, global frequency and damping curve fits are used to estimate modal frequency and modal damping. And then global resonant method is used to evaluate the complex residue of frequency response function, i.e., the imaginary and real parts of the residue. Unlike the polynomial method, the global curve fit method estimates only two modal parameters in each step. Therefore the modal parameters can be better estimated by this method.

3.2.5 Modal Data Presentation

In this phase, modal parameter data obtained from experiment and predicted by the finite element method are presented in a tabular or graphical form so that modal frequencies and modal residues or peak values of frequency response function can be compared. In finite element analysis, damping ratio is usually assumed. Therefore analytically, in this thesis, zero damping is considered as a first step; and then damping values obtained from experiments are used to get damped modal parameters of the structure.

45

3.3 Summary

Modal analysis is the process of characterizing modal parameter using either analytical approach or experimental approach. In this study, analytically, beam elements along with plane strain acoustic elements, provided by package program ABAQUS version 4.9-1, are used to model the cantilever plate vibrating in vacuum and in air. In addition, shell elements are also used to obtain modal frequencies of the plate in air which are then compared with the values obtained using the beam elements. In the experimental part of this study, frequency response function approach is employed to get the modal parameters of the plate for the first five frequencies. The exciter is located at a point of the plate; fast sine sweep signal excites the structure through the frequency range of interest. In spectrum based techniques, the B&K 2034 analyzer is employed to obtained the frequency response functions (FRF) of the vibrating plate; and damping factor and peak magnitudes of the FRF are extracted using STAR computer package program. The result of the analytical study is reported in Chapter 4 and the experimental results are presented in Chapter 5. The comparison of analytical and experimental studies is given in Chapter 6.

Chapter 4

Analysis of Cracked and Uncracked Plates

The plates used in this study (for analytical and experimental purposes) were analyzed using the computer package program, ABAQUS version 4.9-1, to compute the modal vectors, frequencies and frequency response functions. The dimension and crack shape of the plates investigated in this study are shown in Figure 4.1 and 4.2. The plate was 652 mm long, 204 mm wide and 9.5 mm thick. The cracks were "v" shaped and introduced on both sides of the plates; they are located at 110 mm measured from the fixed end. Two crack depths were investigated, i.e., 2x1/32" (2x0.794 mm) and 2x3/32" (2x2.381 mm) crack depth. Since the actual crack width investigated was very small, in the analyses of the plate three crack widths, viz., 1.5 mm, 2 mm and 2.5 mm, were used. For analyzing the plates (cracked and uncracked) in vacuum and in air (air was considered as a fluid medium), five discretizations were employed; in two of them, shell elements were used for discretizing the uncracked plate in vacuum (hence no air discretization is necessary). On the basis of zero damping assumption, the plates were analyzed over several frequency ranges to obtain the natural frequencies, mode shapes and frequency
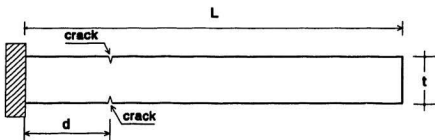
Figure 4.1 Plate dimension and crack location (not to scale)
L = length (652 mm); t = thickness (9.5 mm);
d = 110 mm
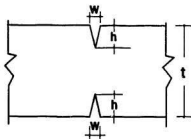
Figure 4.2 Exaggerated crack shape : h = crack depth;
w = crack width

response functions at five nodal points of the vibrating plates; and the results are given in tabular form and plots in Appendix B of this thesis. The response of the structure in water could not be computed, since an appropriate modelling procedure could not be developed due to strong coupling between the plate and water. This chapter highlights the numerical results that were obtained with the finite element discretization of the plates. After detailing the finite element discretization procedure, the results obtained for, the numerical frequency response function, natural frequencies and mode shapes of the plates are presented in this chapter.

4.1 Finite Element Discretization

A total of five different discretizations were used in this study to predict the dynamic behaviour of the plates. Figure 4.3 shows the 4x13 shell elements discretization; the 8x26 shell elements discretization is shown in Figure 4.4. The shell element discretization did not need the discretization of air medium, since it was located in vacuum. The number of degrees of freedom in 4x13 shell elements discretization was reduced to about one fourth by dynamic condensation procedure to shorten the computer processing time; the used discretization is shown in Figure 4.5. In the uncracked beam in vacuum model, the plate was considered as a beam and discretized into 13 beam elements. For the "beam in air model", plain strain fluid elements interact with the beam via the interface elements inserted in between the beam and air interface.
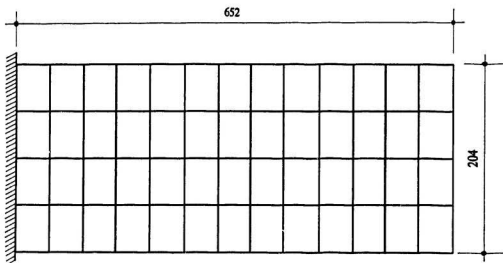
Figure 4.3 4x13 Shell element mesh : plan
(dimension in mm)
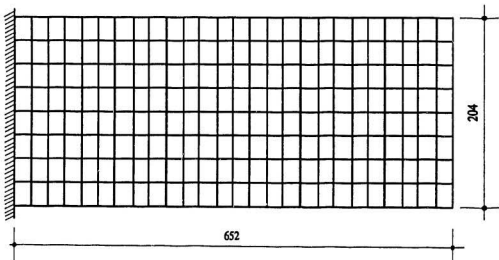
Figure 4.4 8x26 Shell element mesh : plan
(dimension in mm)
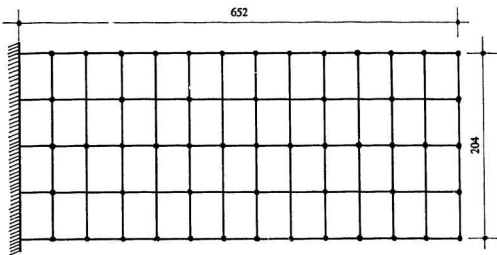
Figure 4.5 Retained nodes used in the reduced shell element discretization : plan
(dimension in mm)

Figure 4.6 shows the "uncracked beam in air" discretization; five nodes, corresponding to the location of transducers (three strain gages and one accelerometer) and excitation point (load cell) in the experiment, are denoted in the figure. The beam in vacuum was modelled by introducing the beam elements as shown in Figure 4.6. The uncracked beam in air discretization was modified to model the cracked beam in air as shown in Figure 4.7. To model the crack, the air and beam elements in the vicinity of the crack were altered. The aspect ratio in that region was maintained as low as possible ($<$ 6), so that reliable results were still obtained. To make the computation simple, the crack was idealized as a "rectangular crack", so that in the analysis, the crack would be considered as a beam element with reduced cross section (the idealization was carried out also due to limitation in computer memory). Further, since the actual crack width was very small, in this study, three different crack widths were considered, viz., 1.5 mm, 2 mm

51

and 2.5 mm. The cracked beam in air discretization is shown in Figure 4.7; the nodes, where the sensors and acceleration were located in the experimental study, are shown in the figure. The finite element mesh around the cracked region for 1.5 mm crack width is shown in Figure 4.8; the idealized crack used in the analysis is shown in Figure 4.9.

Boundary conditions set in these discretizations were made up of plate boundary conditions and fluid boundary conditions. The plate was fixed at one end as shown in Figures 4.6 and 4.7. Since the plate is obviously immersed in the air, in the beam-air discretization, only a half the air discretization was employed taking into consideration the symmetry conditions. To prevent the air pressure from moving back onto the vibrating structure, an absorbing boundary condition was introduced at the farthest end of the air medium by giving a large value of k_i and c_i in Equation (3.1) (k_i and c_i were assumed having value of 10000). These boundaries are located at the bottom and at the right and left sides for the uncracked and cracked beam cases.

4.2   Analytical Frequency Response Function

The analytical frequency response function are obtained by applying a unit force to the structure, in the frequency range of interests; zero damping is assumed in the analysis. This function is the same as the frequency response function used in the experimental study in this thesis, but theoretically these two response functions may be somewhat different in the way they are obtained. ABAQUS uses the equation of motion given in Equation (3.2) to determine the responses; in the experiment, the responses are determined using Equation (3.22) and (3.23) on the basis of auto and power spectra methods. However, physically, these two response functions

52
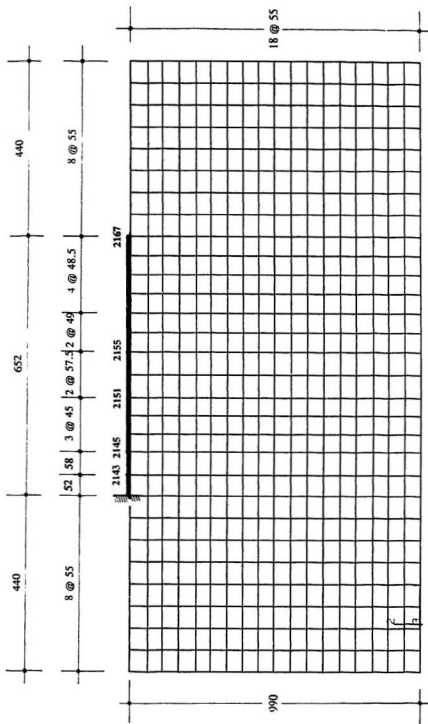
Figure 4.6 Uncracked beam in air discretization (dimension in mm)

53
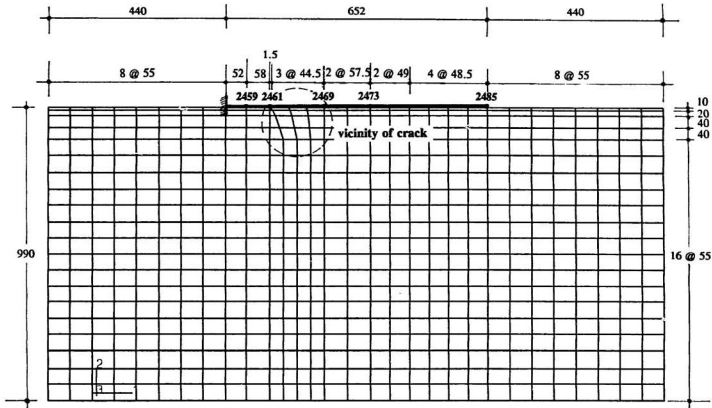
Figure 4.7 Cracked beam in air discretization for 1.5 mm crack width (dimension in mm)
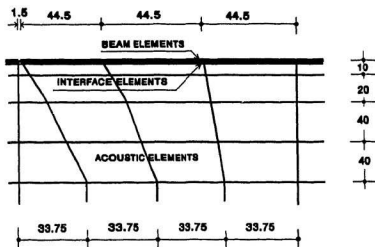
Figure 4.8   Mesh in the vicinity of crack for 1.5 mm crack width
(not to scale; dimension in mm)
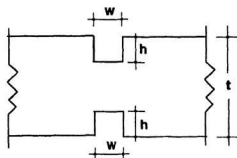
Figure 4.9   Idealized crack : w = crack width; h = crack depth; t = beam's thickness
(not to scale)

are quite similar; the frequency corresponding to the peak response magnitude denotes the natural frequency of the structure. It would be shown later that the acceleration peak magnitudes are proportional to the modal vectors. The purpose of acquiring the functions is to obtain the natural frequencies and peak magnitudes using the discretization given in the previous section. The results are compared with the experimental values in Chapter 6.

The discretization using shell elements, viz., 4x13 shell mesh and 8x26 shell mesh, were used to compute the natural frequencies of the cantilever plate only, since discretizing the plate in air using air and shell elements required a lot of computer memory (9,000 to 11,000 DOFs are involved) and problems were encountered in modelling the "both crack faces" by shell element. The beam element discretization may be adequate to predict the response of the vibrating plates since most of the sensors used in the experimental investigation were located along the center line of the plate; thus only the response in the bending modes could be measured. Using the uncracked beam in vacuum and cracked and uncracked beam in air discretizations, the acceleration and strain response at the five nodes shown in Figures 4.6 and 4.7 were computed. The uncracked beam in vacuum was analyzed in small frequency bands around the peak response. The results, viz., the natural frequencies and peak response magnitudes, are tabulated in Tables B.1.1 and B.1.2 of Appendix B. The beam in air was analyzed in two frequency bands around the resonant peaks; in the smaller one, the frequency resolution used was the same as that used for the beam in vacuum discretization (about 0.025 Hz or 40 points in a one Hz frequency band), so that the results can be compared later. While in the broader bands, the frequency resolution was 0.1 Hz (around the peak) to study the variation of peak magnitudes due to the use of larger frequency resolution. Larger frequency

56

resolution and frequency bands were used in the area where there is no peak. The plots using the broader frequency bands are shown in Appendix B. In obtaining the response of 2x1/32" and 2x3/32" cracked plate in air, frequency resolution used in the vicinity of peak area was the same as the uncracked one. The response peak magnitudes and natural frequencies given by ABAQUS are given in sections B.3 and B.4 in Appendix B.

The analytical frequency response function plot or bode plot, viz., frequency versus response peak magnitude and phase plot, of the uncracked and cracked plate in air for the five nodal points are presented in Appendix B. Two of the response plots, the acceleration and strain response for the uncracked beam at node 2143, are displayed in Figures 4.10 and 4.11. The acceleration and strain response are plotted for the uncracked and cracked plate in air; the displacement responses are only plotted for the uncracked plates. More data on the displacement response were not computed due to time constraint. Since for the uncracked plate ABAQUS gave consistent results in the subsequent frequency ranges, the cracked beams were analyzed in the vicinity of peak response. For the beam with 1.5 mm crack width, the responses are plotted ; and the plots are presented in Appendix B. In several frequency ranges, mostly in the higher frequency ranges, "unexpected peaks" occurred (see Figures B.2.1 to B.2.15 in Appendix B). But it is believed that they are not real peaks since from the preliminary analysis, viz., frequency based analysis, the natural frequencies of the vibrating plates are known and no frequencies were located around these regions. These "errors" might be caused by large time steps used in the time integration procedure; since in zoom frequency bands, the peaks do not come up. The given plots are zoomed around the known resonant frequencies. The strain and displacement phases shift by 180° degrees at the resonant response peaks and around some antiresonant peaks.
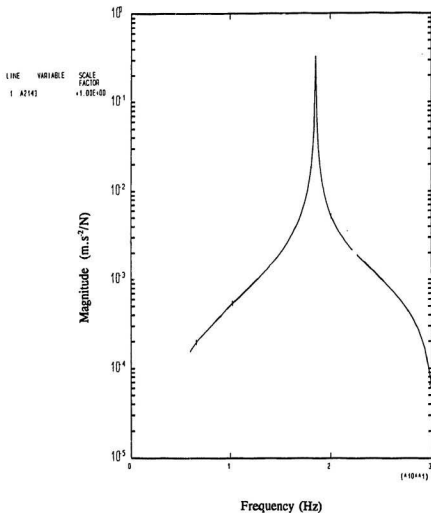
Figure 4.10   Acceleration response of the uncracked plate in air at node 2143 in 6 - 30 Hz frequency band

LINE   VARIABLE   SCALE
                    FACTOR
1 S2143   +1.00E+00

10⁴

10⁵

Magnitude (m.m⁻¹/N)

10⁶

10⁷

10⁸

0   1   2   3
                              (×10⁺⁺¹)
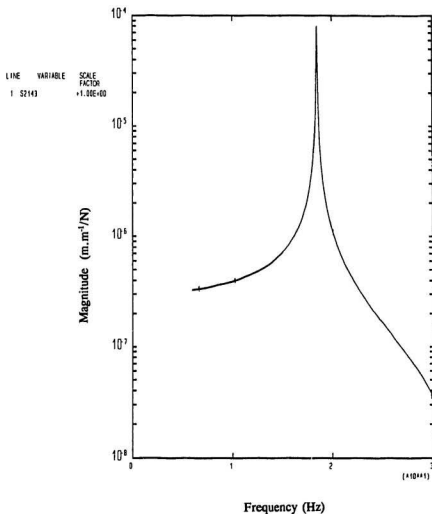
Frequency (Hz)

ABAQUS VERSION 4-9-1

Figure 4.11 Strain response of the uncracked plate in air at node 2143 in 6 - 30 Hz frequency band

4.3 Natural Frequency

The natural frequencies of uncracked plate, computed using the four models mentioned earlier are compared and tabulated in Table 4.1. In-plane transverse mode (mode number 5) and torsion modes (mode 3,6,8,9) were missing when the beam element discretization was used. Figures B.5.1 to B.5.10 display the displacement shapes of the vibrating plate using 4x13 shell element discretization. These figures assist in identifying the modes of the missing frequencies so that Table 4.1 can be constructed. Compared to the 8x26 discretization, the 4x13 shell element discretization gave higher natural frequencies, except for the first mode where the natural frequency was 0.3% lower. The largest difference in natural frequency between these two discretization was 0.4% (for the third mode). The 4x13 shell element reduced model gave good results. A 1.5% difference from the unreduced model (4x13 shell) was found in the ninth mode; for the other modes the difference was lower than the above value. The reduced model consists of 119 variables (DOFs plus langrange multipliers) and 62 nodes; the CPU time utilized was 6 seconds. For the unreduced one, there were 1458 variables and 243 nodes and required 391 seconds to complete the eigenvalue analysis. Hence an enormous saving of computational time was achieved through the reduced model. The natural frequencies obtained using the beam in vacuum discretization were lower than those obtained using the 4x13 shell discretization; the largest difference occurred in the seventh mode (2.3%). Using the same frequency resolution, the resonant frequency changed by a maximum of 1.8% compared to the beam in air (third beam frequency). The natural frequencies of uncracked and cracked beam, in air, for the first five modes are given in Table 4.2. The resonant frequencies only change insignificantly due to the

Table 4.1 Natural frequencies of the uncracked plate

Mode number	Natural frequency (Hz)				
	4x13 shell	8x26 shell	4x13 shell (reduced)	Beam in vacuum	Beam in air
1	19.023	19.081	19.023	18.68	18.48
2	118.82	118.79	118.85	117.00	115.40
3	123.98	123.53	124.04	-	-
4	333.41	333.20	333.90	327.10	321.3
5	375.23	375.21	377.24	-	-
6	387.45	386.09	388.26	-	-
7	654.80	654.06	658.34	640.10	637.8
8	694.62	692.30	699.06	-	-
9	1068.10	1064.60	1084.5	-	-
10	1080.70	1078.40	1095.70	1057.00	1052.00

Table 4.2 Natural frequencies of the cracked and uncracked beam in air

Mode	Natural frequency (Hz)						
	Uncracked beam	2x1/32" cracked beam			2x3/32" cracked beam		
		1.5 mm	2 mm	2.5mm	1.5 mm	2 mm	2.5 mm
1	18.45	18.45	18.42	18.42	18.15	18.04	17.92
2	115.4	115.3	115.4	115.4	115.2	115.2	115.2
3	321.3	319.8	319.8	319.8	319.7	319.7	319.6
4	637.8	637.3	637.3	637.1	632.8	631.2	629.6
5	1052	1051	1051	1050	1041	1039	1039

crack. In the first mode the frequency shift is about 0.2% between the uncracked and cracked beam with a 2x1/32" crack, it is 3% from the uncracked to the beam with the 2x3/32" crack. For the fourth mode the highest shift is 1.3%. The fifth mode shifts by 1.25%. In the second and third modes the natural frequencies shift by less than 0.6%. A "strange thing" occurred in the second mode; when the crack width was increased the natural frequencies reduced. The crack widths were increased further up to 4 mm (with 0.5 mm increment) and the natural frequency did not reduce as expected (the results are not presented in this thesis). The result might imply that the beam crack model used in this study may not be suitable for modelling the crack in the second mode.

4.4 Modal Vectors

According to the modal analysis theory, the acceleration response peak magnitudes are proportional to the modal vectors. In this section, the numerical results are verified to check whether they conform to this. In order to observe the change in the modal vectors due to the presence of the crack, the modal vectors of the uncracked, 2x1/32" and 2x3/32" cracked plates in vacuum were examined.

To be comparable with the modal vectors, the acceleration peak response magnitudes of the uncracked beam in vacuum tabulated in Table B.1.1 in Appendix B are normalized with the largest value of the five points for each mode; the results are given in Table 4.3. The acceleration peak magnitudes of uncracked and cracked beam in air are also normalized to verify the changes in modal vectors due to the presence of air and crack. The peak acceleration

62

response, obtained using the same frequency resolution as the beam in vacuum (Table B.2.1), are compared in Table 4.3. Tables 4.4 to 4.8 give the modal vectors of uncracked beam in vacuum, the normalized peak magnitudes of the uncracked beam in air (from values given in Table B.2.3) and the normalized peak magnitudes of cracked beam in air (from values tabulated in sections B.3 and B.4 in Appendix B). For the cracked beam in air, the values obtained using the three crack widths are presented in these tables. Since the nodes at the same location on the beam are numbered differently in the uncracked and cracked plates discretization, in Tables 4.4 to 4.8 these nodes, where the responses were computed, are numbered from one to five; node number 1 corresponds to node 2143 for the uncracked plate and 2459 for the cracked plate etc.

By comparing the modal vectors and the normalized peak acceleration response of the "beam in vacuum" results given in Table 4.3, it can be concluded that the normalized peak magnitudes are proportional to the modulus of modal vectors. They have same values except at nodes 2151 and 2155 in the first mode where small differences, i.e., 0.0001, occur. Based on the assumption that the peak magnitudes behave similarly, the change of modal vectors can be verified by merely knowing the changed normalized acceleration peak magnitudes; the table also shows that the modal vectors change slightly from "vacuum" to "in air" condition. This result confirms the studies reported by Lindholm *et al.* (1965) and Muthuveerappan *et al.* (1979, 1980). Further, Tables 4.4 to 4.8 examine how the normalized peak response magnitudes or modal vectors, vary due to the assumed crack depths and crack widths. It can be seen that because of the crack, the modal vectors alter slightly; they decrease or increase depending on the modes.

Graphically, the change of modal vectors in vacuum are given in Figures 4.12 to 4.26. The modal vectors of the 2x1/32" and 2x3/32" cracked beams in vacuum with a 1.5 mm crack

Table 4.3 Comparison of modal vector with normalized acceleration response peak magnitudes

Discretization	Mode number	Normalized acceleration peak magnitude or modulus of modal vector at nodes				
		2143	2145	2151	2155	2167
Modal vector in vacuum	1	0.0108	0.0462	0.2056	0.4018	1.0
	2	0.0615	0.2301	0.6558	0.6687	1.0
	3	0.1568	0.4984	0.6155	0.2608	1.0
	4	0.2761	0.7014	0.1385	0.5973	1.0
	5	0.4052	0.7559	0.6954	0.4789	1.0
Beam in vacuum	1	0.0108	0.0462	0.2057	0.4017	1.0
	2	0.0615	0.2301	0.6558	0.6687	1.0
	3	0.1568	0.4984	0.6155	0.2608	1.0
	4	0.2761	0.7014	0.1385	0.5973	1.0
	5	0.4052	0.7559	0.6954	0.4789	1.0
Beam in air	1	0.0108	0.0463	0.2058	0.4020	1.0
	2	0.0600	0.2237	0.6336	0.6395	1.0
	3	0.1471	0.4637	0.5596	0.2478	1.0
	4	0.2774	0.7053	0.1344	0.5972	1.0
	5	0.4039	0.7544	0.6981	0.4768	1.0

Table 4.4 Normalized acceleration response magnitudes in air : mode number 1

Mode	Node	Normalized acceleration peak magnitudes						
		Beam no crack	2x1/32" cracked beam			2x3/32" cracked beam		
			1.5 mm	2.0 mm	2.5 mm	1.5 mm	2.0 mm	2.5 mm
1	1	0.0108	0.0108	0.0108	0.0107	0.0104	0.0103	0.1020
	2	0.0463	0.0461	0.0461	0.0459	0.0446	0.0441	0.0436
	3	0.2060	0.2060	0.2061	0.2060	0.2072	0.2078	0.2083
	4	0.4022	0.4022	0.4023	0.4022	0.4039	0.4047	0.4055
	5	1.0	1.0	1.0	1.0	1.0	1.0	1.0

Table 4.5 Normalized acceleration response magnitudes in air : mode number 2

Mode	Node	Normalized acceleration peak magnitudes						
		Beam no crack	2x1/32" cracked beam			2x3/32" cracked beam		
			1.5 mm	2.0 mm	2.5 mm	1.5 mm	2.0 mm	2.5 mm
2	1	0.0600	0.0560	0.0598	0.0597	0.0590	0.0586	0.0584
	2	0.2237	0.2231	0.2230	0.2229	0.2198	0.2186	0.2175
	3	0.6336	0.6329	0.6330	0.6330	0.6318	0.6314	0.6310
	4	0.6394	0.6385	0.6388	0.6387	0.6376	0.6375	0.6372
	5	1.0	1.0	1.0	1.0	1.0	1.0	1.0

Table 4.6 Normalized acceleration response magnitudes in air : mode number 3

Mode	Node	Beam no crack	2x1/32" cracked beam			2x3/32" cracked beam		
			1.5 mm	2.0 mm	2.5 mm	1.5 mm	2.0 mm	2.5 mm
3	1	0.1471	0.1443	0.1444	0.1445	0.1476	0.1489	0.1500
	2	0.4637	0.4541	0.4544	0.4551	0.4672	0.4717	0.4766
	3	0.5595	0.5420	0.5421	0.5423	0.5462	0.5472	0.5496
	4	0.2477	0.2444	0.2441	0.2442	0.2460	0.2453	0.2479
	5	1.0	1.0	1.0	1.0	1.0	1.0	1.0

Table 4.7 Normalized acceleration response magnitudes in air : mode number 4

Mode	Node	Beam no crack	2x1/32" cracked beam			2x3/32" cracked beam		
			1.5 mm	2.0 mm	2.5 mm	1.5 mm	2.0 mm	2.5 mm
4	1	0.2773	0.2783	0.2780	0.2790	0.2860	0.2895	0.2917
	2	0.7051	0.7093	0.7093	0.7125	0.7245	0.7562	0.7666
	3	0.1344	0.1353	0.1363	0.1359	0.1516	0.1562	0.1616
	4	0.5971	0.5955	0.5954	0.5951	0.5884	0.5856	0.5832
	5	1.0	1.0	1.0	1.0	1.0	1.0	1.0

Table 4.8 Normalized acceleration response magnitudes in air : mode number 5

Mode	Node	Beam no crack	2x1/32" cracked beam			2x3/32" cracked beam		
			1.5 mm	2.0 mm	2.5 mm	1.5 mm	2.0 mm	2.5 mm
5	1	0.4039	0.4035	0.4034	0.4036	0.3992	0.3798	0.3385
	2	0.7544	0.7592	0.7605	0.7622	0.7785	0.7504	0.6767
	3	0.6981	0.6911	0.6905	0.6905	0.6969	0.6740	0.6247
	4	0.4767	0.4809	0.4816	0.4822	0.4950	0.4947	0.4868
	5	1.0	1.0	1.0	1.0	1.0	1.0	1.0

width are shown in Figures 4.12 to 4.16; Figures 4.17 to 4.21 show the cracked beam with a
2 mm crack width and Figures 4.22 to 4.26 show the modal vectors of the beam with 2.5 mm
width. To compare with the cracked beam, the uncracked plate modal vectors are plotted in the
same figures. As observed in the previous sections, the modal vector shifts are more noticeable
in the higher frequencies, i.e, modes 4 and 5, than the lower ones.

The normalized strain response magnitudes do not behave the same as the acceleration
ones; the maximum values occur at different nodes for various modes (the highest value in a
mode of the strain response might be at the nodal point which is very close to the fixed end;
unfortunately the response at that point was not computed). These values are not presented in
this chapter, but they will be compared with the experimental values in Chapter 6.
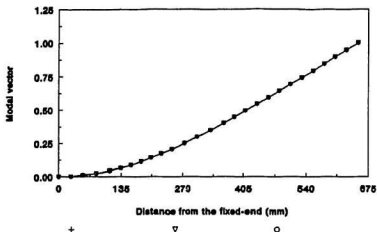
Figure 4.12 Modal vectors of beam in vacuum : 1.5 mm crack width (first mode)
+ uncracked beam; ▽ 2x1/32" cracked and ○ 2x3/32" cracked beam
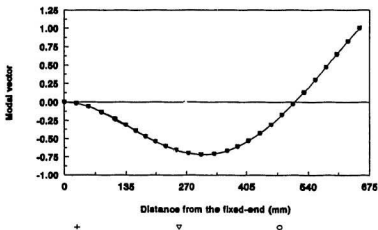
Figure 4.13 Modal vectors of beam in vacuum : 1.5 mm crack width (second mode)
+ uncracked beam; ▽ 2x1/32" cracked and ○ 2x3/32" cracked beam
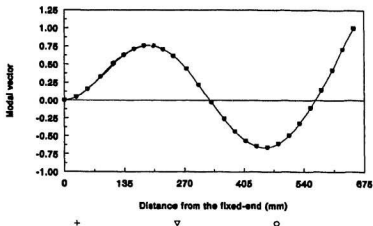
Figure 4.16 Modal vectors of beam in vacuum : 1.5 mm crack width (third mode)
+ uncracked beam; ∇ 2x1/32" cracked and ○ 2x3/32" cracked beam
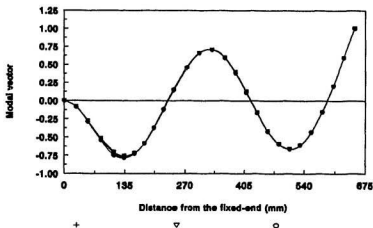
Figure 4.15 Modal vectors of beam in vacuum : 1.5 mm crack width (fourth mode)
+ uncracked beam; ∇ 2x1/32" cracked and ○ 2x3/32" cracked beam
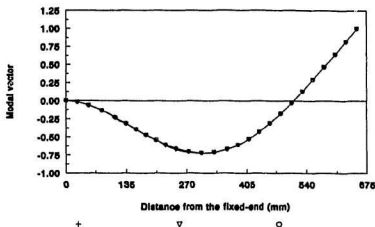
Figure 4.18 Modal vectors of beam in vacuum : 2.0 mm crack width (second mode)
+ uncracked beam; ∇ 2x1/32" cracked and ○ 2x3/32" cracked beam
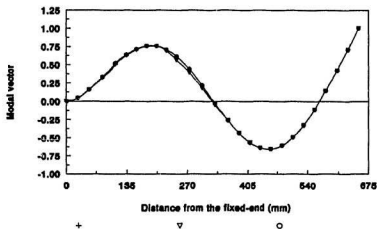
Figure 4.19 Modal vectors of beam in vacuum : 2.0 mm crack width (third mode)
+ uncracked beam; ∇ 2x1/32" cracked and ○ 2x3/32" cracked beam
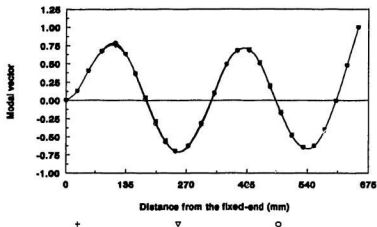
Figure 4.16   Modal vectors of beam in vacuum : 1.5 mm crack width (fifth mode)
+ uncracked beam; ∇ 2x1/32" cracked and ○ 2x3/32" cracked beam
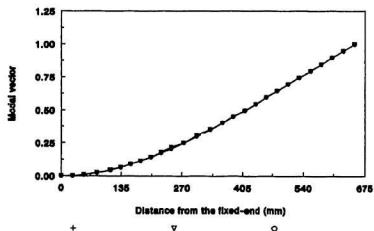
Figure 4.17   Modal vectors of beam in vacuum : 2.0 mm crack width (first mode)
+ uncracked beam; ∇ 2x1/32" cracked and ○ 2x3/32" cracked beam
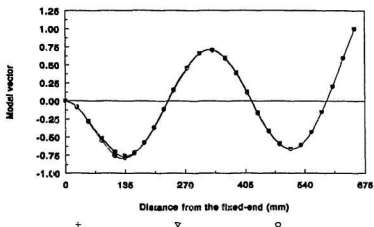
Figure 4.20 Modal vectors of beam in vacuum : 2.0 mm crack width (fourth mode) + uncracked beam; ∇ 2x1/32"cracked and ◯ 2x3/32" cracked beam
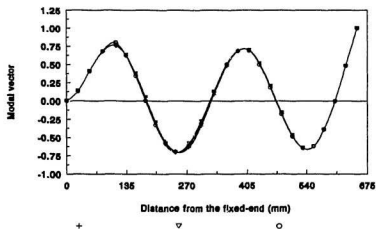
Figure 4.21 Modal vectors of beam in vacuum : 2.0 mm crack width (fifth mode) + uncracked beam; ∇ 2x1/32" cracked and ◯ 2x3/32" cracked beam
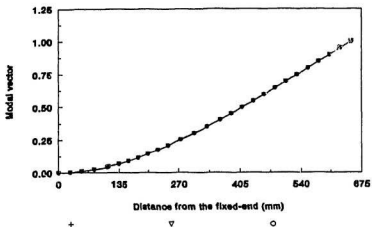
Figure 4.22   Modal vectors of beam in vacuum : 2.5 mm crack width (first mode)
+ uncracked beam; ∇ 2x1/32" cracked and ○ 2x3/32" cracked beam
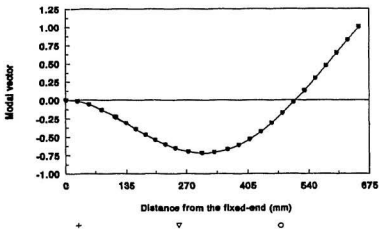
Figure 4.23   Modal vectors of beam in vacuum : 2.5 mm crack width (second mode)
+ uncracked beam; ∇ 2x1/32" cracked and ○ 2x3/32" cracked beam
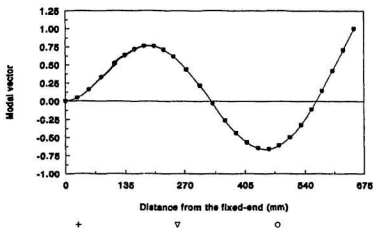
Figure 4.24   Modal vectors of beam in vacuum : 2.5 mm crack width (third mode)
+ uncracked beam; ∇ 2x1/32" cracked and ○ 2x3/32" cracked beam
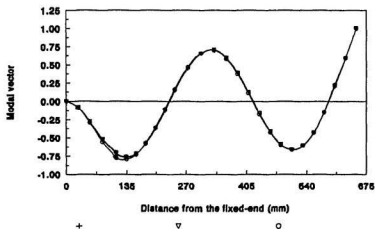
Figure 4.25   Modal vectors of beam in vacuum : 2.5 mm crack width (fourth mode)
+ uncracked beam; ∇ 2x1/32" cracked and ○ 2x3/32" cracked beam
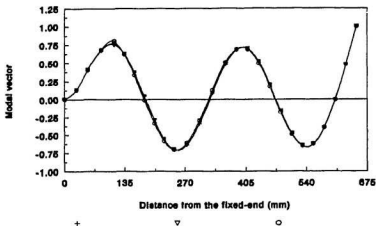
Figure 4.26   Modal vectors of beam in vacuum : 2.5 mm crack beam (fifth mode)
+ uncracked beam; ▽ 2x1/32" cracked and ○ 2x3/32" cracked beam

4.5   Summary

The cracked and uncracked plates are analyzed considering five different models. The natural frequencies obtained from these analyses have been compared. The difference in natural frequencies is less than 0.4% when the results obtained by using the 4x13 shell discretization are compared with the 8x26 ones. The natural frequencies obtained using the 4x13 shell discretization is higher than the beam in vacuum frequencies by a maximum value of 2.3%. Beam in air discretization gives frequencies 1.8% lower than the beam in vacuum discretization. Due to the 2x1/32" crack depth, the natural frequencies reduce by as high as 0.5% from the uncracked one. For the 2x3/32" crack depth the reduction in natural frequency is up to a maximum of 3%. The acceleration response peak magnitudes in vacuum are divided by the

75

largest value in each mode to determine the modal characteristics; it is found that these values are proportional to the modal vectors. By normalizing the acceleration peak magnitudes for the responses obtained for the cracked and uncracked beams in air, and assuming that the peak response magnitudes have the same characteristics as the "in vacuum" ones, it can be concluded that modal vectors change from "in vacuum" to "in air" condition. The modal vectors also change due to the presence of cracks, although the changes are not significant. These changes occur mainly around the location of the crack. At the five nodal points where the responses were computed, the normalized strain magnitudes behave differently form the acceleration ones; these values will be compared with the experimental values.

Chapter 5

Experimental Test in Air and in Water

In the experimental study reported in this thesis, the responses of horizontal cantilever plates (with and without cracks) vibrating in air and in water, were measured for the first five bending modes. The experiment in water was carried out in two water levels, i.e., (i) water level which was approximately at the middle of the plate thickness; and (ii) water level which was about 23 cm above the upper surface of the plate. To carry out the measurements in water, a 130x55x80 cm deep tank was built; the tank was fixed to a rigid platform so that it did not vibrate when the plate was excited. The plates used in this study were rectangular plates, whose dimensions were 652x204x9.5 mm thick. Three plates were tested; the first plate was uncracked while the second and the third ones were fabricated with "v" shaped cracks on both sides of the plate (see Figure 4.2 or the photograph given Appendix E for the crack shape). The crack depths for the second and third plates were 2x1/32" and 2x3/32", respectively; the crack width was very small, compatible with the smallest notch required to produce a crack like feature. The plate was clamped horizontally between two 30.5x30.5x2.75 cm thick steel blocks; the lower

block was attached to a heavy I beam support, which was welded to the bottom of the tank. The complete experimental results obtained in this study are presented in Appendix C; the natural frequencies, damping ratios and peak response magnitudes are tabulated; in addition the acceleration and the strain frequency response functions and coherent functions are also plotted for salient points of interest. In this chapter, the results are discussed and highlighted.

5.1 Experimental Apparatus

To monitor the vibrations of the plate, four strain gages and one accelerometer were mounted on the plate; they were positioned on the plate at the locations shown in Figure 5.1. The positions were predetermined, based on the predicted dynamic behaviour of the structure in the first five bending modes, so that all of the modal response could be obtained (a peak modal responses cannot be obtained if a sensor is located at an inflection point of a vibrating structure). The block diagram of the experiment is shown in Figure 5.2. The apparatus used in this study is tabulated in Table 5.1; and a photograph of the experimental setup is shown in Figure 5.3.

The plate was excited in the frequency ranges of interest by using a function generator. Fast sine sweep or "chirp" excitation was used in this experiment; the time sweep was selected so that the best results for coherence and frequency response functions would be obtained. The signals from the function generator was passed through the power amplifier where the gain was selected. The signals were, then, input to an exciter; the exciter was connected to the driving point on the plate by a 33 mm long rod. A force transducer was attached in between the exciter
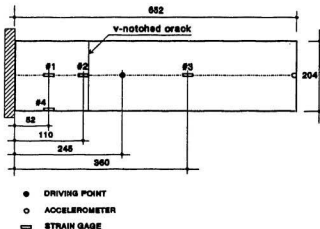
Figure 5.1 Location of the accelerometer and strain gages : plate plan (not to scale; dimension in mm)
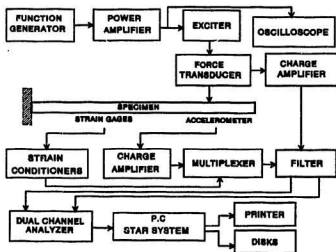
Figure 5.2 Block diagram of experimental setup

Table 5.1 List of the apparatus used in the experiment

No	Name of apparatus	Type or serial number
1	Function Generator	HP 3314A
2	Power Amplifier	B&K type 2706
3	Vibration Exciter	B&K type 4809
4	Force Transducer	B&K type 8200
5	Accelerometer	B&K type 4344
6	Strain Gage	Student gage EA-06-120LZ-120
7	Strain conditioner	Model 2110 Vishay Instrument
8	Charge Amplifier	Model 504E Soundstrand Data control.
9	Multiplexer	B&K 8 Channel type 2811
10	Dual Channel Signal Analyzer	B&K type 2034
11	Filter	Model 442, Rockland Dual Hi/Lo Filter
12	Personal Computer The Star System	386-IBM compatible Star version 3.00D
13	Printer	HP Laserjet II
14	Oscilloscope	Model MM 200 Metermaster
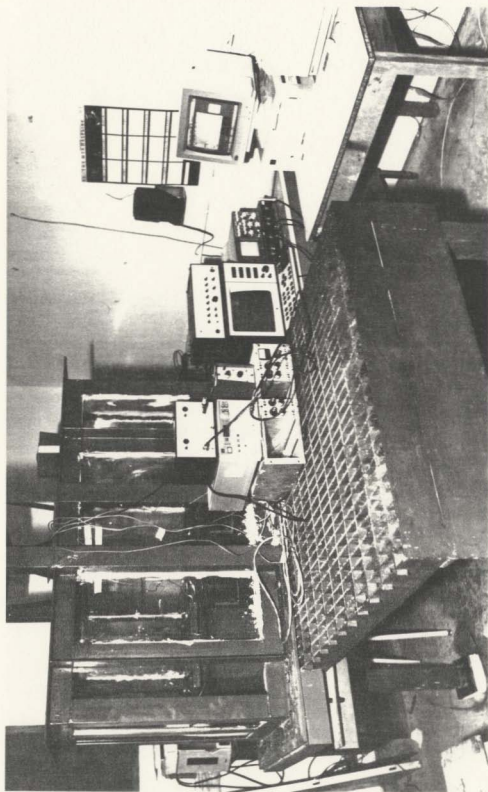
Figure 5.3 A photograph of experimental setup

81

and the connecting rod to monitor the excitation force. The signals generated by strain gages were input to strain conditioners; the signals monitored by the accelerometer and force transducer were input to the charge amplifiers. The strain conditioners and the charge amplifiers converted the voltage charge input signals from the sensors (accelerometer and strain gages) and force transducer, into proportional voltages; the voltages were amplified and output. The gain of the strain conditioners and charge amplifiers were chosen so that the output did not overload (go beyond the measurement range of) the system. Output signals from accelerometer and strain gages were input into a multiplexer, so that only one channel of the sensors was read at time. Then, the signal output from the multiplexer passed through a low pass filter. The signals from the force transducer, after being amplified and converted by the charge amplifier, were input to a low pass filter. The filter was employed to filter out the higher modes of vibration and any noise embedded in the electrical system (filtering in band pass, high pass and without filter modes were tried; it was found that low pass gave almost same results as the band pass but was found to be better than the other two). The signals from the filter were output into the B&K analyzer (two channels) which was calibrated to the charge amplifier/strain conditioner output. In the analyzer, frequency response function and coherence function were computed and displayed. These data were then exported to a PC with the STAR computer package program in it. By using the package program the modal parameters were determined. When the experiment in water was carried out, the strain gages were sealed so that water did not affect the strain gages. The compounds used in the sealing process were polyurethane, acrylic and silicone rubber.

5.2 Experimental Procedure

The 2x1/32" cracked plate was first tested in air along with the uncracked and 2x3/32" cracked plates; then they were tested under partially submerged (where the water level was kept approximately at the middle of the plate thickness - about 27.4 cm above the bottom of the tank) and fully submerged (where the water level was about 50 cm above the bottom of the tank) conditions in water. The experiments in air and in water were carried out using the same setup as that given in section 5.1 so that the changes in modal parameters, i.e., damping, natural frequency and peak response magnitude could be compared.

The data in the experiment were acquired using two types of frequency band, called "the broad " and "zoom" frequency bands. In "the broad frequency bands", five frequency bands were chosen so that in every band, one resonant peak of the frequency response function could be obtained. During the measurement in air, for instance, the chosen frequency bands were 10 to 60 Hz, 60 to 160 Hz, 160 to 360 Hz, 360 to 760 Hz and 760 to 1160 Hz. In "zoom frequency bands", smaller frequency bands than the "broad" ones were selected so that the frequency band produces the highest peak response in the frequency response function. For example, the frequency bands used in the measurement in air were : 5 to 30 Hz, 95 to 120 Hz, 250 to 350 Hz, 585 to 610 and 900 to 1000 Hz. Frequency bands lower than 25 Hz were not used, due to time limitation in this study; at high frequencies, smaller frequency bands do not always give higher peak response magnitudes. The purpose of zooming into smaller frequency bands was to study the change of modal parameters and coherence function due to the increased frequency resolution.

83

Throughout the experiment, linear averaging was used. The number of averages was selected, depending on the condition of the frequency response and coherence functions. The number of averages was increased if a poor frequency response function or coherence was obtained.

5.3   Discussion of the Results

This section discusses the results given in Appendix C. The first part of this section deals with the change of modal parameters due to crack; the experimental results obtained for the uncracked and 2x1/32" cracked plate in air are compared. The modal parameters of 2x3/32" cracked plate are not compared with these two plates, since the results were not consistent with the others; the first three natural frequencies of the 2x3/32" cracked plate were found to be higher than the uncracked ones; the fourth and fifth natural frequencies were lower than the uncracked plate natural frequencies. This may probably have been due to the fact that the plate was too stiff with respect to the crack size. The second part of this section discusses the modal parameter changes due to change of fluid densities between air and water. In this part the relative frequency reductions of uncracked and 2x3/32" cracked plate in air and water are compared. The 2x1/32" cracked plate was not tested in water due to time constraint. The last part of this section discusses the coherence.

5.3.1 Change of Modal Parameters Caused by the Presence of a Crack

The natural frequency and damping of uncracked and 2x1/32" cracked plates are given in Table 5.2. The parameters given in the table are the average values tai *. from Appendix C. The table shows that due to the existence of crack, the frequencies reduce. It can be seen that the natural frequency shifts are larger in the higher modes. In the first mode the natural frequencies are basically the same; the difference between these corresponding frequencies is less than 0.25% (the uncracked plate natural frequency is lower than the cracked one). Figure 5.4 shows the change of natural frequencies in a graphical form; the natural frequencies plotted in this figure are the average values of those measured using strain gagus and the accelerometer (since those values are only slightly different). Table 5.2 also gives the modal parameters for the same plates using zoom frequency bands. Only slight difference in natural frequencies are observed between those measured in "the broad frequency bands" and in "the zoom frequency bands" (the highest difference is about 0.1%). Unlike in "the broad frequency bands", in "the zoom frequency bands", the natural frequency shifts can be identified even in the first mode. (see the lower part of Table 5.2). Figure 5.5 shows the natural frequencies of these two plates graphically.

By comparing damping values for the corresponding modes of these two plates (the second and the fourth column of Table 5.2), it can be concluded that the acceleration damping values vary differently for different modes; in "zoom" frequency bands, the strain damping decreased due to the crack except in the fourth mode (see also Figures 5.6 and 5.7). The values obtained in "the zoom frequency bands" are different from those obtained in the broader bands (the

85

Table 5.2 Modal parameters of the uncracked and 2x1/32" cracked plate in air
(acc : acceleration; str : strain gage)

Mode	Sensor	Modal parameters (broad frequency bands)			
		Uncracked plate		2x1/32" cracked plate	
		Nat. freq	Damping	Nat. freq	Damping
1	Acc	17.0338	0.2825	17.0633	0.2522
	Str	17.0158	0.2599	17.0567	0.2637
2	Acc	106.3433	0.1267	106.2367	0.1460
	Str	106.3283	0.1556	106.2292	0.1712
3	Acc	305.9870	0.1838	305.190	0.1608
	Str	306.0020	0.1768	305.1658	0.1712
4	Acc	602.3133	0.27465	598.280	0.2897
	Str	602.3008	0.2820	598.3258	0.2782
5	Acc	969.9733	0.3776	962.550	0.4164
	Str	969.5833	0.4223	962.6242	0.4140

Mode	Sensor	Modal parameters (zoom frequency bands)			
		Uncracked plate		2x1/32" cracked plate	
		Nat. freq	Damping	Nat. freq	Damping
1	Acc	17.0400	0.1885	17.0167	0.1703
	Str	17.0308	0.1980	16.9992	0.1867
2	Acc	106.2733	0.1669	106.0233	0.1664
	Str	106.2542	0.1838	106.0242	0.1792
3	Acc	306.0067	0.1726	304.5900	0.2028
	Str	306.7508	0.2178	304.4925	0.2076
4	Acc	601.7700	0.2886	597.9067	0.2764
	Str	601.6625	0.2879	597.8625	0.2892
5	Acc	969.4500	0.3643	962.8900	0.3765
	Str	969.5133	0.4394	963.5375	0.3705
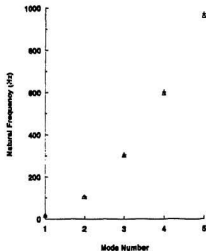
Figure 5.4 Natural frequencies of the uncracked and 2x1/32" cracked plate in air (broad)
+ uncracked plate; ▵ 2x1/32" cracked plate
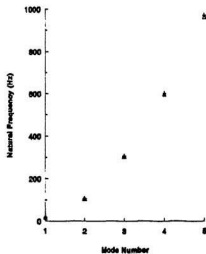
Figure 5.5 Natural frequencies of the uncracked and 2x1/32" cracked plate in air (zoom)
+ uncracked plate; ▵ 2x1/32" cracked plate
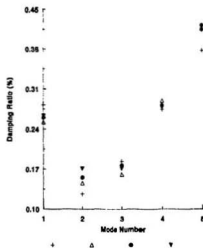
Figure 5.6 Damping ratio of the uncracked and 2x1/32" cracked plate in air (broad)
+ accel. damping (uncracked plate); △ accel. damping (2x1/32" cracked plate)
● strain damping (uncracked plate); ▼ strain damping (2x1/32" cracked plate)
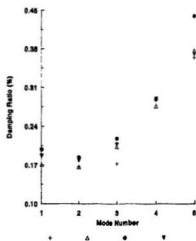
Figure 5.7 Damping ratio of the uncracked and 2x1/32" cracked plate in air (zoom)
+ accel. damping (uncracked plate); △ accel. damping (2x1/32" cracked plate)
● strain damping (uncracked plate); ▼ strain damping (2x1/32" cracked plate)

highest difference is about 50% in the first mode). The change of damping values from the "broad" to the "zoom" frequency bands, are understandable. Since the values were obtained by using curve fit based method, different frequency response function will give different values of damping (even though measurements are made by using a same sensor at a same point). Discrepancies are also found between "strain damping" and "acceleration damping" values even though the differences are not much (see Figures 5.6 and 5.7). The discrepancies between acceleration and damping values may be caused by the nature of these sensors; the acceleration measures "global" behaviour of the vibrating structure; the strain gages measure "local" behaviour of the structure.

As in the case of damping, the change of peak magnitudes at the five measurement points could not be justified in consistent manner; for different modes, they either increase or decrease. When zooming was used, peak response magnitudes of the plates increased. Peak magnitudes of strain gages no. 1, 2 and 3 were examined further. They were divided by the largest value amongst them; and "the normalized peak strain magnitudes" in zoom and broader band frequency ranges were compared for corresponding fit methods; the normalized values are given in Tables D.1 to D.7 of Appendix D. It is found that for uncracked and cracked plates in air, the highest difference between those values is 27.96 % and it occurred in the fourth mode of the uncracked plate; for partially submerged plate, the a maximum difference of 36.98% is found (2x3/32" cracked plate in the third mode) and for full submergence, in the uncracked plate, it is 36.98% maximum (in the fourth mode); in the cracked plate a difference of 206.67% was found in the second mode (in this mode the zoom frequency bands gave lower peak magnitudes than the broader ones).

5.3.2 Change of Modal Parameters for Varying Fluid Densities

Table 5.3 gives damping and natural frequencies of the uncracked plate in air and partially/fully submerged condition in water (partial submergence condition is shortened into part and fully submergence condition is abbreviated to full; acc stands for acceleration and str stands for strain gage in Table 5.3). Natural frequency reduces as high as 40% (in the first mode) for air to fully submerged condition in water. Compared with the values obtained by Lindholm *et al.* (1965) (who found the frequency reduction to be as high as 35% for plate width to plate length ratio equal to 3 and plate thickness to plate width ratio equal to 0.0611), the frequency reduction obtained in this study is a bit higher since the plate size used in this study is not exactly the same as theirs. Figures 5.6 and 5.7 show the natural frequency of the plate in air, and under partially/fully submerged conditions in water for the "broad" and "zoom" frequency bands. Figure 5.8 shows the relative frequency reductions of the plate natural frequencies measured using strain gages under those three conditions. Figure 5.9 displays the natural frequency reductions in "the zoom frequency bands" for the same plate. In Figures 5.8 and 5.9, the relative natural frequency reductions are plotted against the water depth (above the base of the tank) to plate length ratio. The values of relative natural frequency reduction (the ordinate axis of Figures 5.8 and 5.9) are calculated using formula :

$$FR_{0.420} = \frac{(\omega_a - \omega_p)}{\omega_a} \times 100\%$$

$$FR_{0.767} = \frac{(\omega_p - \omega_f)}{\omega_p} \times 100\%$$

Table 5.3 Modal parameters of the uncracked plate in air and in water

Mode	Sensor	Modal parameters (broad frequency bands)					
		Natural frequency (Hz)			Damping (%)		
		Air	Part	Full	Air	Part	Full
1	Acc	17.003	12.490	-	0.2825	0.5731	-
	Str	17.016	12.4875	10.1875	0.2599	0.5378	0.5522
2	Acc	106.343	79.583	-	0.1267	0.64055	-
	Str	106.328	79.582	67.5733	0.1557	0.6770	0.8824
3	Acc	305.987	238.076	-	0.1838	0.8344	-
	Str	306.002	237.990	201.152	0.1769	0.8340	1.05505
4	Acc	602.313	481.143	-	0.2746	0.8311	-
	Str	602.301	481.388	409.272	0.2820	0.8550	1.3450
5	Acc	969.973	808.063	-	0.3776	1.08	-
	Str	969.583	807.332	682.769	0.4223	0.9747	1.5362

Mode	Sensor	Modal parameters (zoom frequency bands)					
		Natural frequency (Hz)			Damping (%)		
		Air	Part	Full	Air	Part	Full
1	Acc	17.04	12.47	-	0.1885	0.5191	-
	Str	17.031	12.462	10.172	0.1980	0.5270	0.5329
2	Acc	106.273	79.4033	-	0.1669	0.7216	-
	Str	106.254	79.3942	67.3033	0.1839	0.7321	0.8601
3	Acc	306.007	237.543	-	0.1726	0.8221	-
	Str	305.751	237.683	199.442	0.2178	0.7920	1.0327
4	Acc	601.77	481.173	-	0.2886	0.9396	-
	Str	601.66	480.923	409.2	0.2879	0.9717	1.6512
5	Acc	969.45	807.367	-	0.3643	0.9311	-
	Str	969.51	806.665	670.412	0.4394	0.9846	1.7675
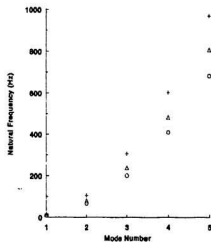
Figure 5.8 Natural frequencies of the uncracked plate in air and in water (broad)
+ in air; △ partially submerged and ○ fully submerged in water
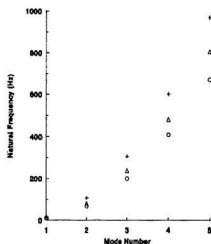
Figure 5.9 Natural frequencies of the uncracked plate in air and in water (zoom)
+ in air; △ partially submerged and ○ fully submerged in water
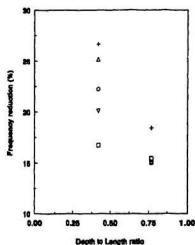
Figure 5.10 Relative natural frequency reductions of the uncracked plate in two water depths (broad): + first mode; △ second mode; ○ third mode; ▽ fourth mode; □ fifth mode
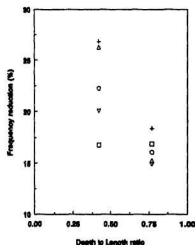
Figure 5.11 Relative natural frequency reductions of the uncracked plate in two water depths (zoom) : + first mode; △ second mode; ○ third mode; ▽ forth mode; □ fifth mode

where :

FR$_{0.420}$ is the relative frequency reduction in percent for water depth to plate length ratio is equal to 0.420 (partially submerged condition),

FR$_{0.767}$ as above except for the ratio equals to 0.767 (fully submerged condition),

ω_a, ω_p and ω_f are the natural frequencies of the plate in air and under partially and fully submerged conditions in water.

It can be noted that there are small discrepancies between natural frequencies measured using strain gages and accelerometer in a measurement (by comparing two rows for a mode in Table 5.3). Unlike the experimental results in air, under full submergence, zooming causes frequency shifts as high as 1.8% (about 12.36 Hz) in the fifth frequency and less than 1% in the other resonant frequencies.

As expected, the damping ratio increases due the increase of the fluid density; Figure 5.12 shows the variation of "strain damping", i.e., damping measured using strain gages under these three conditions. In the "zoom" frequency band, the damping variation is shown in Figure 5.13. From Tables in Appendix C, it can be seen that the damping values vary not only in the "broad" and "zoom" frequency bands, but also at the different sensor locations.

When the peak response magnitudes are examined, it is found that most of them reduce due to vibration in water. In the zoom frequency bands, peak magnitudes are higher than the broader band except in the second and the fifth modes of the plate under full submergence. (unlike the measurement carried in air where in "the zoom frequency band" all of the peak magnitudes were higher than the those measured in the broader frequency bands). The peak response magnitudes were, at least, affected by two factors. The first one was frequency

94
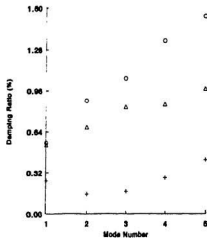
Figure 5.12 Damping ratio variation of the uncracked plate in air and in water (broad)
+ in air; △ partially submerged in water; ○ fully submerged in water
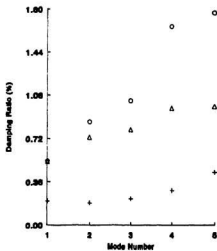
Figure 5.13 Damping ratio variation of the uncracked plate in air and in water (zoom)
+ in air; △ partially submerged in water; ○ fully submerged in water

resolution; by zooming around the area of the peak the number of points in a frequency band increase, so that higher peak magnitudes are obtained. The second one is the frequency response function condition; since the modes of the plates in water are closely separated (see frequency response function plots in sections C.1.2 and C.1.3 in Appendix C), by observing around a smaller frequency band, the contribution of the adjacent modes may be reduced or made insignificant. However, it may be quite reasonable to say that in the zoom band for the experiment in water the peak magnitudes of the two modes (second and fifth) are lower than that obtained using the broader band.

The results of the 2x3/32" cracked plate are presented in Table 5.4 in both frequency bands. This plate was used to examine the frequency variation in air and in water. It can be seen from Table 5.5 that for the first three natural frequencies, the relative frequency reductions from air to partially submerged and from partially submerged to fully submerged are almost similar to the uncracked one (the resonant frequencies given in Table 5.5 are those measured using strain gages) for the first three modes. Differences begin to show for the fourth and fifth modes, indicating the possibility of the influence added water masses due to crack. This needs to be examined further in subsequent studies.

For the second mode of the plate partially submerged in water, the peak response magnitudes decrease in the zoom frequency band. This behaviour was also found to be the same with the uncracked plate. The fifth mode of this plate behaves differently since the experimental results were not consistent.

Table 5.4 Modal parameters of the 2x3/32" cracked plate in air and in water

Mode	Sensor	Modal parameters (broad frequency bands)					
		Natural frequency (Hz)			Damping (%)		
		Air	Part	Full	Air	Part	Full
1	Acc	16.933	12.42	10.1567	0.2725	0.6047	0.6240
	Str	16.933	12.398	10.154	0.27925	0.5566	0.6022
2	Acc	109.033	81.693	69.093	0.17305	0.8073	0.9048
	Str	109.690	81.690	69.081	0.17675	0.8709	0.9394
3	Acc	310.740	239.910	203.233	0.3137	0.8203	1.26
	Str	311.085	239.957	203.233	0.3137	0.7849	1.2737
4	Acc	602.277	449.253	402.610	0.3024	1.1950	1.4878
	Str	602.126	449.093	402.716	0.2952	1.2700	1.4681
5	Acc	966.967	808.190	741.447	0.4657	1.115	1.2850
	Str	967.112	807.726	741.397	0.5161	1.0165	2.3562

Mode	Sensor	Modal parameters (zoom frequency bands)					
		Natural frequency (Hz)			Damping (%)		
		Air	Part	Full	Air	Part	Full
1	Acc	16.983	12.4267	10.11	0.2134	0.4220	0.4880
	Str	16.920	12.373	10.122	0.2302	0.4584	0.4740
2	Acc	108.703	82.1467	68.86	0.1738	0.5321	0.5634
	Str	108.711	82.119	68.932	0.18005	0.5196	0.5456
3	Acc	310.630	240.950	203.306	0.4405	1.2110	1.245
	Str	310.645	240.816	203.362	0.4225	1.1169	1.2575
4	Acc	601.770	465.517	417.313	0.2887	1.1800	1.5770
	Str	601.664	464.600	417.287	0.2878	1.0500	1.5857
5	Acc	966.153	806.497	742.057	0.3691	1.0000	1.5600
	Str	966.352	804.506	742.332	0.3827	1.0005	1.5450

Table 5.5 Comparison of relative frequency reduction of the uncracked and 2x3/32" cracked plate in air and in water

Mode	Natural frequency reduction (%)					
	Uncracked plate			2x3/32" cracked plate		
	Air-Part	Part-Full	Air-Full	Air-Part	Part-Full	Air-Full
1	26.613	18.418	40.130	26.782	18.102	40.035
2	25.155	15.089	36.448	25.062	15.435	36.629
3	22.225	15.478	34.264	22.864	15.283	34.652
4	20.075	14.981	32.049	25.415*	10.327*	33.118*
5	16.734	15.429	29.581	16.481*	8.212*	23.339*

5.3.3 Coherence Function

Coherence functions obtained using the accelerometer were very good; the coherence values were almost one everywhere, except at some points. Strain gages generally gave good coherence in the vicinity of the resonant frequencies. In general, in frequency bands where the first and second mode were located, the coherence was good; in the bands of the third and fifth mode, the values were fair. The worst was around the frequency bands of the fourth mode; the coherence values at several points in the vicinity of the resonant frequency were 0.6 or greater; for other frequencies in the band the coherence was very poor. From the frequency response function presented in figures given in Appendix C, it can be seen that the poor coherence function, generally, corresponds to the region of low peak response amplitudes.

Attempts to improve the coherence were made; one of them was by zooming into smaller
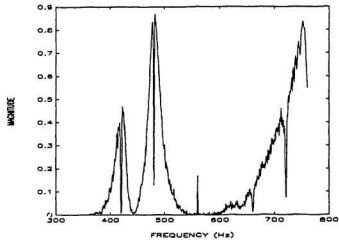
Figure 5.14   Coherence function of the uncracked plate partially submerged in water (broad) : strain gage no. 1
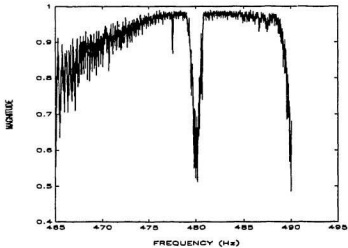
Figure 5.15   Coherence function of the uncracked plate partially submerged in water (zoom) : strain gage no. 1

frequency bands, viz., increasing the number of points in a frequency band. Figures 5.14 and 5.15 show the coherence function in a broad frequency band and in zoom frequency band; this is one of the worst coherence functions obtained in the experiment. By comparing these two, it can be seen that the coherence function is much better in the smaller frequency band (zoom) than in "the broad one".

5.4 Summary

Due to the existence of crack, the natural frequencies reduce; the reductions are higher in the higher modes. Damping and peak magnitudes at the five point of measurement increase/decrease depending on modes. In the zoom frequency bands, damping values differ from those obtained in the broader bands; the peak magnitudes in the zoom band are higher than the peak magnitudes in the broad band.

When the plate is partially submerged in water, the natural frequencies reduce by a maximum of 26.8% and the maximum damping increase is about 5 times. In full submergence condition, the natural frequencies reduce by as much as 40.3%; damping increases as high as 6 times and most of the peak magnitudes decrease. The change of damping and natural frequencies increases as the depth of submergence of the plate increases until a certain depth is reached after which no change is seen. Unlike in air, by zooming into smaller frequency bands, the peak response magnitudes of several modes in water were lower than the broader bands. It was found that the coherence function could be improved by increasing the frequency resolution.

Chapter 6

Comparison of the Experimental and Analytical Study

One of the reasons for doing modal analysis was to compared the predicted dynamic behaviour of a structure with those actually measured in the experiment. This phase should be followed by validation of the modal characteristics of the structure which would lead to the adjustments of the theoretical model so that the model gives results which match with the experimental ones. By this methodology, combination of the theoretical and experimental models can be made; and a better analytical model can be developed. In this chapter, the analytical and experimental results presented in the two previous chapters, viz., natural frequencies and normalized peak strain response magnitudes given in Chapters 4 and 5, are compared and correlated. In addition, the behaviour of peak acceleration and strain response magnitudes of the uncracked plate due to non-zero damping were examined further. The peak response magnitudes and bode plots (frequency versus response magnitude and frequency versus phase plots) are given in Appendix D. The results are discussed in the last part of this chapter. The adjustment of analytical model to correspond to the experimental results was not carried out in this study.

6.1 Measured and Predicted Natural Frequencies

The comparison of natural frequencies of the uncracked plate in air obtained through the present analytical and experimental investigation is given in a tabular form in Table 6.1, both for the "broad" and "zoom" frequency bands. And a in graphical form the natural frequencies obtained using the "broad" frequency bands are shown in Figure 6.1. As given in Table 6.1, the differences between measured and predicted values are found to be within 8.6% for these two frequency bands. In Figure 6.1, the linear fit of the natural frequencies is denoted by the dashed line; the line where the points should lie is denoted by a straight line with slope of one. It can be seen that the points lie in a line which is slightly different from expected one. According to Ewins (1984), this type of discrepancy may be due to "an erroneous material property used in the prediction". This might be true since it was found that the plate thickness along the plate edge, parallel to the plate length, were thicker (more than 25%) than the thickness parallel to the width of the plate (the cross section was not really of uniform thickness). In the analysis, the average value was used; this might not be correct (but this is the only one that could be done). Further analytical study to get results closer to the experimental ones could not be carried out in this thesis.

The comparison of measured and predicted natural frequencies for the 2x1/32" cracked plate in air is displayed in Figure 6.2. It appears that Figures 6.1 and 6.2 are almost similar; the linear fit of the natural frequencies marked by dashed line is slightly different from the

Table 6.1 Comparison of measured and predicted natural frequencies of the uncracked plate in air, in the "broad" and "zoom" frequency bands

Mode	Natural frequency (Hz)				% Difference	
	Predicted		Measured			
	Broad	Zoom	Broad	Zoom	Broad	Zoom
1	18.45	18.48	17.025	17.035	8.37	8.48
2	115.40	115.40	106.336	106.264	8.524	8.60
3	321.30	321.40	305.995	306.379	5.00	4.87
4	637.80	637.80	602.307	601.716	5.89	6.00
5	1052	1052	969.778	969.482	8.48	8.51
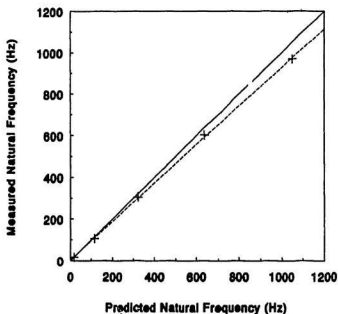
Figure 6.1 Comparison of measured and predicted natural frequencies of the uncracked plate in air

103
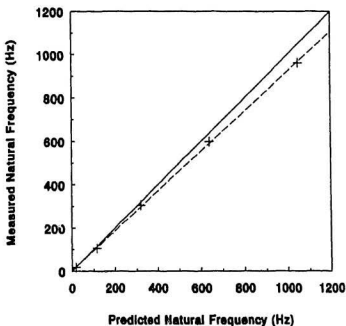
Figure 6.2 Comparison of measured and predicted natural frequencies of the 2x3/32"
cracked plate in air

Table 6.2 Predicted and measured natural frequency reductions due to the 2x1/32" crack

Mode	Natural frequency reduction (%)				
	Predicted			Measured	
	1.5 mm	2.0 mm	2.5 mm	Broad	Zoom
1	0	0.163	0.163	-0.2	0.159
2	0.087	0	0	0.097	0.226
3	0.469	0.469	0.469	0.267	0.603
4	0.078	0.078	0.110	0.669	0.641
5	0.095	0.095	0.191	0.747	0.651

expected line. The same reason as described in the uncracked plate would apply also in the cracked one. Table 6.2 presents the natural frequency reductions obtained (between uncracked and cracked plates) experimentally and numerically due to the presence of cracks; values obtained numerically are given for three different crack widths. It appears that the results of the plate with an assumed 2.5 mm crack width is a good model for the 2x1/32" cracked plate compared with the other two, although the % difference was not close to the experimental ones (this model is the best among these three models, using beam elements). The difference between the measured natural frequencies and those computed using the model with assumed 2.5 mm crack width is 8.65% (maximum) occurs at the second mode in the "zoom" frequency bands. Crack widths larger than 2.5 mm (up to 4 mm), were studied for the second mode; but the natural frequency was not reduced as expected. In higher modes, the larger frequency reductions might be obtained if larger crack widths are introduced. Unfortunately, in this study, the crack widths for those modes were not examined further. Also according to experimental results larger frequency reductions were observed for higher modes than for lower modes. This was not indicated by the numerical model; since the influence of rotatory inertia was not considered in the analytical model, the difference may be due to this.

6.2   Normalized Peak Strain Response Magnitudes

Measured and predicted peak strain response magnitudes of the cracked and uncracked plates were examined further. Three nodes corresponding to the strain gage no. 1, 2 and 3 were normalized by the largest value among them; and the results are given in Appendix D. In Tables

Table 6.3 Analytical and experimental values of the normalized peak strain response magnitudes of the uncracked plate in air

| Mode | Condition | Normalized peak strain response magnitudes at nodes | | | | | |
| | | Predicted | | | Measured | | |
		2143	2145	2155	Str1	Str2	Str3
1	Vacuum	1.0	0.8628	0.3142	-	-	-
	Broad	1.0	0.8616	0.3120	1.0	0.815	0.270
	Zoom	1.0	0.8623	0.3130	1.0	0.812	0.238
2	Vacuum	0.8520	0.2820	1.0	-	-	-
	Broad	0.8486	0.2741	1.0	0.779	0.127	1.0
	Zoom	0.8486	0.2741	1.0	0.636	0.122	1.0
3*	Vacuum	1.0	0.6454	0.8081	-	-	-
	Broad	1.0	0.6934	0.8639	0.395	0.924	1.0
	Zoom	1.0	0.6932	0.8640	0.414	0.920	1.0
4	Vacuum	0.3295	0.9044	1.0	-	-	-
	Broad	0.2116	0.9062	1.0	0.186	1.0	0.958
	Zoom	0.2117	0.9062	1.0	0.238	1.0	0.948
5*	Vacuum	0.1252	1.0	0.6511	-	-	-
	Broad	0.1230	1.0	0.6517	0.639	1.0	0.991
	Zoom	0.1230	1.0	0.6517	0.582	1.0	0.967

Table 6.4 Analytical and experimental values of the normalized peak strain response magnitudes of the 2x1/32* cracked plate in air (cw : crack width)

Mode	Normalized peak strain response magnitudes at nodes							
	Predicted				Measured			
	cw	2143	2145	2155	Band	Str1	Str2	Str3
1	1.5	1.0	0.8625	0.3135	Broad	1.0	0.832	0.344
	2.0	1.0	0.8620	0.3125				
	2.5	1.0	0.8623	0.3131	Zoom	1.0	0.838	0.381
2	1.5	0.8468	0.2729	1.0	Broad	0.742	0.108	1.0
	2.0	0.8460	0.2726	1.0				
	2.5	0.8454	0.2723	1.0	Zoom	0.630	0.103	1.0
3*	1.5	1.0	0.7045	0.8805	Broad	0.413	0.791	1.0
	2.0	1.0	0.7024	0.8793				
	2.5	1.0	0.7003	0.8782	Zoom	0.361	0.776	1.0
4	1.5	0.2157	0.9040	1.0	Broad	0.205	1.0	1.0
	2.0	0.2165	0.9015	1.0				
	2.5	0.2186	0.9026	1.0	Zoom	0.240	1.0	0.958
5*	1.5	0.1185	1.0	0.6579	Broad	0.532	0.759	1.0
	2.0	0.1174	1.0	0.6604				
	2.5	0.1165	1.0	0.6625	Zoom	0.620	0.731	1.0

Table 6.5 Analytical and experimental values of the normalized peak strain response magnitudes of the 2x3/32" cracked plate in air (cw : crack width)

Mode	Normalized peak strain response magnitudes at nodes							
	Predicted				Measured			
	cw	2143	2145	2155	Band	Str1	Str2	Str3
1	1.5	1.0	0.8620	0.3134	Broad	1.0	0.826	0.340
	2.0	1.0	0.8625	0.3132				
	2.5	1.0	0.8621	0.3124	Zoom	1.0	0.861	0.331
2	1.5	0.8330	0.2636	1.0	Broad	0.704	0.115	1.0
	2.0	0.8280	0.2604	1.0				
	2.5	0.8232	0.2574	1.0	Zoom	0.753	0.124	1.0
3*	1.5	1.0	0.6587	0.8530	Broad	0.696	1.0	0.993
	2.0	1.0	0.6443	0.8428				
	2.5	1.0	0.6261	0.8347	Zoom	0.738	1.0	0.994
4**	1.5	0.2492	0.8916	1.0	Broad	-	-	-
	2.0	0.2623	0.8884	1.0				
	2.5	0.2740	0.8821	1.0	Zoom	-	-	-
5**	1.5	0.0985	1.0	0.7267	Broad	-	-	-
	2.0	0.0872	1.0	0.7674				
	2.5	0.0721	1.0	0.8359	Zoom	-	-	-

6.3 to 6.5, the normalized peak strain response magnitudes of the plates in air, obtained through the analytical study are compared with those measured in the experiment. In these tables the experimental values given are obtained using peak fit method since it appears that these values are, in general, good enough to represent the values obtained using polynomial and global fit methods (as could be seen by comparing values given in Tables D.1.1, D.1.4 and D.1.5 in Appendix D). Compared to the predicted values, the values in the first, second and fourth modes are closer to the analytical ones (except the values given by strain gage no. 2 in mode 2 where large discrepancies are observed); the normalized peak response magnitudes in the fourth mode are still acceptable although the highest peak are not the same between the experimental and numerical values (this result is a little surprising since the coherence function for this mode was poorer than the others). The reason is that the peak strain response magnitudes at points 2145 and 2155 (or at strain gages no. 2 and no. 3) are almost the same so that in the measurement the values are not distinguishable. The results for third and fifth modes are not good (marked by superscript *). In the third mode the highest numerical peak is not the same as the one obtained experimentally; and when the peak magnitudes are normalized, the values are reversed, viz., the peak of the numerical FRF occurs at node 2143 while that of the experimental FRF occurs at 2155. In the fifth mode, the discrepancies between values at nodes 2143 and 2155 and strain gage no. 1 and no. 3 are large (a maximum of 4.3 times was observed). Also the maximum values of the uncracked and 2x1/32" cracked plate (Tables 6.3 and 6.4) are not in the same location. The normalized experimental peak strain response magnitudes, in modes 4 and 5 for the 2x3/32" cracked plate are not given in Table 6.5 since these measured amplitudes in the modes are not consistent with the analytical ones (marked by superscript **). Comparing the

values measured in the "broad" and in the "zoom" frequency bands, it appears that measurements made with the "broad" band give better results for the normalized peak response magnitudes (i.e., the values are close to predicted value).

6.3   Response of the Uncracked Plate in Air with Damping

Damping values measured in the experiment for the uncracked plate in air were averaged; and the averaged values were converted into Rayleigh damping by using the formula given by Bathe (1982) and included in the analysis of the plate using ABAQUS computer package program. Since the formula requires two subsequent damping values, the damping at the sixth mode was found by fitting linearly the damping values at the first five modes and assuming that the higher modes give the higher damping. Mass and stiffness proportional damping factors, α_c and β_c, used in the analysis are given in Table D.2.1. The results are given in Appendix D; natural frequencies are tabulated and the response versus frequency plots are presented. The peak response magnitudes decrease, but it is found that for the fourth and fifth modes, the resonant frequencies are different at all five nodes (see Table D.2.2 in Appendix D). The normalized peak acceleration and strain magnitudes of the first two modes are the same as those computed with zero damping. In the third mode, the values change slightly; in the fourth and fifth modes, they change significantly (compare Tables 4.3 and D.2.4 for acceleration response and Tables D.1.1 and D.2.5 for strain response). As comparison to the response in air with zero damping, the acceleration and strain responses at node 2167 of the uncracked beam in air with damping are shown in Figures 6.2 and 6.4.
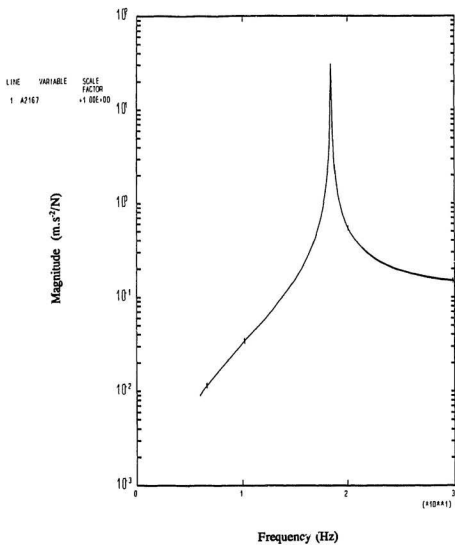
Figure 6.3 Acceleration response of the uncracked beam in air without damping at node 2167 in 6 to 30 Hz frequency band

LINE VARIABLE SCALE FACTOR
1 A2167 +1.00E+00
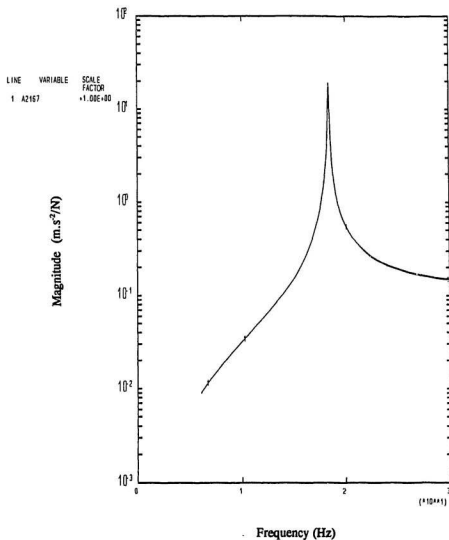
ABAQUS VERSION 4-9-1

Figure 6.4 Acceleration response of the uncracked beam in air with damping at node 2167 in 6 to 30 Hz frequency band
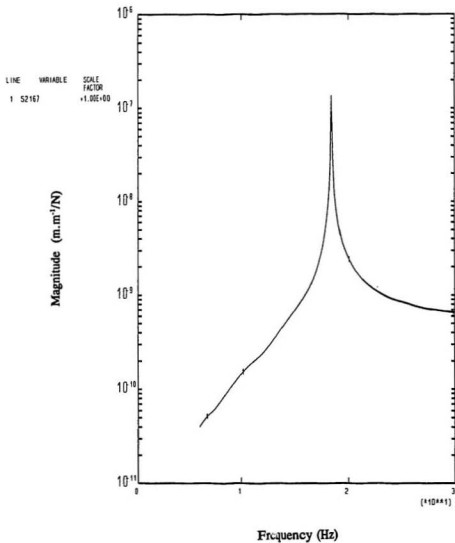
Figure 6.5   Strain response of the uncracked beam in air without damping at node 2167 in 6 to 30 Hz frequency band

113

LINE   VARIABLE   SCALE
                  FACTOR
1 S2167   +1.00E+00

Magnitude (m.m⁻¹/N) $\text{Magnitude (m.m}^{-1}\text{/N)}$
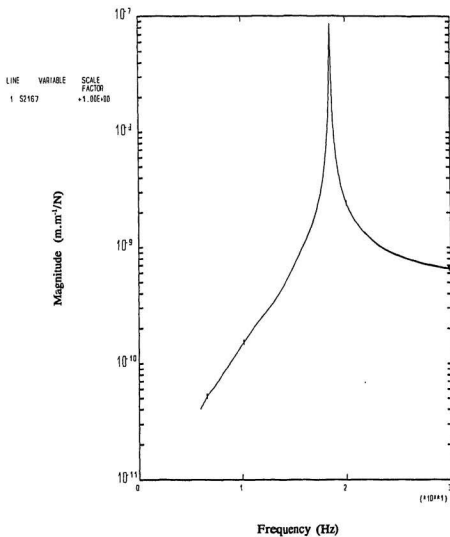
Frequency (Hz)

ABAQUS VERSION 4-9-1

Figure 6.6   Strain response of the uncracked beam in air with damping at node 2167
in 6 to 30 Hz frequency band

6.4 Summary

Measured and predicted natural frequencies of the uncracked and 2x1/32" cracked plate are correlated; it is found that a maximum of 8.60% discrepancy is observed for both "broad" and "zoom" frequency bands. The discrepancies might be because of erroneous material property employed in the analysis. Compared to 1.5 and 2.0 mm crack width, it seems that the 2.5 mm crack width is better to model the 2x1/32" cracked plate in air. Correlation between measured and predicted values of the normalized peak strain response magnitudes are good in modes 1, 2 and 4 for the uncracked and 2x1/32" cracked plates and in mode 1 and 2 for the 2x3/32" cracked plate.

Chapter 7

Conclusion and Recommendation

This thesis investigates the behaviour of vibrating cracked, and uncracked, steel cantilever plates in two media, viz., air and water for two different water levels, through analytical and experimental procedures. The parameters that were considered in this study were the natural frequencies, associated damping and the peak response magnitudes. Three types of plates were studied; an uncracked plate, 2x1/32" and 2x2/32" cracks. The plate dimension was 652 mm long, 204 mm wide and 9.5 mm thick. Symmetrical "v" shaped cracks (located at 110 mm from the fixed end) were introduced on the both side of the plates. The simple structure was chosen to study the phenomena of a structure, with cracks vibrating in air and water, so that the phenomena can be understood clearly without being affected by the complexity of the structure. The primary interest in carrying out this study was to investigate the variation of damping and peak response magnitudes as well as natural frequencies of a structure due to the size of crack and depth of water submergence; very few studies have considered the effect of cracking on damping and response amplitudes. In this study, the plates investigated were excited from 1.00

116

to 1000.0 Hz, using a chirp or fast sine sweep; the response at five nodal points for the first five resonant frequencies were determined using modal analysis/testing approach.

Analytically, the responses of the cracked and uncracked plates were computed by employing a computer package program, ABAQUS version 4.9-1. Five different type of discretizations were considered using plate/shell and beam elements; and natural frequencies obtained by using these discretizations were compared. Beam discretizations were used to investigate the changes of modal parameters due to the existence of cracks and air elements. Since the actual crack width introduced in this study was very small, the cracked beam was analyzed using three assumed crack widths, viz., 1.5 mm, 2.0 mm and 2.5 mm. Conclusions that can be drawn from the analytical study are :

- The natural frequencies computed using 4x13 shell element model were different from those computed using 8x26 shell element model by a maximum of 0.4%; they were 2.3% higher (maximum) than the resonant frequencies obtained using the beam "in vacuum" discretization.

- The beam "in air" discretization gave natural frequencies 1.8% lower than the beam "in vacuum" discretization.

- Due to 2x1/32" crack, the natural frequencies reduced by as high as 0.5%; 2x3/32" crack caused the natural frequency to shift by a maximum value of 3%.

- The modal vectors change from in air to in vacuum condition; the change of modal vectors were also observed when cracks were introduced. The changes due to the presence of crack, were found mainly around the crack region.

Experimental investigations, in air and in water, were carried out in a 130x55x80 cm

117

deep tank. The 2x1/32" cracked plate was investigated in air; the uncracked and 2x3/32" cracked plate was tested in air and in two levels of water submergence. On the plate, four strain gages (three mounted along the centre-line and one near the edge of the plate) and one accelerometer (located at the center of the free end of the plate) were used to monitor the response of the vibrating structure. In addition, one force transducer was located to monitor the force applied to the structure. Measurements were carried out in two type of frequency bands; the "zoom" frequency bands and the "broad" frequency bands. In this two types of frequency bands, only one peak of the frequency response function could be obtained. By using the B&K Analyzer the frequency response function was acquired; the modal parameters (i.e., natural frequencies, damping and peak response magnitudes) were extracted using the STAR computer package program. The 2x3/32" cracked plate in air and in water, gave results which did not go along with the other ones; the first three natural frequencies were higher and the fourth and fifth natural frequencies were lower than the uncracked plate. The results of the 2x3/32" cracked plate in water were compared with the uncracked one. The experimental investigations led to the following conclusion :

- Due to the presence of the crack, a natural frequency reduction of 0.75% (maximum) was observed. In this case zoom frequency bands gave natural frequencies which consistently decreased compared with the uncracked plate natural frequencies (broad frequency bands gave natural frequencies higher than the uncracked plate for the first mode). Peak response magnitudes and acceleration damping ratio either increased or decreased depending on the modes and location of the measurement point. In "zoom" frequency bands, strain damping ratio decreased with the exception of mode 4.

118

- When the plates were partially submerged in water (the water level was just at the middle of the plate thickness), the natural frequencies shifted by 26.8% and damping increased by 5 times; most of the peak response magnitudes decreased.

- Under full submergence conditions where the water level was 50 cm above the tank base, a natural frequency reduction of 40% (maximum) was found; damping increased by 6 times and peak response magnitudes decreased.

The results of the experimental and analytical studies were correlated. It was observed that

- There was a maximum of 8.6% between the measured and computed natural frequencies (see Table 6.1). This discrepancies may be due to thickness variation of the plates used in the analysis as well as due to inherent modelling limitation.

- The best discretization among the assumed crack used, in this thesis, for modelling the 2x1/32" cracked plate was the beam with a 2.5 mm crack width.

- The measured and predicted peak response magnitudes at three nodal points along the middle of the plate were normalized by the highest value among them; and then the values were correlated. There was a good correlation between the measured /predicted values in modes 1, 2 and 4.

7.1 Recommendations for Future Work

Further investigation in this area of study should be in the following areas since there are many unanswered questions. Crack localization is one of them. Although methodologies have

been proposed recently, none of them can localize cracks accurately. Essentially cracks are generated in structures, around the hot spot areas, as multiple small cracks. They grow and coalesce together to form deeper and wider cracks and then towards the end of their crack propagation stage become slit (plane strain) cracks. A proper experimental and analytical study should consider this aspect. Furthermore, different crack shapes and crack widths may generate different response. Consequently, more sophisticated methodologies and experimental techniques should be used to detect/localize them.

In an experimental study, depending on structures boundary (e.g., fixed, free etc) and crack characteristics (shape, width and direction), the use of multiple exciters might become a prerequisite to detect and localize the crack on a structure.

The complexity of the problem would increase when the plate is immersed in water in which case the added mass contributions to the vibrating structure become significant. At a point of measurement where the response is very low, peak value of frequency responses will be comparable with the noise and the amplitudes of torsional mode; this creates little problem in extracting the desired modal parameters. Also modelling of a vibrating structure in water would lead to heavy coupling between water and plate; this would require better finite element formulations for coupled system vibration in water taking into account discontinuous nature of the plate - fluid interface and heavy damping in water. Till now, none of the generally available general purpose finite element program have been able to handle the problem.

References

Akita, Y. (1983). "A Challenge to Structural Failures in Ships", *Proceedings of an International Conference on Marine and Offshore Safety*, Sept. 7-9, Glasgow, Scotland, paper 2, pp. 17-32.

Allemang, R. J. (1990). *Vibrations : Experimental Modal Analysis*, UC-SDRL Publication, 161 pages.

Allemang, R.J., Rost, R.W., Severyn, T.J. and Leuridan, J. (1988). *Mechanical Vibration II*, Course notes at the University of Cincinnati, U.C publication.

Allemang, R.J., Brown, D.L. (1988). "Experimental Modal Analysis", in *Shock and Vibration Handbook*, (Third Edition), ed. Cyril M. Harris, McGraw-Hill Book Company, pp. 21-1 to 21-34.

Almar-Naess, A. (1985). "Weld Imperfection", in *Fatigue Handbook*, Tapir Publishers, Norway, pp. 237-289.

Bathe, K. J. (1982). *Finite Element Procedures in Engineering Analysis*, Prentice Hall, Inc., pp. 527-532.

Bernasconi, O., and Ewins, D.J. (1989a). "Modal Strain/Stress Fields", *The International Journal of Analytical and Experimental Modal Analysis*, Vol. 4, no. 2, pp. 68-76.

Bernasconi, O., and Ewins, D.J. (1989b). "Application of Strain Modal Testing to Real Structures", *Proceeding of the 7th International Modal Analysis Conference*, Orlando, Florida, pp. 1453-1464.

B&K 2043 Dual Channel FFT Analyzer Manual (1987), B&K publ., 138 pages.

Cawley, P., and Adams, R.D. (1979). "The Location of Defects in Structures from Measurements of Natural Frequency", *Journal of Strain Analysis*, Vol. 14, no.2, pp. 49-57.

Chowdhury, M.R. (1991). "Variation in the Modal and System Parameters of Steel Plates Due to Changes in Physical Properties", *Proceeding of the 9th International Modal Analysis Conference*, pp. 1589-1595.

Debao, L., Hongcheng, Z. and Bo, W. (1989). "The Principle and Techniques of Experimental Strain Modal Analysis", *Proceeding of the 7th International Modal Analysis Conference*, Orlando, Florida, pp. 1285-1289.

De Santo, D.F. (1981). "Added Mass and Hydrodynamic Damping of Perforated Plates Vibrating in Water", *Journal of Pressure Vessel Technology*, Vol. 103, pp. 175-182.

De Silva, C.W. (1983). *Dynamic Testing and Seismic Qualification Practise*, LexingtonBooks, pp. 147-152.

Ewins, D.J. (1984). *Modal Testing : Theory and Practice*, Research Studies Press, pp. 217 - 226.

Feng, W. Q., Zhang, K.Y. and Wu, X.Y. (1989). "Research On the Change of Modal Parameters of a Beam Resulted from a Slot", *Proceeding of the 7th International Modal Analysis Conference*, Orlando, Florida, pp. 1100-1108.

Gomes, A.J.M.A., and E Silva, J.M.M. (1990). "On The use of Modal Analysis for Crack Identification", *Proceeding of the 8th International Modal Analysis Conference*, Kissimmee, Florida, pp. 1108-1115.

Hibbitt, Karlsson & Sorensen Inc. (1989). "ABAQUS Manual", 4 vols.

Hillary, B., and Ewins, D.J. (1984). "The use of Strain Gauges in Force Determination and Frequency Response Function Measurements", *Proceedings of the 2nd International Modal Analysis Conference*, Orlando, Florida, pp. 627-634.

Jezequel, L. (1983). "Hydrodynamic Added-Mass Identification from Resonance Tests", *American Institute of Aeronautics and Astronautics Journal*, Vol. 21, no. 4, pp. 608-613.

Kenley, R. M., and Dodds, C.J. (1980). "West Sole We Platform : Detection of Damage by Structural Response Measurements", *Proceedings of the XIIth Offshore Technology Conference*, Paper No. 3866, Houston, Texas, pp. 111-117.

Leibowitz, R.C. (1975). "Vibroacoustic Response of Turbulence Excited Thin Rectangular Finite Plates in Heavy and Light Fluid Media", *Journal of Sound and Vibration*, Vol. 40, no.4, pp. 441-495.

Lieb, B.W., Jacala, A.P. and Glasser, R.P. (1989). "Added Mass for Plates Partially Submerged in Water", *Proceedings of the 7th International Modal Analysis Conference*, Orlando, Florida pp. 453-458.

Lindholm, U.S., Kana, D. D., Chu, W., and Abramson, H.N. (1965). "Elastic Vibration Characteristics of Cantilever Plates in Water", *Journal of Ship Research*, June, pp. 11-22.

Mannan, M.A, and Richardson, M.H. (1990). "Detection and Location of Structural Cracks using FRF Measurements", *Proceedings of the 8th International Modal Analysis Conference*, Orlando Florida, pp. 652-657.

Muthuveerappan, G., Ganesan, N. and Veluswami, M.A. (1979). "A Note On Vibration of A Cantilever Plate Immersed in Water", *Journal of Sound and Vibration*, Vol. 63, no. 3, pp. 385-391.

Muthuveerappan, G., Ganesan, N. and Veluswami, M.A. (1980). "Influence of Fluid Added Mass On the Vibration Characteristics of Plates Under Various Boundary Conditions", *Journal of Sound and Vibration*, Vol. 69, no. 4, pp. 612-615.

Nataraja, R. (1983). "Structural Integrity Monitoring in Real Seas", *Proceedings of the XIVth Offshore Technology Conference*, Paper No. 4538, Houston, Texas, pp. 221-229.

Parfitt, S.H.L, (1986). "Maintenance of Steel Structures", *Proceedings of the IInd International Conference on the Maintenance of Maritime and Offshore Structures*, london, Feb. 19-20, pp. 295-300.

Powell, C.D., and Goldberger, S. (1989). "Modal Analysis and Strain Gage Testing of Finned-tube Heat Exchanger", *Proceedings of the 7th International Modal Analysis Conference*, Orlando Florida, pp. 12-16.

Randal, R.B. (1988). "Vibration Measurement Equipment and Signal Analyzers", in *Shock and Vibration Handbook*, (Third Edition), ed. Cyril M. Harris, McGraw-Hill Book Company, pp. 13-14 to 21-28.

Randall, R. (1985). "Modal Analysis of A Cylinder Structure Immersed in Water", *Proceedings of the 3rd International Modal Analysis Conference*, pp. 738-744.

Richardson, M.H, and Mannan, M.A. (1991). "Determination of Modal Sensitivity Functions for Location of Structural Faults ", *Proceedings of the 9th International Modal Analysis Conference*, pp. 670-676.

Staker, C. H. (1985). "Modal Analysis Efficiency Improved via Strain Frequency Response Functions ", *Proceeding of the 3rd International Modal Analysis Conference*, Orlando Florida, pp. 2-617.

Star Reference Manual (1990). Structural Measurement Systems, January, 58 pages.

Wheeler, G.C. (1982). "An Introduction to the Capabilities of Non-destructive Testing ", Paper No. 13., Short Term Course, on *Introduction to Fracture Mechanics and its Application to Fracture Control*, Paper 13, Union College, New York, July 19-22, 13 pp.

Windows to FFT Analysis (Part I) (1987). Technical Report of Bruel & Kjaer, 58 pages.

Young, J. W., and Joanides, J. (1982). "Development of Test-Derived Strain Modal Models for Structural Fatigue Certification of The Space Shuttle Orbiter ", *Proceedings of the 1st International Modal Analysis Conference*, Orlando, Florida, pp. 479-487.

Appendix A

This appendix consists of three sections: the first section deals with the derivation of equation of motions used in the analysis of structure-acoustic medium. To solve the equation ABAQUS provides two procedures, viz., eigenvalue based solution procedure and direct integration procedure. Both of these procedure are given in the sections A.2 and A.3.

A.1 Coupled Structural Acoustic Medium Analysis

The governing equation of a compressible and inviscid fluid, undergoing small pressure variation through a solid structure motion is given by,

$$\frac{\partial p}{\partial x} + r(\dot{u} - \dot{u}^m) + \rho_f \ddot{u} = 0 \qquad (A-1)$$

where:

p   = the excess pressure in the fluid over any static pressure,

x   = the spatial position of the fluid particle,

$\dot{u}$ = the fluid particle velocity,

$\dot{u}^{\bullet}$ = the velocity of the structure through which the fluid is flowing,

$\ddot{u}$ = the fluid particle acceleration,

ρ_f = the fluid density, and

r = the volumetric drag (force per unit volume per velocity).

The excess of pressure p is defined as,

$$p = -K_f \frac{\partial}{\partial x} \cdot u \tag{A-2}$$

where K_f is the bulk modulus of the fluid.

Dividing Equation (A-1) by ρ_f and taking its gradient with respect to x gives,

$$\frac{\partial}{\partial x}\left(\frac{1}{\rho_f}\frac{\partial p}{\partial x}\right) + \frac{r}{\rho_f}\frac{\partial}{\partial x}\cdot\dot{u} - \frac{r}{\rho_f}\frac{\partial}{\partial x}\cdot\dot{u}^{\bullet} + \frac{\partial}{\partial x}\cdot\ddot{u} = 0 \tag{A-3}$$

Neglecting the third term of the Equation (A-3) and substituting the equation into Equation (A-2) yields,

$$\frac{\partial}{\partial x}\left(\frac{1}{\rho_f}\frac{\partial p}{\partial x}\right) - \frac{r}{\rho_f K_f}\dot{p} - \frac{1}{K_f}\ddot{p} = 0$$

$$\frac{1}{K_f}\ddot{p} + \frac{r}{\rho_f K_f}\dot{p} - \frac{\partial}{\partial x}\cdot\left(\frac{1}{\rho_f}\frac{\partial p}{\partial x}\right) = 0 \tag{A-4}$$

Taking the variational fields δp of Equation (A-4) and integrating over the fluid region gives,

126

$$\int_{V_f} \delta p \left[\frac{1}{K_f} \ddot{p} + \frac{r}{\rho_f K_f} \dot{p} - \frac{\partial}{\partial x} \cdot \left(\frac{1}{\rho_f} \frac{\partial p}{\partial x} \right) \right] dV = 0 \qquad \text{(A-5)}$$

Using Green's theorem, Equation (A-5) can be rewritten as,

$$\int_{V_f} \left[\delta p \left(\frac{1}{K_f} \ddot{p} + \frac{r}{\rho_f K_f} \dot{p} \right) + \frac{1}{\rho_f} \frac{\partial \delta p}{\partial x} \frac{\partial p}{\partial x} \right] dV$$

$$+ \int_S \delta p \left(\frac{1}{\rho_f} n \cdot \frac{\partial p}{\partial x} \right) dS = 0 \qquad \text{(A-6)}$$

where n is direction of outward normal to the fluid.

There are two possibilities of fluid boundary; the first one is prescribe fluid pressure (S_{f_p}) and second is part of fluid which against a solid (S_{f_s}). The solid surface, S_{f_s}, is assumed to be a thin layer which behave as a "reactive surface". With this assumption, the normal component of fluid motion and the motion of the solid surface may not the same; this results in two pressure effects in the fluid, i.e., pressure generated by the stiffness of the layer which is proportional to k_l (the proportionality factor between pressure and displacement) and pressure produced by damping of the layer which is proportional to c_l (proportionality factor between pressure and velocity of the surface).

$$p = -k_l \, n \cdot (u - u^m)$$

$$\qquad \qquad \qquad \qquad \text{(A-7)}$$

$$p = -c_l \, n \cdot (\dot{u} - \dot{u}^m)$$

127

The total acoustic pressure at the reactive surface in the fluid can be defined as,

$$n.(\dot{u} - \dot{u}^m) = -(\frac{1}{k_1}\dot{p} + \frac{1}{c_1}p) \tag{A-8}$$

The fluid-structure coupling equation can be obtained by orthonormalizing Equation (A-1) to the normal to the structure, n, and substituting Equation (A-8),

$$n.\frac{\partial p}{\partial x} + r\,n.(\dot{u} - \dot{u}^m) + \rho_f\,n.\ddot{u} = 0$$

$$\frac{1}{\rho_f}n.\frac{\partial p}{\partial x} + \frac{r}{\rho_f}n.(\dot{u} - \dot{u}^m) + n.(\ddot{u} - \ddot{u}^m) + n.(\ddot{u}^m) = 0$$

$$\frac{1}{\rho_f}n.\frac{\partial p}{\partial x} = \left(\frac{r}{\rho_f c_1}p + \left(\frac{r}{\rho_f}\frac{1}{k_1} + \frac{1}{c_1}\right)\dot{p} + \frac{1}{k_1}\ddot{p}\right) - n.\ddot{u}_m \tag{A-9}$$

By substituting Equation (A-9) into the second integration term in Equation (A-6), one can get

$$\int_{V_f}\left[\delta p\left(\frac{1}{K_f}\ddot{p} + \frac{r}{\rho_f K_f}\dot{p}\right) + \frac{1}{\rho_f}\frac{\partial \delta p}{\partial x}.\frac{\partial p}{\partial x}\right]dV$$

$$-\int_{S_p}\delta p\,\,n.\ddot{u}^m\,dS$$

$$+\int_{S_p}\delta p\left[\frac{r}{\rho_f c_1}p + \left(\frac{r}{\rho_f}\frac{1}{k_1} + \frac{1}{c_1}\right)\dot{p} + \frac{1}{k_1}\ddot{p}\right]dS = 0 \tag{A-10}$$

The behaviour of the structure can be rewritten in the virtual work as,

$$\int_V \delta\varepsilon : \sigma \ dV + \int_v \alpha_c \rho \ \delta u^m . \dot{u}^m \ dV$$

$$+ \int_V \rho \ \delta u^m . \ddot{u}^m \ dV$$

$$+ \int_{S_p} p \, \delta u^m . n \ dS - \int_{S_t} \delta u^m . t \ dS = 0 \qquad (A-11)$$

where:

σ is the stress in the structure,

p is the pressure on the fluid structure interface,

n is the outward normal to the structure,

$\dot{u}^m$ is the velocity of a point in the structure,

ρ is material density,

α_c is the mass proportional damping factor (Rayleigh damping),

$\ddot{u}^m$ is a point acceleration in the structure,

t is surface traction in the structure,

δu^m is variational displacement field,

$\delta\varepsilon$ is the strain variation which is compatible with δu^m.

For the sake of simplicity, only the fluid pressure and surface traction terms are taken into consideration and included in the analysis.

Equations (A-10) and (A-11), the coupled equation for structure and acoustic media, are solved approximately by Galerkin method. Introducing the shape/interpolation functions, in the fluid:

$$p = H^P p^P , \qquad P = 1,2....$$

in the structure :

$$u^m = N^N u^N , \qquad N = 1,2 \ldots$$

where H^P, N^N are the interpolation/shape functions,

In the remainder of this section, superscripts P and Q refer to pressure degrees of freedom in the fluid, superscripts N and M refer to displacement degrees of freedom in the structure.

Taking the variation of the above equations, $\delta p = H^P \, \delta p^P$ and $\delta u^m = N^N . \delta v^N$, Equations (A-10) and (A-11) can be discretized as,

$$-\delta p^P \left\{ -(M_f^{PQ} + M_{f^r}^{PQ}) \ddot{p}^Q - (C_f^{PQ} + C_{f^r}^{PQ}) \dot{p}^Q - (K_f^{PQ} + K_{f^r}^{PQ}) p^Q + S_{f^r}^{PM} \ddot{u}^m \right\}$$

$$+ \delta v^N \left\{ I^N + M^{iNM} \, \ddot{u}^M + C_{(m)}^{NM} \, \dot{u}^M + \left[S_{f^r}^{QN} \right]^T p^Q - P^N \right\} = 0 \qquad (A-12)$$

where:

$$M_f^{PQ} = \int_{V_f} \frac{1}{K_f} H^P H^Q \, dV$$

$$C_f^{PQ} = \int_{V_f} \frac{r}{\rho_f} \frac{1}{K_f} H^P H^Q \, dV$$

$$K_f^{PQ} = \int_{V_f} \frac{1}{\rho_f} \frac{\partial H^P}{\partial x} \frac{\partial H^Q}{\partial x} \, dV$$

$$M_{f^r}^{PQ} = \int_{S_f} \frac{1}{k_1} H^P H^Q \, dS$$

$$C_{f^r}^{PQ} = \int_{S_f} \left(\frac{r}{\rho_f k_1} + \frac{1}{c_1} \right) H^P H^Q \, dS$$

130

$$K_p^{PQ} = \int_{s_p} \frac{r}{\rho_f} \frac{1}{c_1} H^P H^Q \, dS$$

$$S_{f_s}^{PM} = \int_{s_p} H^P n . N^M \, dS$$

$$M^{NM} = \int_V \rho \, N^N . N^M \, dV$$

$$C_{(m)}^{NM} = \int_V \alpha_c \rho \, N^N N^M \, dV$$

$$I^N = \int_V \beta^N : \sigma \, dV$$

$$P^N = \int_{s_t} N^N . t \, dS$$

In direct integration analysis of Equation (A-12) is integrated using an implicit integration method. The Newton equation of the equation is,

$$\delta \dot{p}^{\,P} \left\{ -(M_f^{PQ}) + M_p^{PQ} - \frac{D_v}{D_a}(C_f^{PQ} + C_p^{PQ}) - \frac{1}{D_a}(K_f^{PQ} + K_p^{PQ}) \right\} \partial p^{\,Q}$$

$$+ \delta \dot{p}^{\,P} S_{f_s}^{PM} \partial u^{\,M} + \delta u^{\,N} \left[S_{f_s}^{QN} \right] \partial p^{\,Q} + \delta u^{\,N} \left\{ K^{NM} + D_a M^{NM} + D_v C_{(m)}^{NM} \right\} \partial u^{\,M}$$

$$= \delta \dot{p}^{\,P} \frac{1}{D_a} \left\{ (M_f^{PQ} + M_p^{PQ}) \ddot{p}^{\,Q} + (C_f^{PQ} + C_p^{PQ}) \dot{p}^{\,Q} + (K_f^{PQ} + K_p^{PQ}) p^{\,Q} - S_{f_s}^{PM} \ddot{u}^{\,M} \right\}$$

$$+ \delta u^{\,N} \left\{ -I^N - M^{NM} \ddot{u}^{\,M} - C_{(m)}^{NM} \ddot{u}^{\,M} - \left[S_{f_s}^{QN} \right]^T p^{\,Q} + P^{\,N} \right\} \tag{A-13}$$

where:

$$D_a = \frac{\partial \dot{f}}{\partial f} \; ; \; D_v = \frac{\partial \ddot{f}}{\partial f} \; ; \; \delta \dot{\beta}^P = -D_a \, \delta p^P$$

$f = f(t)$ is one of the solution variables, i.e, pressure, displacement or rotation,

D_a and D_v are determined by the integration method,

∂f is the correction to the solution obtained from the Newton iteration solution,

In steady state harmonic response, the structure is assumed to experience small visco-elastic vibration about a deformed, stressed state σ_0,

$$\sigma = \sigma_0 + D^{el} : (\Delta \varepsilon + \beta_c \dot{\varepsilon}) \tag{A-14}$$

in which D^{el} is the material elasticity matrix and β_c is the stiffness proportional damping factor of the structure (Rayleigh damping).

From discretization assumption,

$$\Delta \varepsilon = \beta^M \Delta v^M \tag{A-15}$$

$$v^N = v_0^N + \Delta v^N \tag{A-16}$$

Defining,

$$K^{NM} = \int_V \left[\frac{\partial \beta^N}{\partial u^M} : \sigma + \beta^N : D^{el} : \beta^M \right] dV \tag{A-17}$$

$$C_{(k)}^{NM} = \int_V \left[\beta_c \, \beta^N : D^{el} : \beta^M \right] dV \tag{A-18}$$

132

$$I^N = I_0^N + K^{NM} \Delta v^M + C_{(k)}^{NM} \dot{v}^M \tag{A-19}$$

$$I_0^N = \int_V \beta^N : \sigma_0 \ dV \tag{A-20}$$

And Equation (A-12) can be rewritten as,

$$-\delta p^P \left\{ -(M_f^{PQ} + M_{FR}^{PQ}) \ddot{p}^Q - (C_f^{PQ} + C_p^{PQ}) \dot{p}^Q - (K_f^{PQ} + K_p^{PQ} p^Q) + S_{fk}^{PM} \dot{v}^M \right\}$$

$$+ \delta v^N \left\{ I_0^N + K^{NM} \Delta v^M + M^{NM} \ddot{v}^M + (C_{(m)}^{NM} + C_{(k)}^{NM}) \dot{v}^M + \left[S_{fk}^{QN} \right]^T p^Q - P^N \right\} = 0 \tag{A-21}$$

If the response is harmonic, one can write,

$$p^Q = p_0^Q + \left(\Re(p^Q) + i \Im(p^Q) \right) e^{i\omega t} \tag{A-22}$$

$$v^M = v_0^M + \left(\Re(v^M) + i \Im(v^M) \right) e^{i\omega t} \tag{A-23}$$

$$P^N = \left(\Re(P^N) + i \Im(P^N) \right) e^{i\omega t} \tag{A-24}$$

where:

p_0^Q and v_0^M are the constant values of p^Q and v^M,

$\Re(p^Q)$, $\Im(p^Q)$ and $\Re(v^M)$, $\Im(v^M)$ are the real and imaginary parts of the amplitude of the response,

$\Re(p^N)$ and $\Im(p^N)$ are the real and imaginary parts of the forcing function applied to the structure,

133

ω is complex circular frequency.

Assuming p_s^Q and v_e^M are in equilibrium with the steady boundary conditions,

$$\begin{bmatrix} \Re[A_f^{PQ}] & \Im[A_f^{PQ}] & S_s^{PM} & 0 \\ \Im[A_f^{PQ}] & -\Re[A_f^{PQ}] & 0 & -S_s^{PQ} \\ [S_s^{QN}]^T & 0 & \Re[A_s^{NM}] & \Im[A_s^{NM}] \\ 0 & -[S_s^{QN}]^T & \Im[A_s^{NM}] & -\Re[A_s^{NM}] \end{bmatrix} \begin{Bmatrix} \Re(p^Q) \\ \Im(p^Q) \\ \Re(v^M) \\ \Im(v^M) \end{Bmatrix} = \begin{Bmatrix} 0 \\ 0 \\ \Re(P^N) \\ -\Im(P^N) \end{Bmatrix} \quad \text{(A-25)}$$

where:

$$\Re[A_f^{PQ}] = \frac{1}{\omega^2}(K_f^{PQ} + K_p^{PQ}) - (M_f^{PQ} + M_{p}^{PQ})$$

$$\Im[A_f^{PQ}] = -\frac{1}{\omega}(C_f^{PQ} + C_p^{PQ})$$

$$\Re[A_s^{NM}] = K^{NM} - \omega^2 M^{NM}$$

$$\Im[A_s^{NM}] = -\omega(C_{(m)}^{NM} + C_{(k)}^{NM})$$

For a one degree of freedom system with excitation $P = \bar{P}\exp{(i\Omega^*t)}$. The response will be,

$$\begin{bmatrix} -m_f + \frac{1}{\Omega^{*2}}k_f & -\frac{1}{\Omega^*}c_f & 1 & \frac{1}{\Omega^*}S_c \\ -\frac{1}{\Omega^*}c_f & m_f - \frac{1}{\Omega^{*2}}k_f & \frac{1}{\Omega^*}S_c & -1 \\ 1 & 0 & k - \Omega^{*2}m & -\Omega_c^* \\ 0 & -1 & -\Omega_c^* & -(k-\Omega^{*2}m) \end{bmatrix} \begin{Bmatrix} \Re(p) \\ \Im(p) \\ \Re(v) \\ \Im(v) \end{Bmatrix} = \begin{Bmatrix} 0 \\ 0 \\ \bar{P} \\ 0 \end{Bmatrix} \quad \text{(A-26)}$$

134

Symmetric approximation term $\dfrac{1}{\Omega^*}\,S_c = 0$,

$$
\begin{bmatrix}
-m_f + \dfrac{1}{\Omega^{*2}}k_f & -\dfrac{1}{\Omega^*}c_f & 1 & 0 \\[2mm]
-\dfrac{1}{\Omega^*}c_f & m_f - \dfrac{1}{\Omega^{*2}}k_f & 0 & -1 \\[2mm]
1 & 0 & k - \Omega^{*2}m & -\Omega_c^* \\[2mm]
0 & -1 & -\Omega_c^* & -(k - \Omega^{*2}m)
\end{bmatrix}
\begin{Bmatrix}
\Re(p) \\[2mm]
\Im(p) \\[2mm]
\Re(v) \\[2mm]
\Im(v)
\end{Bmatrix}
=
\begin{Bmatrix}
0 \\[2mm]
0 \\[2mm]
\tilde{P} \\[2mm]
0
\end{Bmatrix}
\quad \text{(A-27)}
$$

where:

$$
m_f = \frac{1}{K_f}\frac{l}{2} + \frac{1}{k_1}
$$

$$
c_f = \frac{r}{\rho_f}\left(\frac{l}{2}\frac{1}{K_f} + \frac{1}{k_1}\right)
$$

$$
k_f = \frac{1}{\rho_f}\left(\frac{1}{l} + \frac{r}{c_1}\right)
$$

$$
s_c = \frac{r}{\rho_f}
$$

ρ_f is fluid density,

K_f is bulk modulus of fluid,

l is structural length,

r is volumetric drag coefficient,

c_1 is the proportionality factor between pressure and velocity of the surface in the normal

135

direction,

k_i is proportionality factor between pressure and displacement of the surface in the normal direction.

A.2   Steady State Dynamic

The equation of motions of a vibrating structure can be written as,

$$\ddot{q}_i + c_i \dot{q}_i + \Omega_i^2 q_i = \frac{1}{m_i} \{\phi\}_i^T \{F_o\} e^{(i\Omega^* t)} \qquad (A-28)$$

where:

q_i = the amplitude of mode i,

c_i = the damping of mode i,

Ω_i = the undamped frequency of mode i,

m_i = the generalized mass of mode i,

$\{\phi\}_i$ = the eigenvector for mode i,

$\{F_o\} \exp (i\Omega t)$ = the harmonic forcing function,

Ω^* = the forcing frequency.

Damping in a structure may be made up of structural damping $c_i \dot{q}_i$ and modal damping c_i,

$$c_i \dot{q}_i = i s_i \Omega_i^2 m_i q_i$$
$$c_i = 2 \xi_i \Omega_i m_i$$

where:

s = structural damping coefficient,

i = $\sqrt{(-1)}$,

ξ_i = the damping ratio.

By substituting the damping defined above, Equation (A-28) can be expressed as,

$$\ddot{q}_i + 2\xi_i \Omega_i \dot{q}_i + i s_i \Omega_i^2 q_i + \Omega_i^2 q_i = f_o\, e^{(i\Omega^* t)}$$
$$f_o = \frac{1}{m_i} \{\phi\}_i^T \{F_o\}$$

(A-29)

The solution of Equation (A-29) is

$$q_i = \left\{ \Re(Q_i) + i\, \Im(Q_i) \right\} e^{(i\Omega^* t)}$$

(A-30)

where:

$\Re(Q_i)$ and $\Im(Q_i)$ are the real and imaginary part of the response amplitude in mode i which can be written as,

$$\Re(Q_i) = + \frac{(\Omega_i^2 - \Omega_i^{*2})}{m_i \left\{ (\Omega_i^2 - \Omega_i^{*2})^2 + \Omega_i^2 (s_i \Omega_i + 2\xi_i \Omega_i^*)^2 \right\}}\, f_o$$

$$\Im(Q_i) = - \frac{\Omega_i (s_i \Omega_i + 2\xi_i \Omega_i^*)}{m_i \left\{ (\Omega_i^2 - \Omega_i^{*2})^2 + \Omega_i^2 (s_i \Omega_i + 2\xi_i \Omega_i^*)^2 \right\}}\, f_o$$

The amplitude of the response can be written as,

$$\sqrt{\Re(Q_i)^2 + \Im(Q_i)^2} = \frac{1}{m_i} \sqrt{\frac{1}{\left\{ (\Omega_i^2 - \Omega_i^{*2})^2 + \Omega_i^2 (s_i \Omega_i + 2\xi_i \Omega^*)^2 \right\}}}\, f_o$$

$$\psi_i = \arctan\left(\frac{\Im(Q_i)}{\Re(Q_i)} \right)$$

137

A.3 Direct Integration Method

The body force f at a point, can be expressed in terms of an external body force F and a d'Alembert force as,

$$f = F - \rho \ddot{u} \qquad (A-31)$$

where ρ and u are the material density and the displacement at a point.

Using the virtual work term principle, the virtual work done by the body force can be rewritten,

$$\int_V f.\delta v \ dV = \int_V F.\delta v \ dV - \int_V \rho \ \ddot{u}.\delta v \ dV \qquad (A-32)$$

The d'Alembert term in the above equation can be written in term of reference volume V_0 and reference density ρ_0,

$$\int_{V_0} \rho_0 \ddot{u}.\delta v \ dV_0 \qquad (A-33)$$

where $\ddot{u}$ is the acceleration field. In the implicit integration procedure, the equation of motions are solved at the end of each time step viz., $t + \Delta t$; $\ddot{u}$ is computed by the time integration techniques. Further, the displacement at a point is approximated as,

$$u = N^N v^N$$
$$\ddot{u} = N^N \ddot{v}^N$$

where v^N are nodal variables and N^N is the shape/interpolation functions which are assumed to be independent to displacement; with this assumption, the d'Alembert term can be written as,

138

the method proposed by Hilber *et al.* the equation of motion is described as,

$$M^{NM} \ddot{v}^M|_{t+\Delta t} + (1+\alpha)(I^N|_{t+\Delta t} - P^N|_{t+\Delta t}) - \alpha(I^N|_t - P^H|_t) + L^N|_{t+\Delta t} = 0 \qquad \text{(A-35)}$$

where $L^N|_{t+\Delta t}$ is the sum of all Langrange multiplier forces in corresponding degrees of freedom N. Then using the Newmark formulae, the displacement and velocity integration can be expressed as,

$$v|_{t+\Delta t} = v|_t + \Delta t \; \dot{v}|_t + \Delta t^2 \left((0.5 - \beta)\ddot{v}|_t + \beta \ddot{v}|_{t+\Delta t}\right) \qquad \text{(A-36)}$$

$$\dot{v}|_{t+\Delta t} = \dot{v}|_t + \Delta t \left((1-\gamma)\ddot{v}|_t + \gamma \ddot{v}|_{t+\Delta T}\right) \qquad \text{(A-37)}$$

where:

$$\beta = 0.25(1-\alpha)^2 \; ; \quad \gamma = 0.50 - \alpha \quad ; \quad -\frac{1}{3} \le \alpha \le 0$$

And the rotation is also integrated using the Newmark's formula which gives velocity at a time $t + \Delta t$ as,

$$\dot{\phi}^n|_{t+\Delta t} = \dot{\phi}^n|_t + \Delta t \left[\gamma \ddot{\phi}|_{t+\Delta t} + (1-\gamma)\ddot{\phi}^n|_t\right] \qquad \text{(A-38)}$$

where:

$\dot{\phi}^n$ and $\ddot{\phi}^n$ are angular velocity and acceleration of the node,

Δt is time increment.

In a global system, the velocity is written as,

$$\dot{\phi}|_{t+\Delta t} = \Delta t \; \gamma \; \ddot{\phi}|_{t+\Delta t} + \left[e^n|_{t+\Delta t} \; e^n|_t\right] \cdot \left\{\dot{\phi}|_t + \Delta t(1-\gamma)\ddot{\phi}|_t\right\} \qquad \text{(A-39)}$$

where $e^n = e^n(\phi)$ are orthonormal base vectors where variations can be written as,

140

$$-\left(\int_{V_0} \rho_0 N^N . N^M \, dV_0 \right) \ddot{u}^M$$

The equation of motion is then can be written as,

$$M^{NM} \ddot{u}^M + I^N - P^N = 0 \qquad \qquad (A-34)$$

where:

$$M^{NM} = \int_{V_0} \rho_0 N^N . N^M \, dV_0$$

$$I^N = \int_{V_0} \beta^N : \sigma \, dV_0$$

$$P^N = \int_S N^N . t \, dS + N^N . F \, dV$$

M^{NM} is the consistent mass matrix,

I^N is the internal force vector,

P^N is the external force vector,

t is the load vector.

It was noted that in the case of first order element, the mass matrix, M^{NM} is lumped so that the matrix is diagonal.

In ABAQUS the time integration scheme proposed by Hilber, Hughes and Taylor (1978)[1] is used with the automatic time stepping method developed by Hibbitt and Karlsson (1979)[2]. In

[1] Hilber, H.M., Hughes, T.J.R., Taylor, R.L. (1978). "Collocation, Dissipation and 'Overshoot' for Time Integration Schemes in Structural Dynamics," Earthquake Engineering and Structural Dynamics, Vol. 6, pp. 99-117.

[2] Hibbitt, H.D. and Karlsson, B.I. (1979). "Analysis of Pipe Whip", EPRI, Report NP-1208.

$$\partial e^{*}(\phi) = \partial \phi \times e^{*}(\phi) \tag{A-40}$$

By eliminating $\tilde{v}|_{t+\Delta t}$ from Equation (A-36) and Equation (A-37), $\Delta\phi$, the change of ϕ, can be defined as,

$$\Delta\phi = \Delta t \left(1 - \frac{\beta}{\gamma}\right) \dot{\phi}|_{t} + \Delta t \frac{\beta}{\gamma} \dot{\phi}|_{t+\Delta t} + \Delta t^{2} \left(\frac{1}{2} - \frac{\gamma}{\gamma}\right) \ddot{\phi}|_{t} \tag{A-41}$$

Equation (A-39) and (A-41) can be used to obtain $\dot{\phi}|_{t+\Delta t}$ and $\ddot{\phi}|_{t+\Delta t}$,

$$\dot{\phi}|_{t+\Delta t} = \frac{\gamma}{\beta \Delta t} \Delta\phi + \left(1 - \frac{\gamma}{\beta}\right) \dot{\phi}|_{t} + \Delta t \left(1 - \frac{\gamma}{2\beta}\right) \ddot{\phi}|_{t} \tag{A-42}$$

$$\ddot{\phi}|_{t+\Delta t} = \frac{1}{\gamma \Delta t} \dot{\phi}|_{t+\Delta t} + \left[e^{*}|_{t+\Delta t} e^{*}|_{t}\right] \cdot \left\{-\frac{1}{\gamma \Delta t} \dot{\phi}|_{t} + \left(1 - \frac{1}{\gamma}\right) \ddot{\phi}|_{t}\right\} \tag{A-43}$$

The variation of Equation (A-42) is,

$$\partial\dot{\phi}|_{t+\Delta t} = \frac{\gamma}{\beta \Delta t} \partial\phi|_{t+\Delta t} \tag{A-44}$$

And using Equation (A-40), the variation of Equation (A-43) is,

$$\partial\ddot{\phi}|_{t+\Delta t} = \frac{1}{\gamma \Delta t} \partial\dot{\phi}|_{t+\Delta t} + \partial\phi|_{t+\Delta t} \times \left[e^{*}|_{t+\Delta t} e^{*}|_{t}\right] \cdot \left\{-\frac{1}{\gamma \Delta t} \dot{\phi}|_{t} + \left(1 - \frac{1}{\gamma}\right) \ddot{\phi}|_{t}\right\} \tag{A-45}$$

Using Equation (A-39) and Equation (A-44), and Equation (A-45) can be rewritten as,

141

$$\partial \bar{\phi}\,|_{t+\Delta t} = \frac{1}{\beta \Delta t}\, \partial \phi\,|_{t+\Delta t} + \partial \phi\,|_{t+\Delta t} \times \left\{ \dot{\phi}\,|_{t+\Delta t} - \frac{1}{\gamma \Delta t}\, \phi\,|_{t+\Delta t} \right\} \qquad \text{(A-46)}$$

The automatic time stepping based on the half step residual (Hibbitt & Karlsson, 1979)[2] is used in the ABAQUS for solving the dynamic problem. The half step residual method ensures the equilibrium of Equation (A-34) at a intermediate time point $(t + \Delta t)$ by computing and assessing the equilibrium residual error, i.e, the left hand side of Equation (A-34) at the time step.

On the basis of Newmark formulae, the half step residual technique assumes the linear variation of accelerations over the time of interval; for any nodal variable v, viz., displacement or rotation,

$$\ddot{v}\,|_{\tau} = (1-\tau)\,\ddot{v}\,|_{t} + \tau\,\ddot{v}\,|_{t+\Delta t} \qquad 0 \le \tau \le 1 \qquad \text{(A-47)}$$

For solving at time $t + \Delta t$, the Newmark formulae require displacement, velocity and acceleration written as,

$$v\,|_{\tau} = v\,|_{t} + \tau^{3}\Delta v\,|_{t+\Delta t} + (1-\tau^{2})\,\Delta t\,\dot{v}\,|_{t} + \tau^{2}(1-\tau)\frac{\Delta t^{2}}{2}\,\ddot{v}\,|_{t}$$

$$\dot{v}\,|_{\tau} = \frac{\tau^{2}\gamma}{\beta \Delta t}\Delta v\,|_{t+\Delta t} + \left(1 - \frac{\tau^{2}\gamma}{\beta}\right)\dot{v}\,|_{t} + \Delta t\left(1 - \frac{\gamma \tau}{2\beta}\right)\ddot{v}\,|_{t}$$

$$\ddot{v}\,|_{\tau} = \frac{\tau}{\beta \Delta t}\Delta v\,|_{t+\Delta t} - \frac{\tau}{\beta \Delta t}\dot{v}\,|_{t} + \left(1 - \frac{\tau}{2\beta}\right)\ddot{v}\,|_{t} \qquad \text{(A-48)}$$

[2] Hibbitt, H.D. and Karlsson, B.I. (1979). "Analysis of Pipe Whip", EPRI, Report NP-1208.

where:

$$\Delta \upsilon \,|_{t+\Delta t} = \upsilon \,|_{t+\Delta t} - \upsilon \,|_t$$

is the displacement increment for the step Δt at the end.

If the residual is relatively small, Equation (A-47) and Equation (A-48) are employed to evaluate Equation (A-34),

The residual at the end of the time step is written as,

$$R^N |_{t+\Delta t} = M^{NM} \ddot{u}^M |_{t+\Delta t} + (1-\alpha)(I^N |_{t+\Delta t} - P^N |_{t+\Delta t}) - \alpha (I^N |_t - P^N |_t) + L^N |_{t+\Delta t} \quad (A\text{-}49)$$

The residual at the start of the time is,

$$R^N |_t = M^{NM} \ddot{u}^M |_t + (1-\alpha)(I^N |_t - P^N |_t) - \alpha (I^N |_{t^-} - P^N |_{t^-}) + L^N |_t \quad (A\text{-}50)$$

where:

$t^{\cdot}$ is t for the first increment after an initial acceleration or t for the time at the start of the previous time in the regular stepping.

Further, the residual at $t + \Delta t/2$ is,

$$R^N |_{t+\Delta t/2} = M^{NM} \ddot{u}^M |_{t+\Delta t/2} + (1+\alpha)\left(I^N |_{t+\Delta t/2} - P^N |_{t+\Delta t/2}\right)$$
$$- \frac{1}{2}\alpha\left(I^N |_t - P^N |_t + I^N |_{t^-} - P^N |_{t^-}\right) + L^N |_{t+\Delta t/2} \quad (A\text{-}51)$$

where:

$$L^N |_{t+\Delta t/2} = \frac{1}{2}\left(L^N |_{t+\Delta t} + L^N |_t\right)$$

143

In each time step the residual is assessed, so that the value is smaller than the tolerance set by users. The algorithm of the technique is,

1. Setting the maximum half step residual, by giving a tolerance (HAFTOL) value which could be 0.1 to 10 times the excitation force **P**.

2. In some time step, find out a convergence solution at $t + \Delta t$.

3. Calculating $|\mathbf{R}^N|_{t+\Delta t/2}|$.

4. If $\mathbf{HAFTOL} < |\mathbf{R}^N|_{t+\Delta t/2}|$, changing Δt to $\Delta t/2$ and start again from t.

5. $\mathbf{HAFTOL} \geq |\mathbf{R}^N|_{t+\Delta t/2}| > \mathbf{HAFTOL}/2$, updating the state to $t + \Delta t$; the time step is used in the next to analysis.

6. If $\mathbf{HAFTOL}/2 > |\mathbf{R}^N|_{t+\Delta t/2}|$, the time increment, Δt, is increased to 1.25 Δt for the next analysis.

7. In the two consecutive increment the time set must not be increased.

Appendix B

Analytical Results

Using the finite element discretization given in Chapter 4, the analyses based on zero damping assumption are carried out over the frequency bands of interest. In this Appendix, the natural frequencies and peak response magnitudes, of the beams for five nodes corresponding to the points of measurement and excitation in the experimental study (see Figures 4.6 and 4.7), are tabulated; the analytical frequency response function plots, viz., the response magnitude versus frequency, are also presented. The appendix is broken into five sections. In the first section, the natural frequencies, peak response magnitudes and frequency response function plots obtained by using uncracked beam in vacuum discretization are given. The analytical results and the plots for uncracked beam in air are presented in the second section. The results of 2x1/32" cracked beam in air for three crack widths, i.e., 1.5 mm, 2 mm and 2.5 mm, are tabulated in the third section; the response for 1.5 mm crack width are displayed. Section B.4 gives the 2x3/32" cracked beam in air with the same crack width as section B.3. Section B.5 gives the displaced shape of the uncracked plate when the plate is analyzed using 4x13 shell elements.

B.1   Uncracked Plate in Vacuum

The uncracked plate "in vacuum" model was analyzed in small frequency bands of 1.0 Hz around the resonant frequencies, to shorten the computer time and to examine the influence of fluid (air) on the peak response magnitudes and natural frequencies of the plates. The responses of the five nodes shown in Figure 4.6 are given in Tables B.1.1 and B.1.2.

Table B.1.1   Beam in vacuum : acceleration response

No.	Natural Frequency (Hz)	Peak magnitudes at nodes (ms^{-2}/N)				
		2143	2145	2151	2155	2167
1	18.68	5.76	24.66	109.8	214.40	533.70
2	117.0	3113	1.1643.10^4	3.3177.10^4	3.3834.10^4	5.0593.10^4
3	327.1	2307	7334	9057	3838	1.4715.10^4
4	640.1	1.4535.10^4	3.6928.10^4	7291	3.1450.10^4	5.2650.10^4
5	1057	1.8816.10^5	3.5106.10^5	3.2293.10^5	2.2240.10^5	4.6441.10^5

Table B.1.2   Beam in vacuum : strain response

No.	Natural Frequency (Hz)	Peak magnitudes at nodes (m/m/N) x 10^{-6}				
		2143	2145	2151	2155	2167
1	18.68	1.3543.10^3	1.1685.10^3	7.4789.10^3	4.2557.10^3	2.3393
2	117	1.4251.10^4	4.7167.10^3	1.2472.10^4	1.6726.10^4	1.9219.10^2
3	327.10	9.0287.10^2	5.8267.10^2	1.3698.10^3	7.2956.10^2	4.8182.10^1
4	640.10	9.3020.10^2	2.5533.10^3	6.4367.10^2	2.8231.10^3	1.4429.10^2
5	1057	2.1812.10^3	1.7426.10^4	1.7315.10^4	1.1346.10^4	1.0289.10^3

B.2   Uncracked Plate in Air

It is known that air introduces damping in the vibrating structures. In this thesis, the effect of air on the response peak magnitudes and the natural frequencies are examined. For this purpose, the uncracked plate in air discretization is used in two frequency bands, i.e in small frequency bands which resolution is the same as the beam in vacuum one (with a maximum frequency resolution of 0.025 Hz) and in broad frequency bands for examining the influence of frequency resolution on the peak magnitudes. The results of the analyses are given in Tables B.2.1 and B.2.2 for small frequency bands and Tables B.2.3 to B.2.5 for the wider frequency bands. It could be observed that the introduction of air into the analysis shifts the natural frequencies to lower values and reduces the magnitudes of the response. Also it could be seen from Tables B.2.1 to B.2.5 that the higher frequency resolution gives larger responses and slightly different natural frequencies. The frequency response function plots for the phase, strain, acceleration and displacement response at the above nodes are shown in Figures B.2.1 to B.2.15.

Table B.2.1   Beam in air : acceleration response (higher frequency resolution)

No.	Natural Frequency (Hz)	Peak magnitudes at nodes (ms⁻²/N)				
		2143	2145	2151	2155	2167
1	18.48	5.186	22.20	98.76	192.90	479.8
2	115.4	181.80	678.30	1921	1939	3032
3	321.4	1212	3821	4611	2042	8240
4	637.8	1104	2807	534.9	2377	3980
5	1052	$1.0822.10^4$	$2.0211.10^4$	$1.8704.10^4$	$1.2774.10^4$	$2.6792.10^4$

Table B.2.2 Beam in air : strain response (higher frequency resolution)

No.	Natural Frequency (Hz)	Peak magnitudes at nodes (m/m/N) x 10^{-6}				
		2143	2145	2151	2155	2167
1	18.48	$1.2458.10^4$	$1.0742.10^3$	$6.8658.10^2$	$3.8999.10^2$	2.1346
2	115.4	$8.5125.10^2$	$2.7496.10^2$	$7.5416.10^2$	$1.0031.10^3$	$1.1449.10^1$
3	321.3	$4.7692.10^2$	$3.3058.10^2$	$7.2251.10^2$	$4.1207.10^2$	$2.5810.10^1$
4	637.3	$4.5518.10^1$	$1.9490.10^2$	$4.8707.10^1$	$2.1506.10^2$	$1.0964.10^1$
5	1052	$1.2473.10^2$	$1.0142.10^3$	$1.0098.10^3$	$6.6098.10^2$	$5.9961.10^1$

Table B.2.3 Beam in air : acceleration response

No.	Natural Frequency (Hz)	Peak magnitudes at nodes (ms²/N)				
		2143	2145	2151	2155	2167
1	18.45	0.3314	1.418	6.307	12.31	30.61
2	115.4	278.6	1040	2945	2972	4648
3	321.3	244.7	771.6	931	412.1	1664
4	637.8	5073	$1.2898.10^4$	2459	$1.0923.10^4$	$1.8293.10^4$
5	1052.0	5785	$1.0804.10^4$	9999	6828	$1.4322.10^4$

Table B.2.4 Beam in air: strain response

No	Natural Frequency (Hz)	Peak magnitudes at nodes (m/m/N) x 10^{-6}				
		2143	2145	2151	2155	2167
1	18.45	$7.9821.10^1$	$6.8771.10^2$	$4.3809.10^1$	$2.4884.10^1$	$1.3619.10^{-1}$
2	115.4	$1.3048.10^3$	$4.2145.10^2$	$1.1558.10^3$	$1.5376.10^3$	$1.7550.10^1$
3	321.3	$9.6293.10^1$	$6.6773.10^1$	$1.4583.10^2$	$8.3190.10^1$	5.2108
4	637.8	$2.0916.10^2$	$8.9565.10^1$	$2.2375.10^2$	$9.8840.10^2$	$5.0392.10^1$
5	1052	$6.6679.10^1$	$5.4216.10^2$	$5.3977.10^2$	$3.5332.10^2$	$3.2053.10^1$

Table B.2.5 Beam in air : displacement response

No.	Natural Frequency (Hz)	Peak magnitudes at nodes (m x 10^{-6})				
		2143	2145	2151	2155	2167
1	18.45	$2.4654.10^1$	$1.0551.10^2$	$4.6915.10^3$	$9.1581.10^2$	$2.2770.10^3$
2	115.4	$5.3031.10^2$	$1.9792.10^3$	$5.6049.10^3$	$5.6568.10^3$	$8.8471.10^3$
3	321.3	$1.7564.10^1$	$6.6867.10^2$	$6.6867.10^1$	$2.9702.10^1$	$1.1946.10^2$
4	637.8	$3.1589.10^2$	$1.5312.10^2$	$1.5312.10^3$	$6.8014.10^2$	$1.1390.10^2$
5	1052.0	$1.3251.10^3$	$2.2903.10^2$	$2.2903.10^2$	$1.5640.10^3$	$3.2806.10^2$
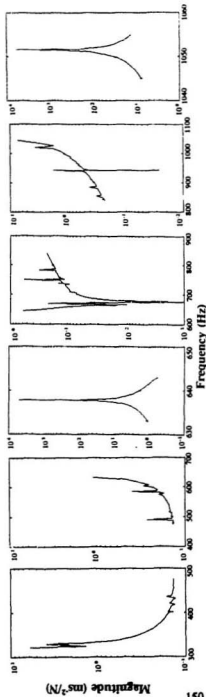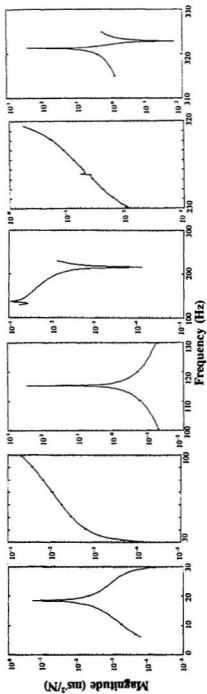
Figure B.2.1 Acceleration response of the uncracked plate in air at node 2143
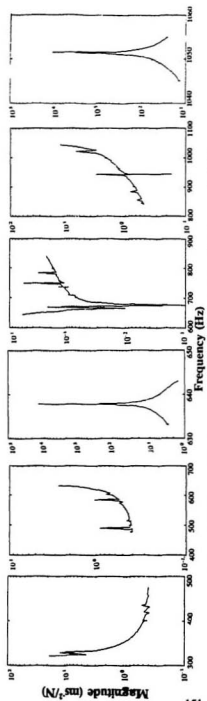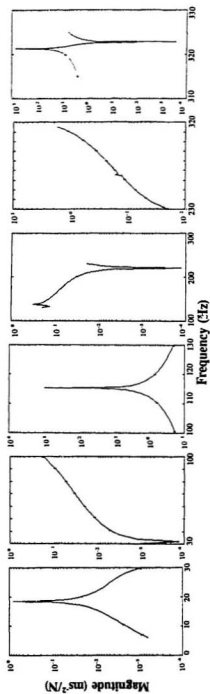
Figure B.2.2 Acceleration response of the uncracked plate in air at node 2145

151
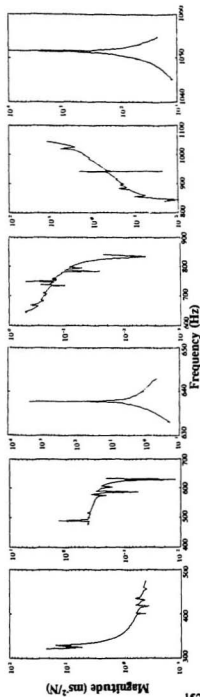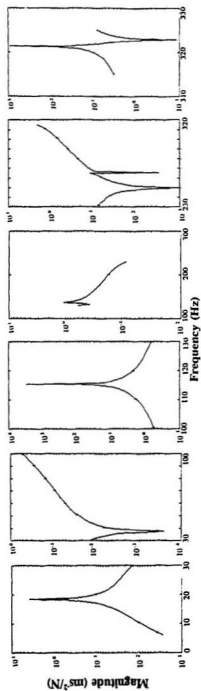
Figure B.2.3 Acceleration response of the uncracked plate in air at node 2151

152
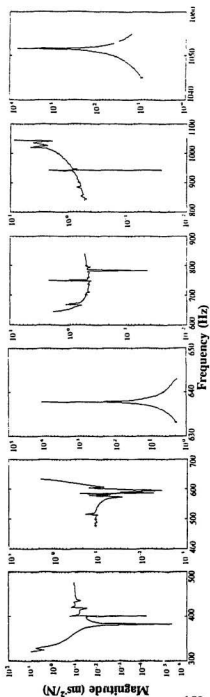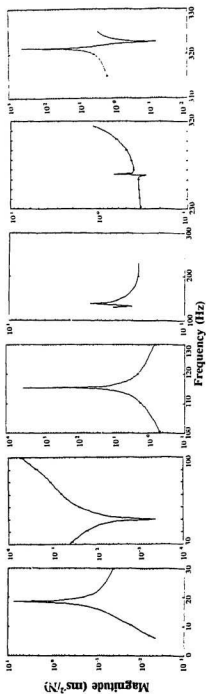
Figure B.2.4 Acceleration response of the uncracked plate in air at node 2155

153
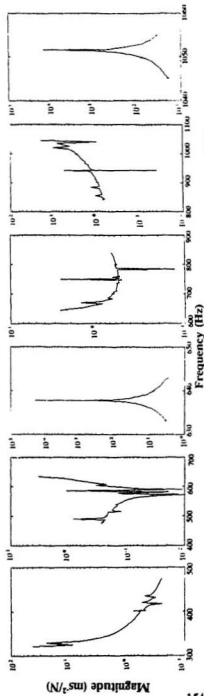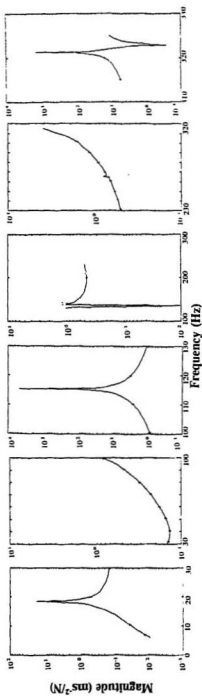
Figure B.2.5 Acceleration response of the uncracked plate in air at node 2167

154
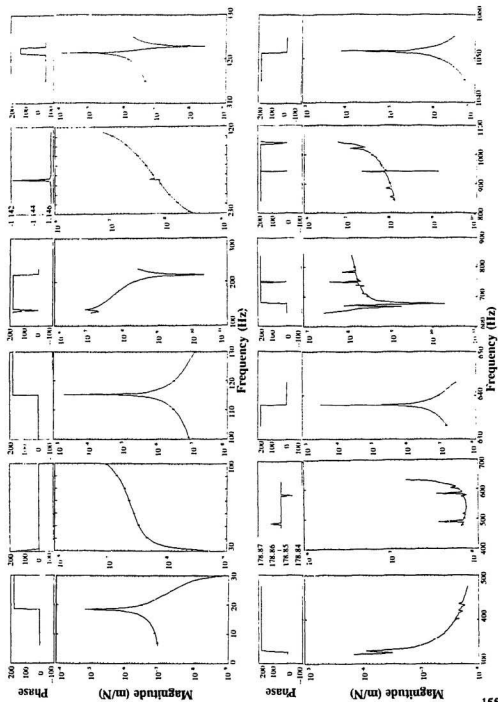
Figure B.2.6 Displacement response of the uncracked plate in air at node 2143

155
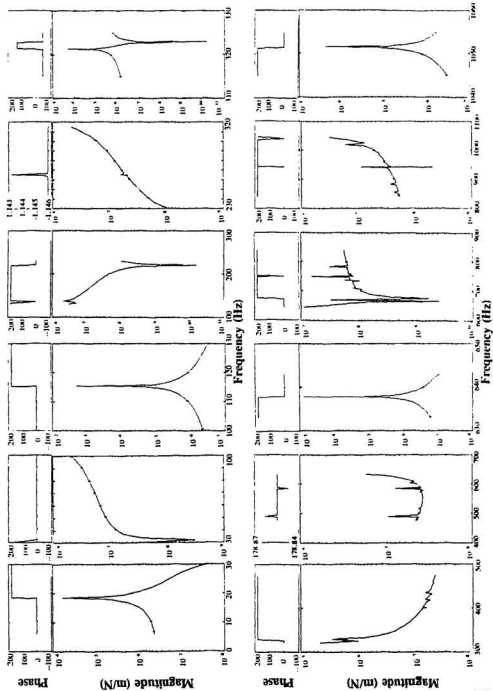
Figure B.2.7 Displacement response of the uncracked plate in air at node 2145

156
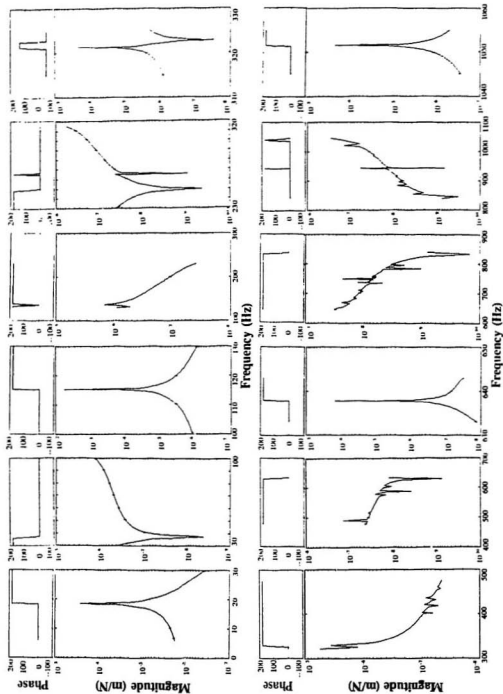
Figure B.2.8 Displacement response of the uncracked plate in air at node 2151

157
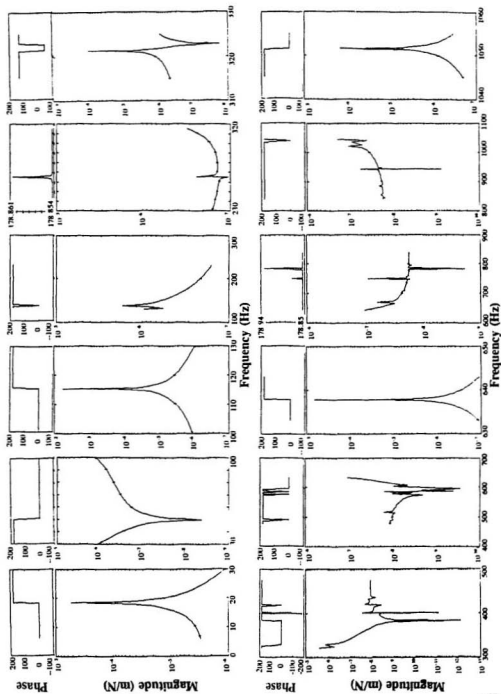
Figure B.2.9 Displacement response of the uncracked plate in air at node 2155

158
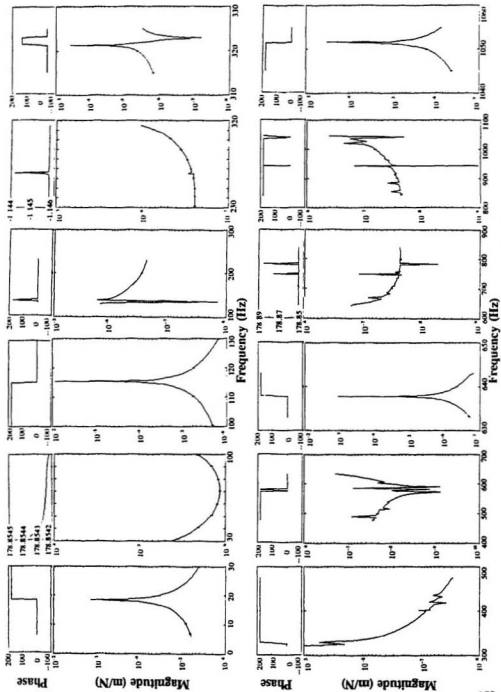
Figure B.2.10 Displacement response of the uncracked plate in air at node 2167

159
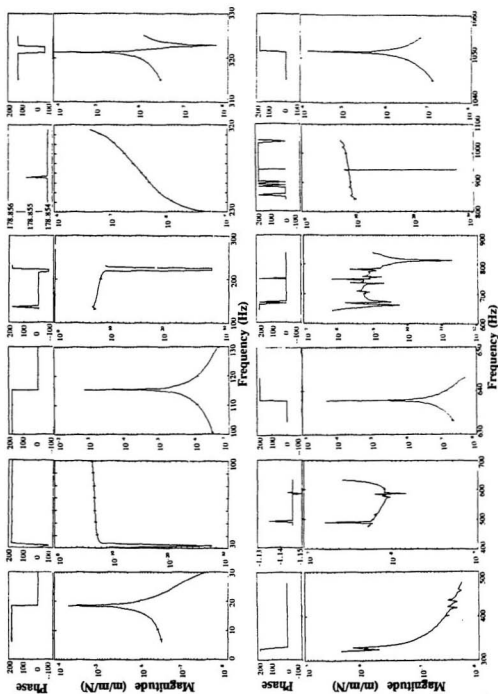
Figure B.2.11 Strain response of the uncracked plate in air at node 2143

160
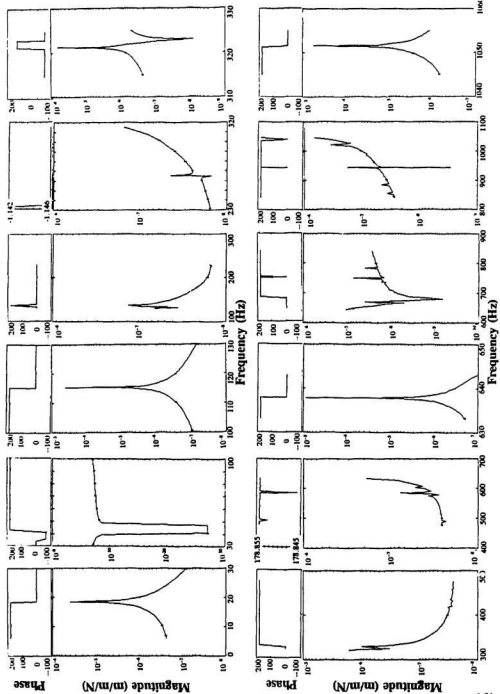
Figure B.2.12 Strain response of the uncracked plate in air at node 2145

161
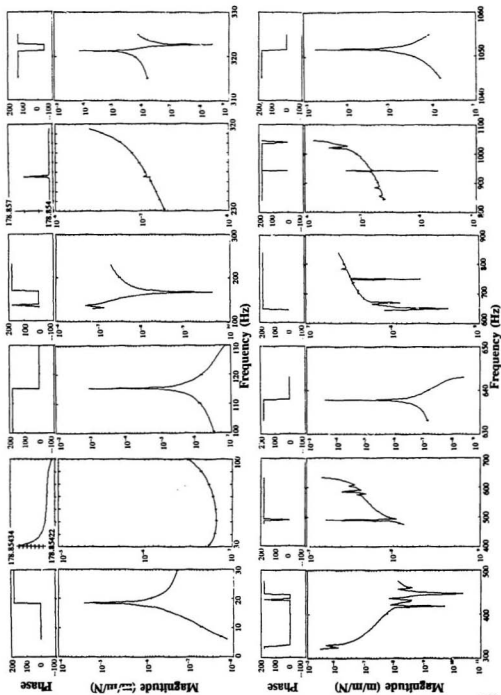
Figure B.2.13 Strain response of the uncracked plate in air at node 2151

162
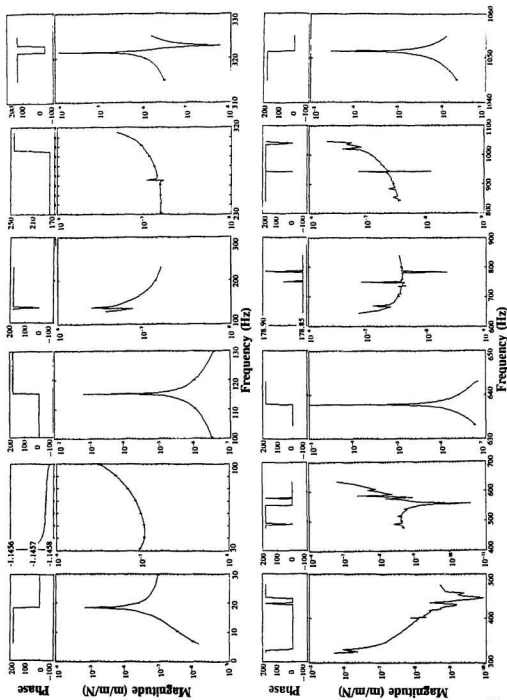
Figure B.2.14 Strain response of the uncracked plate in air at node 2155

163
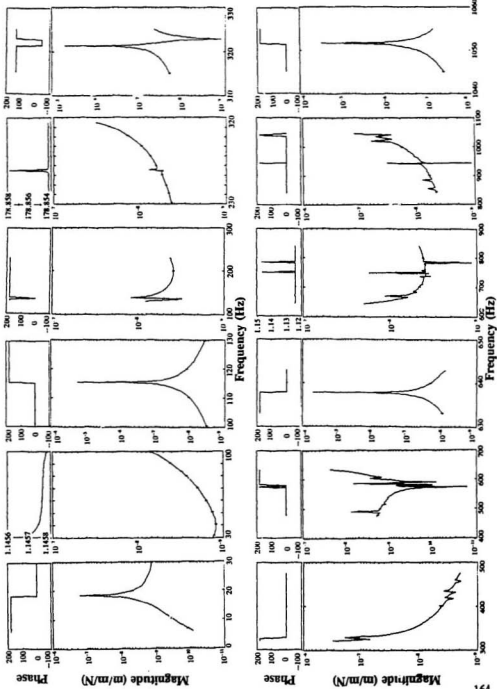
Figure B.2.15 Strain response of the uncracked plate at node 2167

164

B.3 2x1/32" Cracked Plate in Air

Since the actual crack widths introduced in the specimen are very small, analytically the cracks are modeled by three different widths, viz., 1.5 mm, 2 mm and 2.5 mm. The choice of 1.5 mm for the smallest crack width in this study is to accommodate the crack to "breath" (to open and close) freely and to maintain the aspect ratio of the finite element mesh as small as possible. Further study on the crack width is not done due to time constraint. Tables B.3.1 to B.3.6 give the results for the corresponding nodes. The phase, strain and acceleration plots around the peak response at the five nodes shown in Figure 4.7 are presented in Figures B.3.1 to B.3.10. The results indicate that the responses are very sensitive to the finite element discretization used in this study.

Table B.3.1 Beam with 2x1/32 inch (2x0.794 mm) crack depth modeled using 1.5 mm crack width : acceleration response

No.	Natural Frequency (Hz)	Peak magnitudes at nodes (ms²/N)				
		2159	2161	2169	2173	2185
1	18.45	0.6839	2.927	13.09	25.56	63.55
2	115.3	117.6	438.90	1245.0	1256.0	1967
3	319.8	77.53	244.00	291.20	131.3	537.3
4	637.3	355.90	907.20	173.0	761.60	1279.0
5	1051	3508	6601.0	6009.0	4181.0	8695.0

Table B.3.2 Beam with 2x1/32 inch (2x0.794 mm) crack depth modeled using 1.5 mm crack width : strain response

No.	Natural Frequency (Hz)	Peak magnitudes at nodes (m/m/N) x 10^-6				
		2159	2161	2169	2173	2185
1	18.45	$1.6478.10^2$	$1.4212.10^2$	$9.0954.10^1$	$5.1662.10^1$	$2.8276.10^{-1}$
2	115.3	$5.5099.10^2$	$1.7759.10^2$	$4.8936.10^2$	$6.5066.10^2$	7.4246
3	319.3	$3.0539.10^1$	$2.1507.10^1$	$4.5994.10^1$	$2.6890.10^1$	1.6562
4	637.3	$1.4892.10^1$	$6.2410.10^1$	$1.5924.10^1$	$6.9034.10^1$	3.5230
5	1051	$3.8616.10^1$	$3.2596.10^2$	$3.2656.10^2$	$2.1446.10^2$	$1.9394.10^1$

Table B.3.3 Beam with 2x1/32 inch (2x0.794 mm) crack depth modeled using 2 mm crack width : acceleration response

No.	Natural Frequency (Hz)	Peak magnitudes at nodes (ms^2/N)				
		2459	2461	2469	2473	2495
1	18.42	1.029	4.405	19.71	38.48	95.64
2	115.4	24.72	92.25	261.8	264.20	413.60
3	319.8	56.98	179.30	213.9	96.34	394.60
4	637.3	150.90	385.0	73.97	323.20	542.80
5	1051	766.50	1445.0	1312.0	915.0	1900.0

Table B.3.6 Beam with 2x1/32 inch (2x0.794 mm) crack depth modeled using 2.5 mm crack width : strain response

No.	Natural Frequency (Hz)	Peak magnitudes at nodes (m/m/N) x 10^{-6}				
		2459	2461	2469	2473	2485
1	18.42	$4.8670.10^2$	$4.1969.10^2$	$2.6831.10^2$	$1.5239.10^2$	$8.3404 \ 10^{-1}$
2	115.40	$1.0742.10^2$	$3.4592.10^1$	$9.5490.10^1$	$1.2706.10^2$	1.4504
3	319.40	$2.1564.10^1$	$1.5102.10^1$	$3.2352.10^1$	$1.8937.10^1$	1.1663
4	637.10	6.5701	$2.1727.10^1$	7.0212	$3.0053.10^1$	1.5324
5	1050	$1.9303.10^1$	$1.6571.10^2$	$1.6677.10^2$	$1.0978.10^2$	9.9018

Table B.3.4 Beam with 2x1/32 inch (2x0.794 mm) crack depth modeled using 2 mm crack width: strain response

No	Natural Frequency (Hz)	Peak magnitudes at nodes (m/m/N) x 10⁻⁶				
		2459	2461	2469	2473	2485
1	18.42	$2.4878.10^2$	$2.1445.10^2$	$1.3689.10^2$	$7.7752.10^1$	$4.2552.10^1$
2	115.4	$1.1572.10^2$	$3.7283.10^2$	$1.0279.10^2$	$1.3679.10^2$	1.5614
3	319.8	$2.2454.10^1$	$1.5772.10^1$	$3.3740.10^1$	$1.9744.10^1$	1.2160
4	637.3	6.3428	$2.6408.10^1$	6.7571	$2.9294.10^1$	1.4953
5	1051.0	8.3402	$7.1063.10^1$	$7.1353.10^1$	$4.6927.10^1$	4.2366

Table B.3.5 Beam with 2x1/32 inch (2x0.794 mm) crack depth modeled using 2.5 mm crack width : acceleration response

No.	Natural Frequency (Hz)	Peak magnitudes at nodes (ms⁻²/N)				
		2459	2461	2469	2473	2485
1	18.42	2.013	8.617	38.63	75.42	187.50
2	115.4	22.95	85.64	243.20	245.40	384.20
3	319.8	54.68	172.20	205.20	92.39	378.40
4	637.3	155.40	396.80	75.68	331.40	556.90
5	1051	1792.0	3384.0	3066.0	2141.0	4440.0
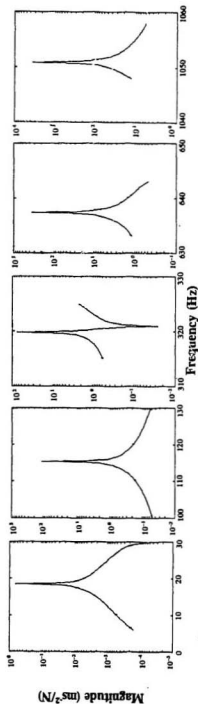
Figure B.3.1 Acceleration response of the 2x1/32" cracked plate in air at node 2459
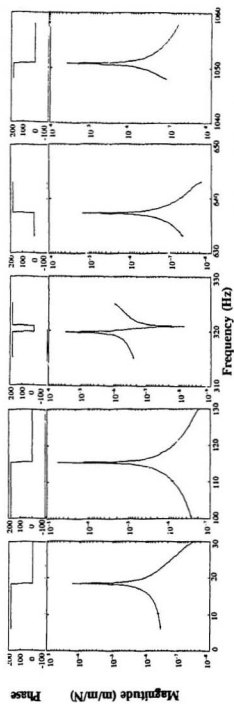
Figure B.3.2 Strain response of the 2x1/32" cracked plate in air at node 2459

169
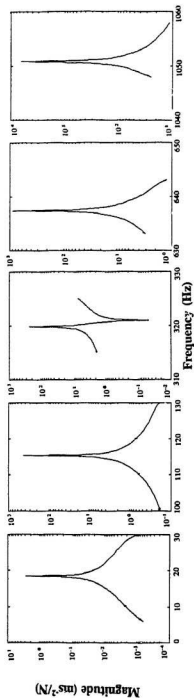
Figure B.3.3 Acceleration response of the 2x1/32" cracked plate in air at node 2461
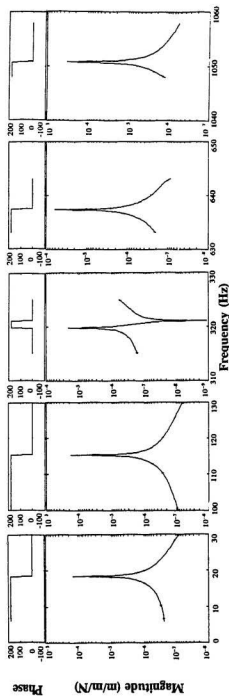
Figure B.3.4 Strain response of the 2x1/32" cracked plate in air at node 2461

170
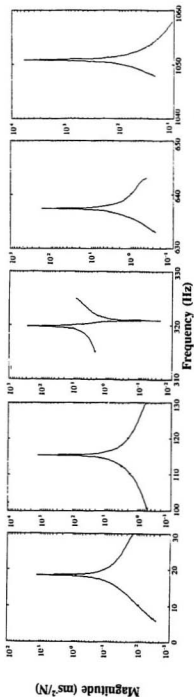
Figure B.3.5 Acceleration response of the 2x1/32" cracked plate in air at node 2469

Magnitude (ms⁻²/N)

Frequency (Hz)
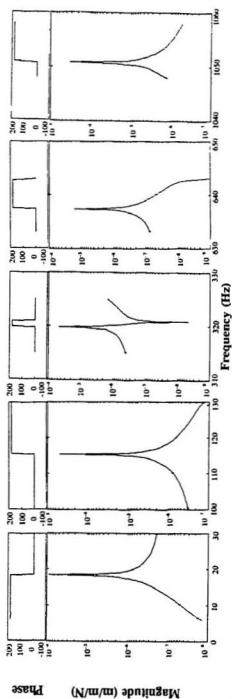
Figure B.3.6 Strain response of the 2x1/32" cracked plate in air at node 2469

Magnitude (m/m/N)   Phase

Frequency (Hz)

171
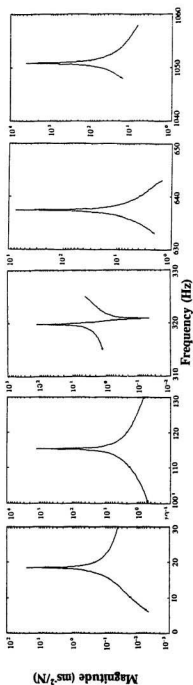
Figure B.3.7 Acceleration response of the 2x1/32" cracked plate in air at node 2473

Frequency (Hz)

Magnitude (ms⁻²/N)
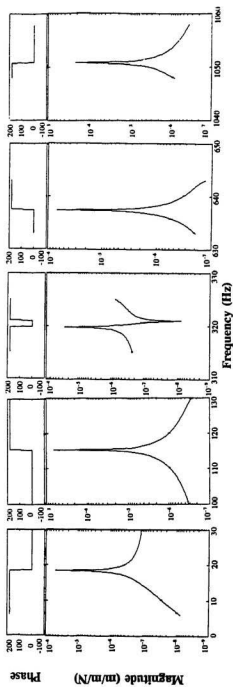
Figure B.3.8 Strain response of the 2x1/32" cracked plate in air at node 2473

Frequency (Hz)

Magnitude (m/m/N)

Phase

172
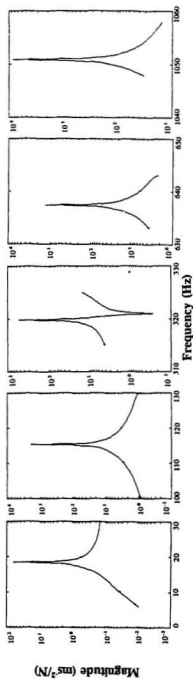
Figure B.3.9 Acceleration response of the 2x1/32" cracked plate in air at node 2485
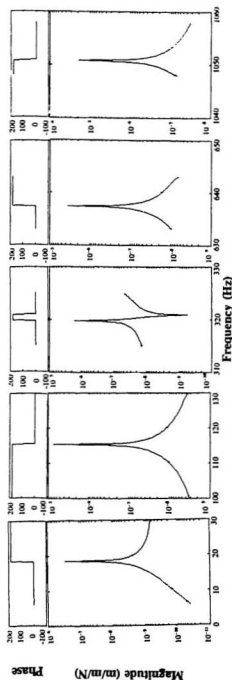
Figure B.3.10 Strain response of the 2x1/32" cracked plate in air at node 2485

173

B.4 2x3/32" Cracked Plate in Air

The discretization for 2x3/32" cracked plate is the same as the one used for the 2x1/32" case. The only difference is the crack depth used in this analysis; the results are given in Tables B.4.1 to B.4.6. Figures B.4.1 to B.4.10 show the phase, strain and acceleration response plots at the five nodes displayed in Figure 4.7. As could be seen from Tables B.2.1 to B.2.5, B.3.1 to B.3.1 to B.3.6 and B.4.1 to B.4.6, the presence of cracks influences both the frequencies and the amplitudes of response.

Table B.4.1 Beam with 2x3/32 inch (2x2.381 mm) crack depth modeled using 1.5 mm crack width : acceleration response

No.	Natural Frequency (Hz)	Peak magnitudes at nodes (ms²/N)				
		2459	2461	2469	2473	2485
1	18.15	0.6120	2.620	12.17	23.72	58.72
2	115.20	24.18	90.13	259.10	261.50	410.10
3	319.70	178.50	564.80	660.40	297.40	1209.0
4	632.8	150.90	391.80	80.00	310.50	527.70
5	1041	4377.0	8536.0	7641.0	5428.0	1.0965.10⁴

Table B.4.2 Beam with 2x3/32 inch (2x2.381 mm) crack depth modeled using 1.5 mm crack width : strain response

No.	Natural Frequency (Hz)	Peak magnitudes at nodes (m/m/N) x 10^{-6}				
		2459	2461	2469	2473	2485
1	18.15	$1.5247.10^2$	$1.3151.10^2$	$8.4146.10^1$	$4.7776.10^1$	$2.6130.10^1$
2	115.20	$1.1327.10^2$	$1.0271.10^1$	$1.0271.10^2$	$1.3598.10^2$	1.5489
3	319.70	$7.1453.10^1$	$4.7068.10^1$	$1.0353.10^2$	$6.0946.10^1$	3.7404
4	623.80	7.0640	$2.5278.10^1$	7.5168	$2.8350.10^1$	1.4568
5	1041	$3.8522.10^1$	$3.9094.10^2$	$4.1817.10^2$	$2.8411.10^2$	$2.4567.10^1$

Table B.4.3 Beam with 2x3/32 inch (2x2.381 mm) crack depth modeled using 2 mm crack width : acceleration response

No.	Natural Frequency (Hz)	Peak magnitudes at nodes (ms^{-2}/N)				
		2459	2461	2469	2473	2485
1	18.04	0.6908	2.957	13.93	27.13	67.04
2	115.2	1025	3820	$1.1035.10^4$	$1.1141.10^4$	$1.7476.10^4$
3	319.70	28.67	90.85	105.40	47.25	192.60
4	631.20	291.20	760.70	157.10	589.10	1006.0
5	1039	$3.9993.10^4$	$7.9021.10^4$	$7.0979.10^4$	$5.2094.10^4$	$1.0522.10^5$

Table B.4.4 Beam with 2x3/32 inch (2x2.382 mm) crack depth modeled using 2 mm crack width : strain response

No.	Natural Frequency (Hz)	Peak magnitudes at nodes (m/m/N) x 10^{-6}				
		2459	2461	2469	2473	2485
1	18.04	$1.7422.10^2$	$1.5026.10^2$	$9.6115.10^1$	$5.4563.10^1$	$2.9834 \ 10^{-1}$
2	115.20	$4.7987.10^3$	$1.5090.10^3$	$4.3795.10^3$	$5.7952.10^3$	$6.6003 \ 10^1$
3	319.7	$1.1526.10^1$	7.4264	$1.6426.10^1$	9.7142	$5.9595 \ 10^{-1}$
4	631.2	$1.4152.10^1$	$4.7940.10^1$	$1.5086.10^1$	$5.3961.10^1$	2.7791
5	1039	$3.0764.10^2$	$3.5281.10^3$	$3.8961.10^3$	$2.7074.10^3$	$2.3309 \ 10^2$

Table B.4.5 Beam with 2x3/32 inch (2x2.382 mm) crack depth modeled using 2.5 mm crack width : acceleration response

No.	Natural Frequency (Hz)	Peak magnitudes at nodes (ms^{-2}/N)				
		2459	2461	2469	2473	2485
1	17.92	3.679	15.75	75.14	146.30	360.80
2	115.20	27.04	100.70	292.20	295.10	463.10
3	319.60	63.56	201.9	232.80	105.0	423.60
4	629.60	294.60	774.30	163.20	589.0	1010.0
5	1039	2095.0	4189.0	3867.0	3013.0	6190.0

Table B.4.6 Beam with 2x3/32 inch (2x2.382 mm) crack depth modeled using 2.5 mm crack width : strain response

No.	Natural Frequency (Hz)	Peak magnitudes at nodes (m/m/N) x 10⁻⁶				
		2459	2461	2469	2473	2485
1	17.92	$9.4018.10^2$	$8.1054.10^2$	$5.1753.10^2$	$2.9375.10^2$	1.6057
2	115.20	$1.2644.10^2$	$3.9526.10^1$	$1.1613.10^2$	$1.5359.10^2$	1.7490
3	319.6	$2.5747.10^1$	$1.6121.10^1$	$3.6334.10^1$	$2.1492.10^1$	1.3154
4	629.6	$1.4819.10^1$	$4.7713.10^1$	$1.5736.10^1$	$5.4090.10^1$	2.7924
5	1039	$1.3234.10^1$	$1.8365.10^2$	$2.1294.10^2$	$1.5351.10^2$	$1.3327.10^1$
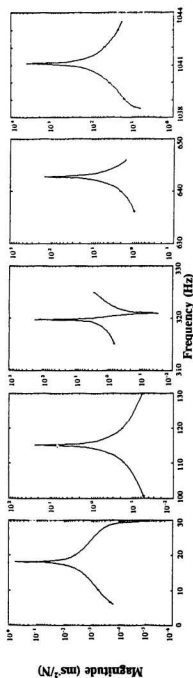
Figure B.4.1 Acceleration response of the 2x3/32" cracked plate in air at node 2459
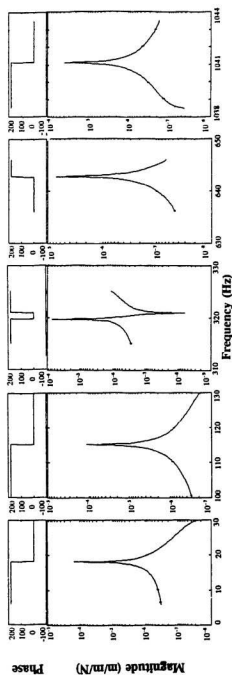
Figure B.4.2 Strain response of the 2x3/32" cracked plate in air at node 2459

178
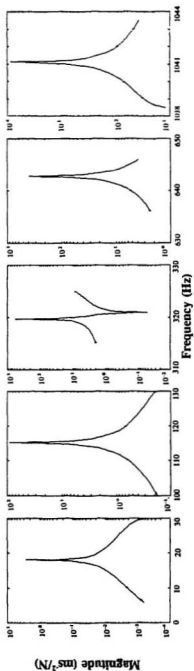
Figure B.4.3 Acceleration response of the 2x3/32" cracked plate in air at node 2461

Magnitude (ms⁻²/N)

Frequency (Hz)
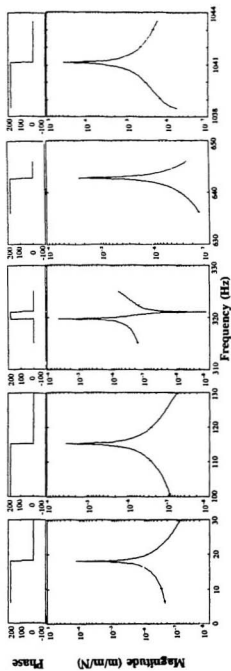
Figure B.4.4 Strain response of the 2x3/32" cracked plate in air at node 2461

Phase   Magnitude (m/m/N)

Frequency (Hz)

179
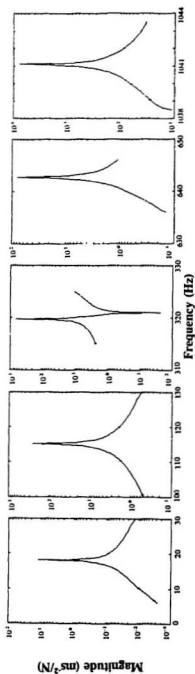
Figure B.4.5 Acceleration response of the 2x3/32" cracked plate in air at node 2469
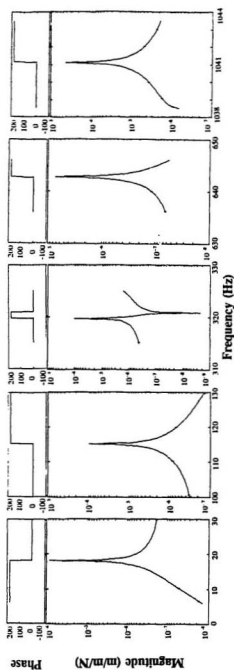
Figure B.4.6 Strain response of the 2x3/32" cracked plate in air at node 2469

180
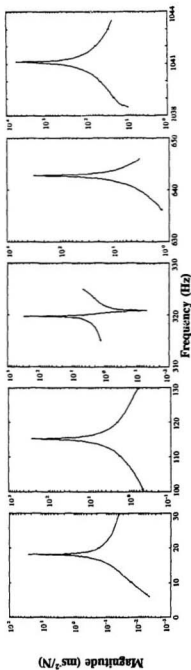
Figure B.4.7 Acceleration response of the 2x3/32" cracked plate in air at node 2473
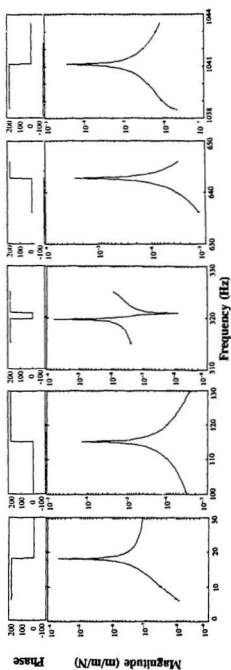
Figure B.4.8 Strain response of the 2x3/32" cracked plate in air at node 2473

181
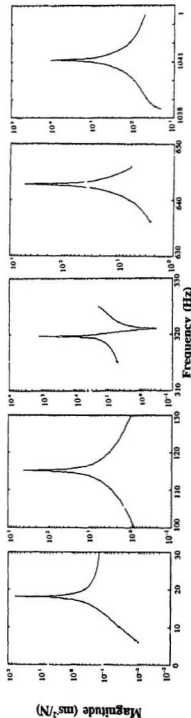
Figure B.4.9 Acceleration response of the 2x3/32" cracked plate in air at node 2485
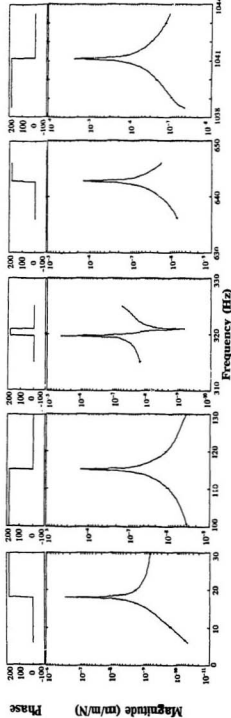
Figure B.4.10 Strain response of the 2x3/32" cracked plate in air at node 2485

182

B.5 Displaced Shape of the Vibrating Plate

Using a 4x13 shell element discretization, the displaced/deformed shape on the first ten modes presented in this section were obtained. By knowing the displaced shape, the in-plane, torsion and bending modes can be recognized, so that the resonant frequencies determined using this discretization can be correlated to those obtained using the beam element discretization given in Chapter 4.
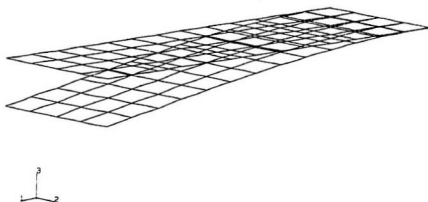
Figure B.5.1 Deformed shape of the 4x13 shell discretization : first mode
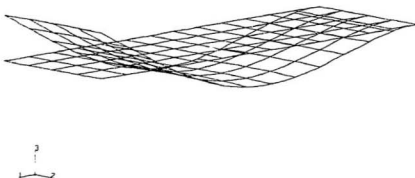
Figure B.5.2 Deformed shape of the 4x13 shell discretization : second mode
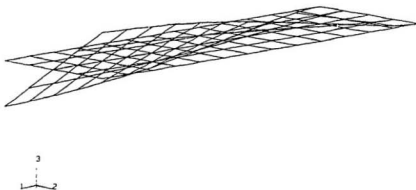
Figure B.5.3 Deformed shape of the 4x13 shell discretization : third mode
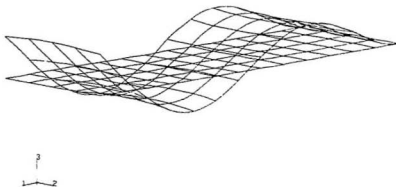
Figure B.5.4 Deformed shape of the 4x13 shell discretization : fourth mode
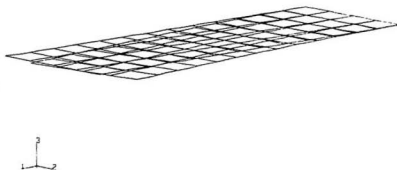
Figure B.5.5 Deformed shape of the 4x13 shell discretization : fifth mode
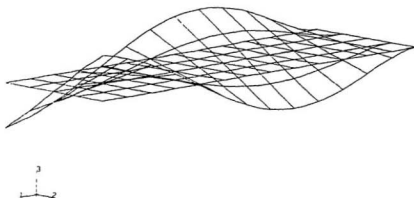
Figure B.5.6 Deformed shape of the 4x13 shell discretization : sixth mode
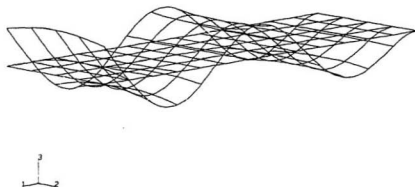
Figure B.5.7 Deformed shape of the 4x13 shell discretization : seventh mode
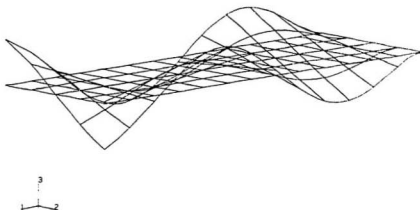
Figure B.5.8 Deformed shape of the 4x13 shell discretization : eighth mode
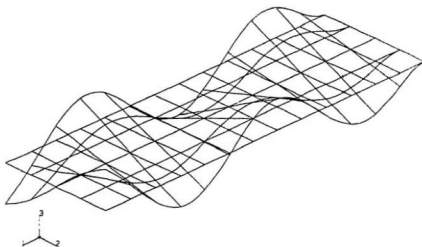
Figure B.5.9 Deformed shape of the 4x13 shell discretization : ninth mode
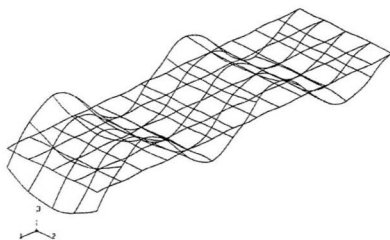
Figure B.5.10   Deformed shape of the 4x13 shell discretization : tenth mode

Appendix C
Experimental Results

The experiment in air and in water were conducted in a 130x55x80 cm deep tank. To measure the responses of vibrating plate in air and in water under partially/fully submerged conditions, four strain gages and one accelerometer were mounted on the plate; the response in the first five modes were acquired. The measurement was carried out in two type of frequency bands, i.e., "the broad frequency bands" and "the zoom frequency bands". "The broad frequency bands" were the bands chosen so that in every band, one peak of frequency response function, viz., natural frequency of a mode, could be found. These bands ranged from 50 Hz (in the first mode) to 400 Hz (in the fifth mode). The "zoom frequency bands" were much smaller than the broad ones. These bands, depending on the mode, varied from 25 Hz (in the first mode) to 100 Hz (in the fifth mode). The purpose of zooming into smaller frequency bands was to study the peak response characteristics, natural frequency and damping of the structure when the higher frequency resolution (i.e., greater number in a frequency band) was used. Modal parameters were extracted using three fit methods, i.e., peak, polynomial and global fit methods; the results were compared. In the tables given in this Appendix, these fit methods are

shortened to peak, poly and global. Sensor and transducer terms are also abbreviated; these refer to accelerometer (which is abbreviated to acc) and strain gages (which are shortened to str). The transducer locations are depicted in Figure 5.1 of Chapter 5. The average and standard deviation of natural frequency and damping obtained using accelerometer and strain gages are given for every mode, both in the "broad" and "zoom" frequency bands; the values obtained using accelerometer are given in bracket. Several values in the tables, presented in this Appendix are not used, since they are extracted from poor frequency response functions so that the values deviate too much compared to those obtained using sensors in other locations or other fit methods. These values are marked by superscript * in the tables. The frequency response functions are also given in this Appendix. Since the frequency response functions were taken in five bands for the five modes, there are several "discontinuities" in the plots. Because the frequency response functions were measured with different frequency resolutions for each mode (and the frequencies were divided into discrete frequency bands), the response magnitude in the highest frequency in a frequency band is little bit different from the lowest frequency in the subsequent frequency band. The experimental results of the uncracked plate in air, and those of the partially/fully submerged plates in water are presented in the first section of this Appendix. The results of the 2x1/32" cracked plate in air are given in the second section. And in the third section, the results of the 2x3/32" cracked plate in air and water are given.

C.1 Uncracked Plate

The frequency response function and modal parameters of the uncracked plate vibrating

in three conditions mentioned above, are given in this section. The results of the plate in air can be found in subsection C.1.1, the partially submerged plate in subsection C.1.2 and fully submerged plate in C.1.3.

C.1.1 Uncracked Plate in Air

In Tables C.1.1.1 to C.1.1.5, natural frequency and damping values are given. Peak response magnitudes are tabulated in Tables C.1.1.6 to C.1.1.10; the acceleration magnitudes are in ms^{-2}/N and strain response ones are given in m/m/N x 10^6 (micro strain). The coherence function and frequency response function plots are shown in Figures C.1.1.1 to C.1.1.10. In general, strain frequency response functions are more "noisy" than the acceleration frequency response function; the coherence function obtained using strain sensors are poorer than the accelerometer ones.

Table C.1.1.1   Modal parameters of the uncracked plate in air : 1st mode (broad band)

| Transducer | Modal Parameters | | | | | |
| | Natural Frequency (Hz) | | | Damping (%) | | |
	Peak	Poly	Global	Peak	Poly	Global
Acc	17.00	17.00	17.01	-	0.28379	0.28117
Str1	17.00	17.01	17.02	-	0.21645	0.24242
Str2	17.00	17.01	17.02	-	0.24376	0.27724
Str3	17.00	17.00	17.01	-	0.27499	0.29771
Str4	17.06	17.04	17.02	-	0.25125	0.27534
Average	17.0158 (17.0033)			0.259895 (0.2825)		
Stand. Dev.	0.01754 (0.0047)			0.0243 (0.0013)		

Table C.1.1.1.1 Modal parameters of the uncracked plate in air : 1st mode (zoom)

Transducer	Modal Parameters					
	Natural Frequency (Hz)			Damping (%)		
	Peak	Poly	Global	Peak	Poly	Global
Acc	17.03	17.05	17.04	-	0.18664	0.19038
Str1	17.00	17.03	17.03	-	0.19129	0.21743
Str2	17.03	17.04	17.05	-	0.18678	0.21114
Str3	17.03	17.03	17.04	-	0.17753	0.20834
Str4	17.03	17.03	17.03	-	0.18235	0.20816
Average	17.0309 (17.04)			0.1979 (0.1885)		
Stand. Dev.	0.01115 (0.0082)			0.0141 (0.0019)		

Table C.1.1.2 Modal parameters of the uncracked plate in air : 2nd mode (broad band)

Transducer	Modal Parameters					
	Natural Frequency (Hz)			Damping (%)		
	Peak	Poly	Global	Peak	Poly	Global
Acc	106.38	106.35	106.30	-	0.12290	0.13046
Str1	106.38	106.37	106.35	-	0.13336	0.13866
Str2	106.25	106.35	106.34	-	0.15363	0.15248
Str3	106.25	106.37	106.32	-	0.17706	0.18404
Str4	106.25	106.37	106.34	-	0.15204	0.15412
Average	106.3283 (106.3433)			0.1557 (0.1267)		
Stand. Dev.	0.0480 (0.0330)			0.0161 (0.0038)		

Table C.1.1.2.1 Modal parameters of the uncracked plate in air : 2nd mode (zoom)

Transducer	Modal Parameters					
	Natural Frequency (Hz)			Damping (%)		
	Peak	Poly	Global	Peak	Poly	Global
Acc	106.28	106.27	105.27	-	0.16487	0.16896
Str1	106.28	106.25	106.26	-	0.18107	0.18315
Str2	106.28	106.26	106.27	-	0.18235	0.18196
Str3	106.22	106.24	106.25	-	0.18794	0.18875
Str4	106.22	106.25	106.27	-	0.17791	0.18742
Average	106.2542 (106.2733)			0.1838 (0.1669)		
Stand. Dev.	0.01935 (0.0047)			0.0036 (0.0020)		

Table C.1.1.3 Modal parameters of the uncracked plate in air : 3rd mode (broad band)

Transducer	Modal Parameters					
	Natural Frequency (Hz)			Damping (%)		
	Peak	Poly	Global	Peak	Poly	Global
Acc	306.0	305.99	305.97	-	0.16613	0.20145
Str1	306.0	305.97	305.84	-	0.17611	0.20900
Str2	306.0	306.02	306.09	-	0.16328	0.18675
Str3	306.0	306.10	305.98	-	0.16141	0.17223
Str4	306.0	306.02	306.0	-	0.16368	0.18241
Average	306.0017 (305.9867)			0.1769 (0.1838)		
Stand. Dev.	0.0618 (0.0125)			0.0149 (0.0177)		

Table C.1.1.3.1   Modal parameters of the uncracked plate in air : 3rd mode (zoom)

Transducer	Modal Parameters					
	Natural Frequency (Hz)			Damping (%)		
	Peak	Poly	Global	Peak	Poly	Global
Acc	306.00	306.02	306.00	-	0.16316	0.18206
Str1	306.00	305.66	305.98	-	0.21878	0.21371
Str2	305.81	305.66	305.67	-	0.22095	0.22024
Str3	305.81	305.67	305.64	-	0.21785	0.21697
Str4	305.81	305.66	305.64	-	0.21862	0.21552
Average	305.7508 (306.0067)			0.2178 (0.1726)		
Stand. Dev.	0.1250 (0.0094)			0.0022 (0.00945)		

Table C.1.1.4   Modal parameters of the uncracked plate in air : 4th mode (broad band)

Transducer	Modal Parameters					
	Natural Frequency (Hz)			Damping (%)		
	Peak	Poly	Global	Peak	Poly	Global
Acc	602.50	602.48	601.96	-	0.26022	0.28909
Str1	602.50	602.04	602.16	-	0.34668	0.31693
Str2	602.50	602.31	601.91	-	0.26794	0.26983
Str3	602.50	602.33	602.23	-	0.26869	0.27414
Str4	602.50	602.40	602.23	-	0.25560	0.25641
Average	602.3008 (602.3133)			0.2820 (0.27465)		
Stand. Dev.	0.1871 (0.2500)			0.0303 (0.0144)		

Table C.1.1.4.1 Modal parameters of the uncracked plate in air : 4th mode (zoom)

Transducer	Modal Parameters					
	Natural Frequency (Hz)			Damping (%)		
	Peak	Poly	Global	Peak	Poly	Global
Acc	601.84	601.70	601.77	-	0.29467	0.28247
Str1	601.63	601.53	601.62	-	0.27891	0.27309
Str2	601.66	601.60	601.74	-	0.29088	0.28721
Str3	601.66	601.65	601.76	-	0.29070	0.28940
Str4	601.66	601.64	601.80	-	0.29430	0.29881
Average	601.6625 (601.77)			0.2879 (0.2886)		
Stand. Dev.	0.0704 (0.05715)			0.0077 (0.0061)		

Table C.1.1.5 Modal parameters of the uncracked plate in air : 5th mode (broad band)

Transducer	Modal Parameters					
	Natural Frequency (Hz)			Damping (%)		
	Peak	Poly	Global	Peak	Poly	Global
Acc	970.00	969.47	970.45	-	0.36806	0.38712
Str1	969.50	969.16	969.36	-	0.43553	0.43345
Str2	969.50	969.49	969.76	-	0.42750	0.42885
Str3	969.50	969.47	969.43	-	0.40839	0.43260
Str4	970.00	969.70	970.13	-	0.39731	0.41463
Average	969.5833 (969.9733)			0.4223 (0.3776)		
Stand. Dev.	0.2602 (0.4005)			0.0130 (0.0095)		

Table C.1.1.5.1 Modal parameters of the uncracked plate in air : 5ᵗʰ mode (zoom)

Transducer	Modal Parameters					
	Natural Frequency (Hz)			Damping (%)		
	Peak	Poly	Global	Peak	Poly	Global
Acc	969.38	969.39	969.58	-	0.36619	0.36237
Str1	969.63	969.29	969.29	-	0.40816	0.42115
Str2	969.38	969.65	969.88	-	0.41336	0.44901
Str3	969.13	969.50	969.69	-	0.42708	0.47115
Str4	969.88	969.39	969.45	-	0.44093	0.48406
Average	969.5133 (969.4500)			0.4394 (0.3643)		
Stand. Dev.	0.2266 (0.0920)			0.0256 (0.0019)		

Table C.1.1.6 Peak response magnitudes of the uncracked plate in air : 1ˢᵗ mode

Mode	Sensor	Peak Magnitudes (ms⁻²/N) for acc; (m/m/N x 10⁻⁶) for str					
		Broad band			Zoom		
		Peak	Poly	Global	Peak	Poly	Global
1	Acc	1.6	0.93597	0.88887	2.72	0.91896	0.93755
	Str1	45.52	22.20	22.05	46.55	24.33	22.48
	Str2	37.10	20.01	20.15	37.78	21.42	21.91
	Str3	12.27	7.29	7.32	11.07	8.01	8.07
	Str4	52.78	29.82	28.13	55.41	30.22	30.37

Table C.1.1.7   Peak magnitudes of the uncracked plate in air : 2nd mode

Mode	Sensor	Peak Magnitudes (ms^{-2}/N) for acc; (m/m/N x 10^{-6}) for str					
		Broad band			Zoom		
		Peak	Poly	Global	Peak	Poly	Global
2	Acc	12.78	22.76	22.92	65.03	145.51	146.83
	Str1	25.32	51.09	51.48	124.71	313.57	314.46
	Str2	4.13	9.41	9.28	23.91	57.57	57.32
	Str3	32.52	84.54	84.74	196.03	496.66	496.37
	Str4	32.48	75.18	73.60	186.03	449.03	459.63

Table C.1.1.8   Peak magnitudes of the uncracked plate in air : 3rd mode

Mode	Sensor	Peak Magnitudes (ms^{-2}/N) for acc; (m/m/N x 10^{-6}) for str					
		Broad band			Zoom		
		Peak	Poly	Global	Peak	Poly	Global
3	Acc	6.41	40.22	43.83	7.35	42.03	43.80
	Str1	1.61	10.84	11.06	2.13	17.21	16.87
	Str2	3.77	23.49	24.80	4.73	38.91	38.46
	Str3	4.08	25.22	25.72	5.14	41.96	42.08
	Str4	2.73	17.04	17.94	3.30	27.34	27.08

Table C.1.9 Peak magnitudes of the uncracked plate in air : 4ᵗʰ mode

Mode	Sensor	Peak Magnitudes (ms⁻²/N) for acc; (m/m/N x 10⁻⁶) for str					
		Broad band			Zoom		
		Peak	Poly	Global	Peak	Poly	Global
4	Acc	2.06	40.06	42.43	2.46	53.17	50.73
	Str1	0.20806	4.48	4.43	0.33093	6.78	6.63
	Str2	1.12	22.79	22.54	1.34	29.96	29.34
	Str3	0.98574	21.80	21.58	1.27	28.42	27.87
	Str4	0.17839	3.46	3.42	0.22010	4.95	5.01

Table C.1.10 Peak magnitudes of the uncracked plate in air : 5ᵗʰ mode

Mode	Sensor	Peak Magnitudes [ms⁻²/N] for acc; [m/m/N x 10⁻⁶] for str					
		Broad band			Zoom		
		Peak	Poly	Global	Peak	Poly	Global
5	Acc	28.76	1290	1300	120.58	5280	5130
	Str1	6.15	326.01	316.87	24.61	1170	1200
	Str2	9.62	495.28	484.84	42.31	2100	2240
	Str3	9.53	480.34	483.54	40.90	2070	2230
	Str4	8.62	412.53	419.52	33.54	1730	1830
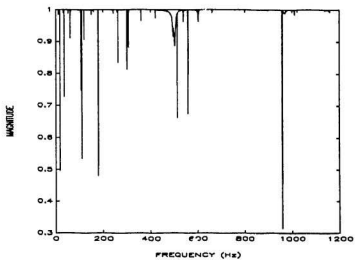
Figure C.1.1.1 Acceleration coherence function of the uncracked plate in air
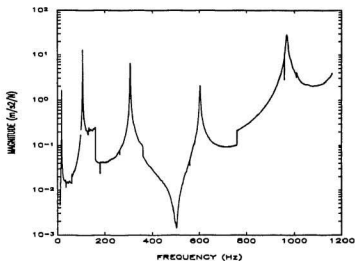
Figure C.1.1.2 Acceleration frequency response function of the uncracked plate in air
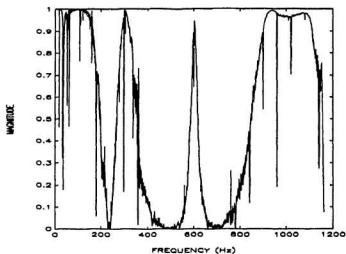
Figure C.1.1.3 Strain coherence function of the uncracked plate in air : strain gage no. 1
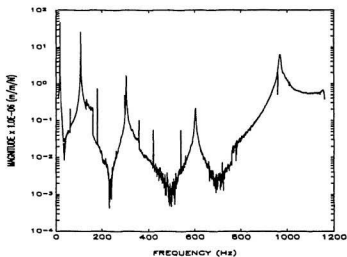
Figure C.1.1.4 Strain frequency response function of the uncracked plate in air : strain gage no. 1
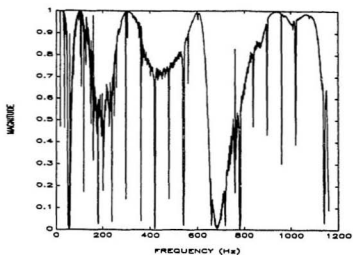
Figure C.1.1.5 Strain coherence function of the uncracked plate in air : strain gage no. 2
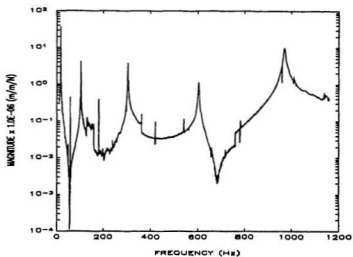
Figure C.1.1.6 Strain frequency response function of the uncracked plate in air : strain gage no. 2
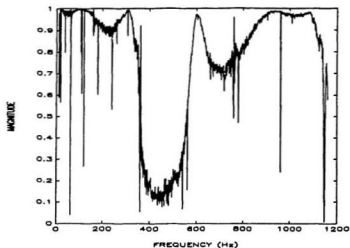
Figure C.1.1.7 Strain coherence function of the uncracked plate in air : strain gage no. 3
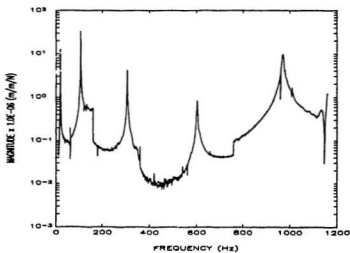
Figure C.1.1.8 Strain frequency response function of the uncracked plate in air : strain gage no. 3
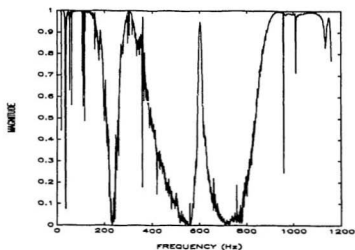
Figure C.1.1.9 Strain coherence function of the uncracked plate in air : strain gage no. 4
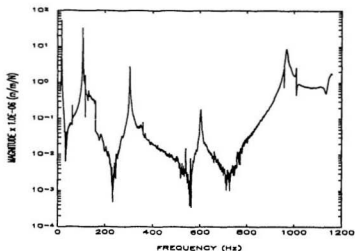
Figure C.1.1.10 Strain frequency response function of the uncracked plate in air : strain gage no. 4

C.1.2 Uncracked Plate Partially Submerged in Water

Tables and figures in this subsection are organized in the same way as the previous section. Natural frequency and damping are given in Tables C.1.2.1 to C.1.2.5; the peak response magnitudes for the broad and zoom frequency bands in Tables C.1.2.6 to C.1.2.10 and the coherence function and frequency response function in Figures C.1.2.1 to C.1.2.10.

Table C.1.2.1 Modal parameters of the uncracked plate partially submerged in water : 1ˢᵗ mode (broad band)

Transducer	Modal Parameters					
	Natural Frequency (Hz)			Damping (%)		
	Peak	Poly	Global	Peak	Poly	Global
Acc	12.50	12.49	12.48	-	0.57754	0.56866
Str1	12.50	12.49	12.49	-	0.52310	0.54501
Str2	12.50	12.48	12.48	-	0.51374	0.54173
Str3	12.50	12.48	12.48	-	0.56612	0.54515
Str4	12.50	12.47	12.48	-	0.51823	0.54944
Average	12.4875 (12.49)			0.5378 (0.5731)		
Stand. Dev.	0.0101 (0.0082)			0.0167 (0.0044)		

204

Table C.1.2.1.1 Modal parameters of the uncracked plate partially submerged in water : 1st mode (zoom)

Transducer	Modal Parameters					
	Natural Frequency (Hz)			Damping (%)		
	Peak	Poly	Global	Peak	Poly	Global
Acc	12.47	12.47	12.47	-	0.52443	0.51379
Str1	12.47	12.47	12.46	-	0.51850	0.52044
Str2	12.47	12.45	12.46	-	0.51322	0.51745
Str3	12.47	12.45	12.46	-	0.53909	0.53511
Str4	12.47	12.46	12.47	-	0.53604	0.53654
Average	12.4625 (12.4700)			0.52705 (0.5191)		
Stand. Dev.	0.0072 (0.0000)			0.0099 (0.0053)		

Table C.1.2.2 Modal parameters of the uncracked plate partially submerged in water : 2nd mode (broad band)

Transducer	Modal Parameters					
	Natural Frequency (Hz)			Damping (%)		
	Peak	Poly	Global	Peak	Poly	Global
Acc	79.63	79.53	79.59	-	0.61319	0.66791
Str1	79.63	79.53	79.57	-	0.61292	0.69014
Str2	79.63	79.53	79.57	-	0.65695	0.69085
Str3	79.63	79.53	79.60	-	0.67241	0.70031
Str4	79.63	79.52	79.61	-	0.66877	0.72343
Average	79.5817 (79.5833)			0.6770 (0.64055)		
Stand. Dev.	0.0434 (0.0411)			0.03095 (0.0274)		

Table C.1.2.2.1 Modal parameters of the uncracked plate partially submerged in water : 2nd mode (zoom)

Transducer	Modal Parameters					
	Natural Frequency (Hz)			Damping (%)		
	Peak	Poly	Global	Peak	Poly	Global
Acc	79.31	79.39	79.51	-	0.69247	0.75074
Str1	79.31	79.38	79.55	-	0.69468	0.71786
Str2	79.31	79.35	79.54	-	0.76715	0.80322
Str3	79.31	79.32	79.50	-	0.68944	0.72986
Str4	79.31	79.34	79.51	-	0.71810	0.73615
Average	79.3942 (79.4033)			0.7321 (0.7216)		
Stand. Dev.	0.09535 (0.0822)			0.0352 (0.0291)		

Table C.1.2.3 Modal parameters of the uncracked plate partially submerged in water : 3rd mode (broad band)

Transducer	Modal Parameters					
	Natural Frequency (Hz)			Damping (%)		
	Peak	Poly	Global	Peak	Poly	Global
Acc	238.25	238.07	237.91	-	0.78683	0.88202
Str1	238.00	238.03	237.90	-	0.79556	0.83309
Str2	238.00	237.93	237.97	-	0.81248	0.87201
Str3	238.00	238.00	238.05	-	0.86515	0.89093
Str4	238.00	238.00	237.97	-	0.79368	0.80933
Average	237.9900 (238.0767)			0.8340 (0.8344)		
Stand. Dev.	0.0406 (0.1389)			0.0351 (0.0476)		

Table C.1.2.3.1 Modal parameters of the uncracked plate partially submerged in water : 3rd mode (zoom)

Transducer	Modal Parameters					
	Natural Frequency (Hz)			Damping (%)		
	Peak	Poly	Global	Peak	Poly	Global
Acc	237.34	237.59	237.77	-	0.82202	0.82220
Str1	237.75	237.67	237.77	-	0.78710	0.78095
Str2	237.56	237.63	237.79	-	0.78951	0.78099
Str3	237.56	237.48	237.80	-	0.80760	0.80795
Str4	237.56	237.67	237.96	-	0.77924	0.79306
Average	237.6833 (237.5433)			0.79205 (0.8221)		
Stand. Dev.	0.1303 (0.1506)			0.0108 (0.0001)		

Table C.1.2.4 Modal parameters of the uncracked plate partially submerged in water : 4th mode (broad band)

Transducer	Modal Parameters					
	Natural Frequency (Hz)			Damping (%)		
	Peak	Poly	Global	Peak	Poly	Global
Acc	481.50	481.11	480.82	-	0.82449	0.83780
Str1	482.00	481.10	481.10	-	0.84268	0.80387
Str2	481.00	481.02	480.94	-	0.84034	0.80855
Str3	481.50	481.14	481.45	-	0.86906	0.87463
Str4	482.00	481.65	481.76	-	0.92699	0.87399
Average	481.3883 (481.1433)			0.8550 (0.83115)		
Stand. Dev.	0.3749 (0.2786)			0.0375 (0.0067)		

Table C.1.2.5.1 Modal parameters of the uncracked plate partially submerged in water : 5th mode (zoom)

Transducer	Modal Parameters					
	Natural Frequency (Hz)			Damping (%)		
	Peak	Poly	Global	Peak	Poly	Global
Acc	807.50	807.36	807.30	-	0.92306	0.93918
Str1	807.00	806.92	807.18	-	0.96006	0.96740
Str2	806.50	806.66	806.71	-	0.98752	0.96395
Str3	806.00	806.50	806.70	-	0.99548	0.98698
Str4	807.00	806.32	806.49	-	0.99512	1.02
Average	806.6650 (807.3867)			0.9846 (0.9311)		
Stand. Dev.	0.3168 (0.0838)			0.0188 (0.0081)		

Table C.1.2.6 Peak response magnitude of uncracked plate partially submerged in water : 1st mode

Mode	Sensor	Peak Magnitudes (ms^2/N) for acc; (m/m/N x 10^{-6}) for str					
		Broad band			Zoom		
		Peak	Poly	Global	Peak	Poly	Global
1	Acc	0.434	0.38884	0.38130	0.545	0.42872	0.41635
	Str1	22.88	18.25	18.09	23.85	18.74	18.42
	Str2	20.34	15.77	15.94	21.10	16.37	16.07
	Str3	6.75	5.75	5.52	7.07	5.83	5.71
	Str4	28.29	23.66	23.08	29.71	24.39	23.96

Table C.1.2.4.1 Modal parameters of the uncracked plate partially submerged in water : 4ᵗʰ mode (zoom)

Transducer	Modal Parameters					
	Natural Frequency (Hz)			Damping (%)		
	Peak	Poly	Global	Peak	Poly	Global
Acc	481.47	480.90	481.15	-	0.93975	0.93949
Str1	479.66	480.85	480.99	-	0.93341	0.93164
Str2	480.25	480.87	480.96	-	0.95556	0.94639
Str3	482.28	481.38	481.35	-	0.98877	0.98756
Str4	480.03	481.27	481.19	-	1.0	1.03
Average	480.9233 (481.1733)			0.9717 (0.9396)		
Stand. Dev.	0.6636 (0.2333)			0.0330 (0.0001)		

Table C.1.2.5 Modal parameters of the uncracked plate partially submerged in water : 5ᵗʰ mode (broad band)

Transducer	Modal Parameters					
	Natural Frequency (Hz)			Damping (%)		
	Peak	Poly	Global	Peak	Poly	Global
Acc	808.00	807.79	808.40	-	1.05	1.11
Str1	808.50	807.81	807.93	-	0.97852	0.94271
Str2	808.00	807.51	807.51	-	0.98421	0.99581
Str3	806.50	807.45	807.33	-	0.97690	0.94189
Str4	808.50	806.97	806.97	-	0.99479	0.98312
Average	807.3317 (808.0633)			0.9747 (1.08)		
Stand. Dev.	0.7519 (0.2530)			0.0198 (0.03)		

Table C.1.2.7   Peak response magnitudes of the uncracked plates partially submerged in water : 2ⁿᵈ mode

Mode	Sensor	Peak Magnitudes (ms⁻²/N) for acc; (m/m/N x 10⁶) for str					
		Broad band			Zoom		
		Peak	Poly	Global	Peak	Poly	Global
2	Acc	1.21	7.32	7.55	17.40	120.84	121.81
	Str1	4.30	25.98	27.29	62.74	436.11	422.76
	Str2	0.62328	4.05	4.06	8.93	67.21	64.58
	Str3	6.22	41.28	41.43	98.60	689.44	663.46
	Str4	5.66	37.37	38.30	89.16	629.59	604.90

Table C.1.2.8   Peak response magnitudes of the uncracked plate partially submerged in water : 3ʳᵈ mode

Mode	Sensor	Peak Magnitudes (ms⁻²/N) for acc; (m/m/N x 10⁶) for str					
		Broad band			Zoom		
		Peak	Poly	Global	Peak	Poly	Global
3	Acc	0.71084	16.58	17.50	1.36	33.62	33.58
	Str1	0.24707	5.95	6.07	0.46014	10.92	10.69
	Str2	0.62163	14.87	15.36	1.24	28.03	27.98
	Str3	0.63012	15.99	15.79	1.26	28.92	28.21
	Str4	0.43868	10.49	10.54	0.91275	21.53	22.07

Table C.1.2.9   Peak response magnitudes of the uncracked plates partially submerged in water : 4ᵗʰ mode

Mode	Sensor	Peak Magnitudes (ms⁻²/N) for acc; (m/m/N x 10⁻⁶) for str					
		Broad band			Zoom		
		Peak	Poly	Global	Peak	Poly	Global
4	Acc	0.43229	21.38	21.49	1.89	114.76	113.70
	Str1	0.07107	3.64	3.49	0.32548	19.20	19.06
	Str2	0.353	18.05	17.59	1.42	85.94	83.84
	Str3	0.32385	15.60	16.21	1.35	80.10	78.51
	Str4	0.05374	3.00	2.82	0.28398	15.73	16.44

Table C.1.2.10   Peak response magnitudes of the uncracked plate partially submerged in water : 5ᵗʰ mode

Mode	Sensor	Peak Magnitudes (ms⁻²/N) for acc; (m/m/N x 10⁻⁶) for str					
		Broad band			Zoom		
		Peak	Poly	Global	Peak	Poly	Global
5	Acc	3.22	344.70	357.46	15.23	1410	1430
	Str1	0.93913	89.91	86.75	4.66	447.84	445.04
	Str2	1.37	131.53	132.94	6.18	598.94	577.04
	Str3	1.35	130.25	132.71	6.08	590.57	568.55
	Str4	1.31	129.55	126.86	4.91	488.27	491.27
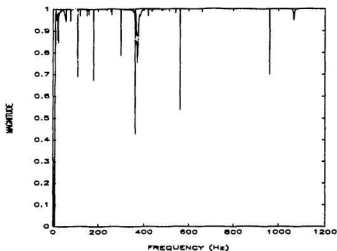
Figure C.1.2.1 Acceleration coherence function of the uncracked plate partially submerged in water
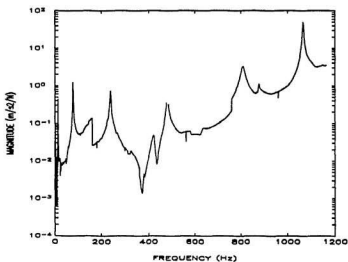
Figure C.1.2.2 Acceleration frequency response function of the uncracked plate partially submerged in water

Figure C.1.2.3   Strain coherence function of the uncracked plate partially submerged in water : strain gage no. 1

Figure C.1.2.4   Strain frequency response function of the uncracked plate partially submerged in water : strain gage no. 1
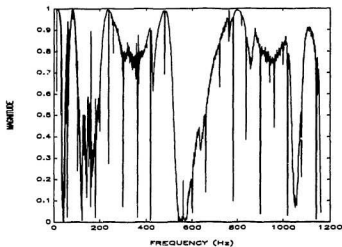
Figure C.1.2.5 Strain coherence function of the uncracked plate partially submerged in water : strain gage no. 2
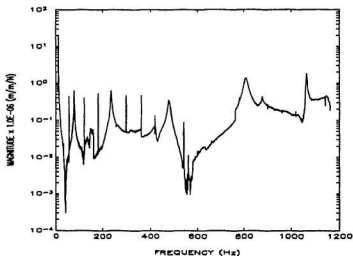
Figure C.1.2.6 Strain frequency response function of the uncracked plate partially submerged in water : strain gage no. 2
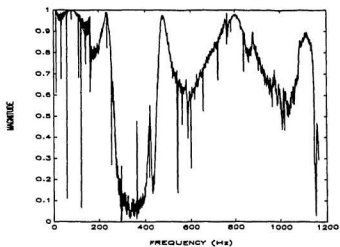
Figure C.1.2.7 Strain coherence function of the uncracked plate partially submerged in water : strain gage no. 3
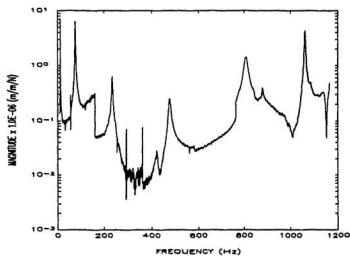
Figure C.1.2.8 Strain frequency response function of the uncracked plate partially submerged in water : strain gage no. 3
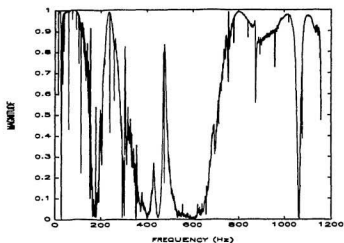
Figure C.1.2.9 Strain coherence function of the uncracked plate partially submerged in water : strain gage no. 4
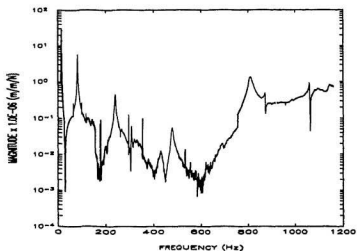
Figure C.1.2.10 Strain frequency response function of the uncracked plate partially submerged in water : strain gage no. 4

C.1.3 Uncracked Plate Fully Submerged in Water

The accelerometer was not working properly when this experiment was carried out. Therefore only the data acquired using strain gages are presented here. Unlike the measurement carried out in air, for fully submergence, the natural frequency shifts by nearly 2% from "broad" to "zoom" frequency band. Several values marked by superscript * in Table C.1.3.5 were not averaged since the difference with the other values in that table were high. These values are extracted from poor strain frequency response function.

Table C.1.3.1 Modal parameters of the uncracked plate fully submerged in water : 1st mode (broad band)

Transducer	Modal Parameters					
	Natural Frequency (Hz)			Damping (%)		
	Peak	Poly	Global	Peak	Poly	Global
Acc	-	-	-	-	-	-
Str1	10.19	10.19	10.19	-	0.53904	0.54138
Str2	10.19	10.19	10.19	-	0.56101	0.55835
Str3	10.19	10.18	10.19	-	0.5600	0.55069
Str4	10.19	10.19	10.17	-	0.54396	0.54326
Average	10.1875			0.5522		
Stand. Dev.	0.0595			0.0078		

Table C.1.3.1.1 Modal parameters of the uncracked plate fully submerged in water : 1st mode (zoom)

Transducer	Modal Parameters					
	Natural Frequency (Hz)			Damping (%)		
	Peak	Poly	Global	Peak	Poly	Global
Acc	-	-	-	-	-	-
Str1	10.17	10.17	10.17	-	0.54570	0.54685
Str2	10.17	10.17	10.17	-	0.51712	0.52853
Str3	10.19	10.17	10.17	-	0.52790	0.53224
Str4	10.17	10.17	10.17	-	0.52071	0.54401
Average	10.1717			0.5329		
Stand. Dev.	0.0055			0.01075		

Table C.1.3.2 Modal parameters of the uncracked plate fully submerged in water : 2nd mode (broad band)

Transducer	Modal Parameters					
	Natural Frequency (Hz)			Damping (%)		
	Peak	Poly	Global	Peak	Poly	Global
Acc	-	-	-	-	-	-
Str1	67.69	67.57	67.45	-	0.87235	0.88927
Str2	67.69	67.56	67.39	-	0.85493	0.90218
Str3	67.75	67.54	67.45	-	0.86302	0.89238
Str4	67.75	67.59	67.45	-	0.88380	0.90101
Average	67.5733			0.8824		
Stand. Dev.	0.1192			0.0163		

218

Table C.1.3.2.1 Modal parameters of the uncracked plate fully submerged in water : 2nd mode (zoom)

Transducer	Modal Parameters					
	Natural Frequency (Hz)			Damping (%)		
	Peak	Poly	Global	Peak	Poly	Global
Acc	-	-	-	-	-	-
Str1	67.38	67.36	67.10	-	0.76815	0.99390
Str2	67.44	67.37	67.18	-	0.75637	0.88948
Str3	67.47	67.38	67.13	-	0.74800	0.95957
Str4	67.38	67.36	67.09	-	0.77011	0.99493
Average	67.3033			0.8601		
Stand. Dev.	0.1314			0.1041		

Table C.1.3.3 Modal parameters of the uncracked plate fully submerged in water : 3rd mode (broad band)

Transducer	Modal Parameters					
	Natural Frequency (Hz)			Damping (%)		
	Peak	Poly	Global	Peak	Poly	Global
Acc	-	-	-	-	-	-
Str1	201.00	200.95	200.98	-	0.97792	1.12000
Str2	201.25	201.04	201.34	-	0.97416	0.93310
Str3	201.25	201.05	201.33	-	0.97570	0.98026
Str4	201.25	201.20	201.19	-	1.18930	1.29000
Average	201.1525			1.05505		
Stand. Dev.	0.1342			0.12078		

Table C.1.3.3.1 Modal parameters of the uncracked plate fully submerged in water : 3rd mode (zoom)

Transducer	Modal Parameters					
	Natural Frequency (Hz)			Damping (%)		
	Peak	Poly	Global	Peak	Poly	Global
Acc	-	-	-	-	-	-
Str1	199.00	199.33	199.71	-	1.14000	1.14000
Str2	198.88	198.87	199.02	-	0.93777	0.93574
Str3	198.72	199.20	199.26	-	0.93961	0.95638
Str4	199.69	201.2	200.42	-	1.11000	1.10000
Average	199.4417			1.03267		
Stand. Dev.	0.6966			0.09089		

Table C.1.3.4 Modal parameters of the uncracked plate fully submerged in water : 4th mode (broad band)

Transducer	Modal Parameters					
	Natural Frequency (Hz)			Damping (%)		
	Peak	Poly	Global	Peak	Poly	Global
Acc	-	-	-	-	-	-
Str1	410.00	409.41	409.63	-	1.46000	1.50000
Str2	409.25	408.90	408.86	-	1.25000	1.23000
Str3	410.00	410.09	410.12	-	1.41000	1.48000
Str4	409.75	407.73	407.52	-	1.30000	1.13000
Average	409.2717			1.345		
Stand. Dev.	0.8456			0.1276		

Table C.1.3.4.1 Modal parameters of the uncracked plate fully submerged in water : 4th mode (zoom)

Transducer	Modal Parameters					
	Natural Frequency (Hz)			Damping (%)		
	Peak	Poly	Global	Peak	Poly	Global
Acc	-	-	-	-	-	-
Str1	409.68	409.92	408.94	-	1.82000	1.74000
Str2	409.38	409.17	408.94	-	1.36000	1.30000
Str3	409.19	409.52	409.34	-	1.76000	1.80000
Str4	409.56	408.92	408.84	-	1.73000	1.70000
Average	409.20			1.65125		
Stand. Dev.	0.4180			0.18944		

Table C.1.3.5 Modal parameters of the uncracked plate fully submerged in water : 5th mode (broad band)

Transducer	Modal Parameters					
	Natural Frequency (Hz)			Damping (%)		
	Peak	Poly	Global	Peak	Poly	Global
Acc	-	-	-	-	-	-
Str1	682.75	683.27	683.25	-	1.47000	1.47000
Str2	682.75	684.32*	683.88*	-	1.61000	1.59000
Str3	682.25	684.45*	679.71*	-	1.57000	1.57000
Str4	682.50	681.22	682.88	-	1.52000	1.51000
Average	682.7692			1.53625		
Stand. Dev.	1.2603			0.0517		

Table C.1.3.5.1 Modal parameters of the uncracked plate fully submerged in water : 5th mode (zoom)

Transducer	Modal Parameters					
	Natural Frequency (Hz)			Damping (%)		
	Peak	Poly	Global	Peak	Poly	Global
Acc	-	-	-	-	-	-
Str1	670.63	670.75	670.60	-	1.75000	1.77000
Str2	670.50	670.37	670.70	-	1.71000	1.75000
Str3	669.88	670.00	670.71	-	1.72000	1.74000
Str4	670.00	670.23	670.58	-	1.78000	1.92000
Average	670.4125			1.7675		
Stand. Dev.	0.2975			0.0616		

Table C.1.3.6 Peak response magnitudes of the uncracked plate fully submerged in water : 1st mode

Mode	Sensor	Peak Magnitudes (m/m/N x 10^{-6})					
		Broad band			Zoom		
		Peak	Poly	Global	Peak	Poly	Global
1	Acc	-	-	-	-	-	-
	Str1	18.19	14.27	13.06	27.82	15.25	15.59
	Str2	16.50	12.63	11.43	24.59	13.45	13.59
	Str3	5.94	4.38	4.28	8.12	4.63	4.63
	Str4	26.18	18.63	17.39	34.95	19.58	20.03

Table C.1.3.7   Peak response magnitude of the uncracked plate fully submerged in water : 2nd mode

Mode	Sensor	Peak Magnitudes (ms^{-2}/N) and $(m/m/N \times 10^{-6})$					
		Broad band			Zoom		
		Peak	Poly	Global	Peak	Poly	Global
2	Acc	-	-	-	-	-	-
	Str1	26.44	187.19	184.18	2.93	18.57	20.74
	Str2	3.53	24.85	25.01	0.38759	2.42	2.59
	Str3	41.87	295.32	294.66	4.82	29.72	33.11
	Str4	37.21	268.24	263.39	4.20	26.76	29.82

Table C.1.3.8   Peak response magnitudes of the uncracked plate fully submerged in water : 3rd mode

Mode	Sensor	Peak Magnitudes $(m/m/N \times 10^{-6})$					
		Broad band			Zoom		
		Peak	Poly	Global	Peak	Poly	Global
3	Acc	-	-	-	-	-	-
	Str1	0.19423	3.8	4.41	0.21621	3.82	4.17
	Str2	0.62043	11.27	11.69	0.65123	12.26	12.65
	Str3	0.66832	12.40	13.60	0.72071	13.54	13.89
	Str4	0.30925	6.51	7.62	0.34122	11.54	4.57

Table C.1.3.9   Peak response magnitudes of the uncracked plate fully submerged in water : 4th mode

Mode	Sensor	Peak Magnitudes (m/m/N x 10⁻⁶)					
		Broad band			Zoom		
		Peak	Poly	Global	Peak	Poly	Global
4	Acc	-	-	-	-	-	-
	Str1	0.11219	9.72	10.28	0.07975	8.78	8.02
	Str2	0.39129	25.24	24.77	0.27248	29.62	26.40
	Str3	0.35216	22.72	22.24	0.24211	26.68	23.74
	Str4	0.08524	5.81	5.16	0.06234	9.91	11.83

Table C.1.3.10   Peak response magnitudes of the uncracked plate fully submerged in water : 5th mode

Mode	Sensor	Peak Magnitudes (m/m/N x 10⁻⁶)					
		Broad band			Zoom		
		Peak	Poly	Global	Peak	Poly	Global
5	Acc	-	-	-	-	-	-
	Str1	0.26033	32.92	32.24	0.16041	22.00	22.46
	Str2	0.33880	43.27	41.31	0.18566	23.81	24.35
	Str3	0.32047	40.88	39.43	0.17157	17.67	18.50
	Str4	0.26309	29.12	28.34	0.13630	17.35	20.12
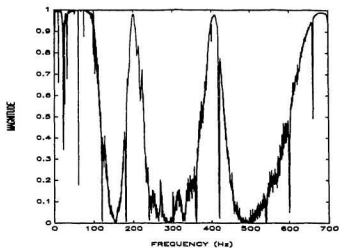
Figure C.1.3.1 Strain coherence function of the uncracked plate fully submerged in water : strain gage no. 1
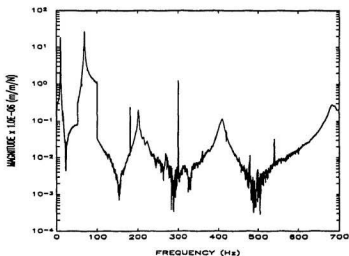
Figure C.1.3.2 Strain frequency response function of the uncracked plate fully submerged in water : strain gage no. 1
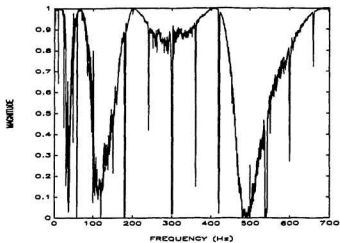
Figure C.1.3.3 Strain coherence function of the ' cracked plate fully submerged in water : strain gage no. 2
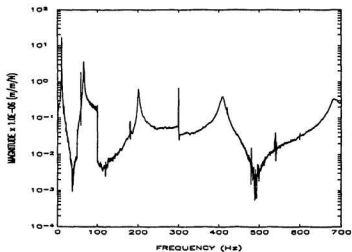
Figure C.1.3.4 Strain frequency response function of the uncracked plate fully submerged in water : strain gage no. 2
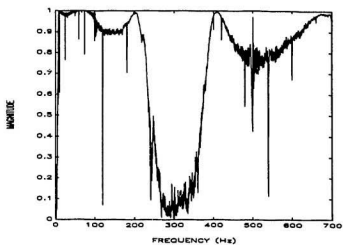
Figure C.1.3.5 Strain coherence function of the uncracked plate fully submerged in water : strain gage no. 3
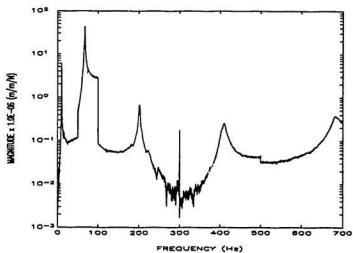
Figure C.1.3.6 Strain frequency response function of the uncracked plate fully submerged in water : strain gage no. 3
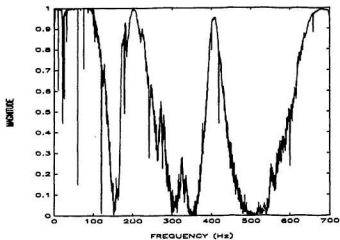
Figure C.1.3.7 Strain coherence function of the uncracked plate fully submerged in water : strain gage no. 4
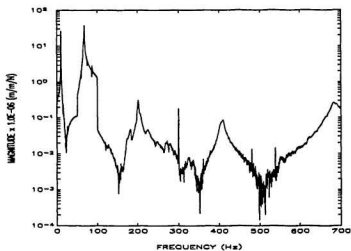
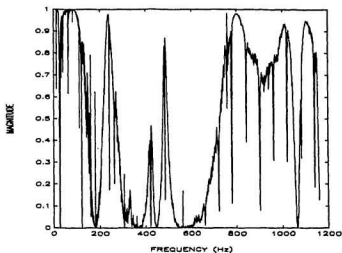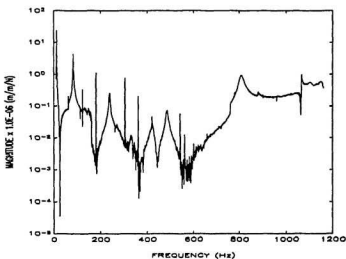**Figure C.1.3.8** Strain frequency response function of the uncracked plate fully submerged in water : strain gage no. 4

C.2 2x1/32" Cracked Plate

The response of the plate is measured only in air, due to time limitation; the results are given in tables of subsection C.2.1. The average and standard deviation of the natural frequencies and damping are given in the last two rows of the tables; values in the brackets are those obtained using accelerometer.

C.2.1 2x1/32" Cracked Plate in Air

Natural frequency and damping are given in Tables C.2.1.1 to C.2.1.5; peak response magnitudes are tabulated in Tables C.2.1.6 to C.2.1.10. Frequency response function and coherence function are shown in Figures C.2.1.1 to C.2.1.10.

Table C.2.1.1   Modal parameters of the 2x1/32" cracked plate in air : 1st mode (broad band)

Transducer	Modal Parameters					
	Natural Frequency (Hz)			Damping (%)		
	Peak	Poly	Global	Peak	Poly	Global
Acc	17.06	17.06	17.07	-	0.25217	0.25227
Str1	17.06	17.06	17.06	-	0.27491	0.27496
Str2	17.06	17.05	17.05	-	0.26443	0.26474
Str3	17.06	17.05	17.07	-	0.26088	0.26027
Str4	17.06	17.05	17.05	-	0.25451	0.25458
Average	17.0567 (17.0633)			0.2637 (0.2522)		
Stand. Dev.	0.0062 (0.0047)			0.0074 (0.00005)		

Table C.2.1.1.1 Modal parameters of the 2x1/32" cracked plate in air : 1ˢᵗ mode (zoom)

Transducer	Modal Parameters					
	Natural Frequency (Hz)			Damping (%)		
	Peak	Poly	Global	Peak	Poly	Global
Acc	17.00	17.01	17.02	-	0.17061	0.17045
Str1	17.00	17.01	17.02	-	0.19351	0.19808
Str2	17.00	17.01	17.00	-	0.17757	0.18834
Str3	16.97	17.00	17.01	-	0.17527	0.18605
Str4	16.97	17.00	17.00	-	0.18427	0.19098
Average	16.9992 (17.0167)			0.1868 (0.1703)		
Stand. Dev.	0.0144 (0.0047)			0.0072 (0.00015)		

Table C.2.1.2 Modal parameters of the 2x1/32" cracked plate in air : 2ⁿᵈ mode (broad band)

Transducer	Modal Parameters					
	Natural Frequency (Hz)			Damping (%)		
	Peak	Poly	Global	Peak	Poly	Global
Acc	106.25	106.24	106.22	-	0.14449	0.14754
Str1	106.25	106.23	106.23	-	0.15701	0.15776
Str2	106.38	106.24	106.22	-	0.16317	0.16269
Str3	106.13	106.24	106.23	-	0.19871	0.19623
Str4	106.13	106.24	106.23	-	0.16716	0.16713
Average	106.2292 (106.2367)			0.1712 (0.1460)		
Stand. Dev.	0.0601 (0.0125)			0.01555 (0.0015)		

Table C.2.1.2.1 Modal parameters of the 2x1/32" cracked plate in air : 2nd mode (zoom)

Transducer	Modal Parameters					
	Natural Frequency (Hz)			Damping (%)		
	Peak	Poly	Global	Peak	Poly	Global
Acc	106.03	106.02	106.02	-	0.16622	0.16660
Str1	106.06	106.02	106.03	-	0.17635	0.17662
Str2	106.00	106.02	106.02	-	0.17609	0.17608
Str3	106.00	106.02	106.02	-	0.18765	0.18916
Str4	106.06	106.02	106.02	-	0.17536	0.17628
Average	106.0242 (106.0233)			0.1792 (0.1664)		
Stand. Dev.	0.0180 (0.0047)			0.0053 (0.0002)		

Table C.2.1.3 Modal parameters of the 2x1/32" cracked plate in air : 3rd mode (broad band)

Transducer	Modal Parameters					
	Natural Frequency (Hz)			Damping (%)		
	Peak	Poly	Global	Peak	Poly	Global
Acc	305.25	305.16	305.16	-	0.15793	0.16370
Str1	305.25	305.12	305.11	-	0.15972	0.15963
Str2	305.25	305.16	305.17	-	0.16569	0.16635
Str3	305.25	305.14	305.15	-	0.17326	0.17418
Str4	305.25	305.11	305.03	-	0.18285	0.18776
Average	305.1658 (305.1900)			0.1712 (0.160815)		
Stand. Div.	0.0684 (0.0424)			0.0096 (0.0029)		

Table C.2.1.3.1   Modal parameters of the 2x1/32" cracked plate in air : 3rd mode (zoom)

| Transducer | Modal Parameters | | | | | |
| | Natural Frequency (Hz) | | | Damping (%) | | |
	Peak	Poly	Global	Peak	Poly	Global
Acc	304.63	304.54	304.60	-	0.20507	0.20052
Str1	304.53	304.49	304.52	-	0.20603	0.21721
Str2	304.53	304.48	304.50	-	0.20448	0.20404
Str3	304.44	304.48	304.51	-	0.20195	0.20854
Str4	304.47	304.47	304.49	-	0.20300	0.21563
Average	304.4925 (304.5900)			0.2076 (0.2030)		
Stand. Div.	0.0259 (0.0374)			0.0054 (0.0023)		

Table C.2.1.4   Modal parameters of the 2x1/32" cracked plate in air : 4th mode (broad band)

| Transducer | Modal Parameters | | | | | |
| | Natural Frequency (Hz) | | | Damping (%) | | |
	Peak	Poly	Global	Peak	Poly	Global
Acc	598.50	598.21	598.13	-	0.28914	0.29037
Str1	598.50	598.33	598.10	-	0.27852	0.27857
Str2	598.50	598.30	598.29	-	0.27903	0.27921
Str3	598.50	598.20	598.22	-	0.26740	0.26737
Str4	598.50	598.27	598.20	-	0.28685	0.28845
Average	598.3258 (598.2800)			0.2782 (0.28975)		
Stand. Dev.	0.1355 (0.15895)			0.0072 (0.0006)		

Table C.2.1.4.1   Modal parameters of the 2x1/32" cracked plate in air : 4th mode (zoom)

Transducer	Modal Parameters					
	Natural Frequency (Hz)			Damping (%)		
	Peak	Poly	Global	Peak	Poly	Global
Acc	598.03	597.82	597.87	-	0.28066	0.27221
Str1	597.94	597.81	598.01	-	0.28580	0.27337
Str2	597.63	597.71	597.91	-	0.28792	0.27046
Str3	598.03	597.76	597.97	-	0.30281	0.29438
Str4	597.84	597.77	597.97	-	0.29426	0.30439
Average	597.8625 (597.9067)			0.2892 (0.2764)		
Stand. Dev.	0.12275 (0.0896)			0.0116 (0.0042)		

Table C.2.1.5   Modal parameters of the 2x1/32" cracked plate in air : 5th mode (broad band)

Transducer	Modal Parameters					
	Natural Frequency (Hz)			Damping (%)		
	Peak	Poly	Global	Peak	Poly	Global
Acc	963.00	962.41	962.24	-	0.41610	0.41681
Str1	963.00	962.55	962.14	-	0.41215	0.41205
Str2	963.00	962.61	962.32	-	0.41428	0.41434
Str3	963.00	962.58	962.23	-	0.41240	0.41277
Str4	963.00	962.68	962.38	-	0.41628	0.41798
Average	962.6242 (962.5500)			0.4140 (0.41645)		
Stand. Dev.	0.3052 (0.3257)			0.0020 (0.00035)		

Table C.2.1.5.1 Modal parameters of the 2x1/32" cracked plate in air : 5th mode (zoom)

Transducer	Modal Parameters					
	Natural Frequency (Hz)			Damping (%)		
	Peak	Poly	Global	Peak	Poly	Global
Acc	962.88	962.96	962.83	-	0.37631	0.37677
Str1	963.38	963.51	963.39	-	0.36753	0.36709
Str2	963.50	963.55	963.57	-	0.37163	0.37738
Str3	963.50	963.61	963.48	-	0.37028	0.37715
Str4	963.63	963.61	963.72	-	0.36639	0.36611
Average	963.5375 (962.8900)			0.37045 (0.3765)		
Stand. Dev.	0.0944 (0.0535)			0.0043 (0.0002)		

Table C.2.1.6 Peak response magnitudes of the 2x1/32" cracked plate in air : 1st mode

Mode	Sensor	Peak Magnitudes (ms⁻²/N) for acc; (m/m/N x 10⁻⁶) for str					
		Broad band			Zoom		
		Peak	Poly	Global	Peak	Poly	Global
1	Acc	1.64	0.89461	0.86371	2.67	0.98186	0.91017
	Str1	36.18	22.60	22.32	52.50	24.52	22.32
	Str2	30.10	18.62	18.28	43.98	20.17	17.60
	Str3	12.46	7.94	7.75	20.00	8.74	7.75
	Str4	45.09	28.01	27.45	67.82	30.38	26.96

Table C.2.1.7 Peak response magnitudes of the 2x1/32" cracked plate in air : 2ⁿᵈ mode

Mode	Sensor	Peak Magnitudes (ms^{-2}/N) for acc; (m/m/N x 10^6) for str					
		Broad band			Zoom		
		Peak	Poly	Global	Peak	Poly	Global
2	Acc	12.24	22.73	22.32	65.21	137.69	136.62
	Str1	25.33	51.77	50.79	135.67	311.86	309.85
	Str2	3.68	9.00	8.68	22.16	51.82	51.42
	Str3	34.12	95.61	93.92	215.43	552.56	552.30
	Str4	28.52	70.55	69.30	169.57	412.69	409.78

Table C.2.1.8 Peak response magnitudes of the 2x1/32" cracked plate in air : 3ʳᵈ mode

Mode	Sensor	Peak Magnitudes (ms^{-2}/N) for acc; (m/m/N x 10^6) for str					
		Broad band			Zoom		
		Peak	Poly	Global	Peak	Poly	Global
3	Acc	6.40	39.11	38.64	10.41	69.83	66.49
	Str1	0.13550	0.85726	0.83498	0.17978	1.32	1.35
	Str2	0.25962	1.69	1.65	0.38643	2.81	2.79
	Str3	0.32829	2.20	2.16	0.49778	3.63	3.68
	Str4	0.17810	1.27	1.26	0.27358	2.01	2.07
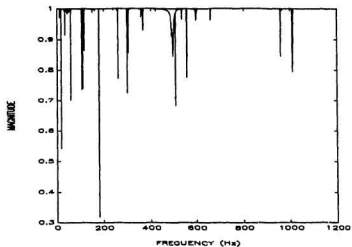
Figure C.2.1.1 Acceleration coherence function of the 2x1/32" cracked plate in air
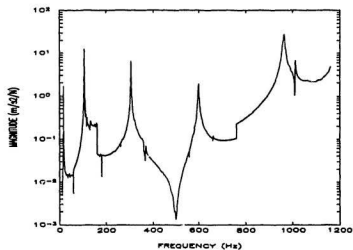
Figure C.2.1.2 Acceleration frequency response function of the 2x1/32" cracked plate in air

Table C.2.1.9 Peak response magnitudes of the 2x1/32" cracked plate in air : 4th mode

Mode	Sensor	Peak Magnitudes (ms^{-2}/N) for acc; (m/m/N x 10^{-6}) for str					
		Broad band			Zoom		
		Peak	Poly	Global	Peak	Poly	Global
4	Acc	1.84	39.14	38.37	2.38	48.59	46.88
	Str1	0.20704	4.24	4.16	0.29793	6.26	5.93
	Str2	1.01	20.89	20.52	1.21	25.05	23.14
	Str3	1.00	19.85	19.46	1.15	23.92	22.10
	Str4	0.15456	3.13	3.06	0.22496	4.76	4.88

Table C.2.1.10 Peak response magnitudes of the 2x1/32" cracked plate in air : 5th mode

Mode	Sensor	Peak Magnitudes (ms^{-2}/N) for acc; (m/m/N x 10^{-6}) for str					
		Broad band			Zoom		
		Peak	Poly	Global	Peak	Poly	Global
5	Acc	27.15	1350	1350	132.81	5910	5930
	Str1	6.68	323.34	320.24	38.52	1640	1590
	Str2	9.52	464.89	459.34	45.42	1970	1960
	Str3	12.55	608.30	602.36	62.13	2660	2650
	Str4	6.51	315.59	310.66	36.33	1550	1500
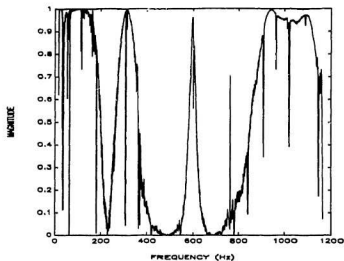
Figure C.2.1.3   Strain coherence function of the 2x1/32" cracked plate in air : strain gage no.1
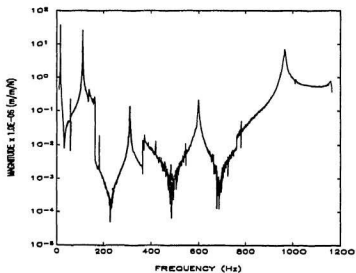
Figure C.2.1.4   Strain frequency response function of the 2x1/32" cracked plate in air : strain gage no. 1
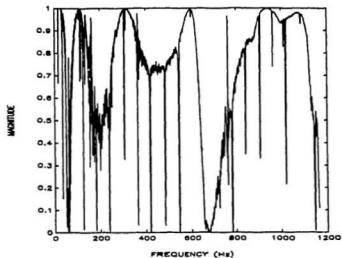
Figure C.2.1.5 Strain coherence function of the 2x1/32" cracked plate in air : strain gage no. 2
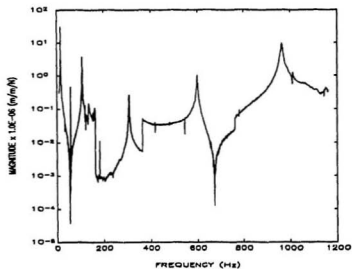
Figure C.2.1.6 Strain frequency response function of the 2x1/32" cracked plate in air : strain gage no. 2
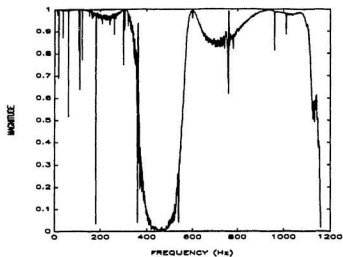
Figure C.2.1.7   Strain coherence function of the 2x1/32" cracked plate in air : strain gage no. 3
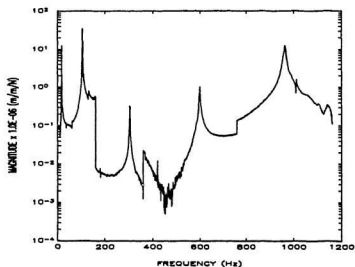
Figure C.2.1.8   Strain frequency response function of the 2x1/32" cracked plate in air : strain gage no. 3
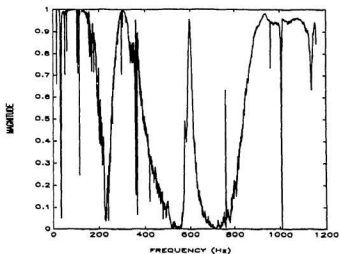
Figure C.2.1.9 Strain coherence function of the 2x1/32" cracked plate in air : strain gage no. 4
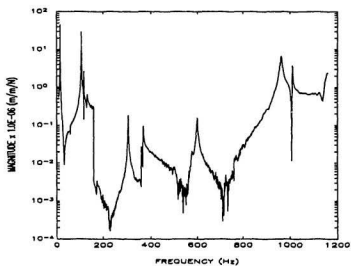
Figure C.2.1.10 Strain frequency response function of the 2x1/32" cracked plate in air : strain gage no. 4

C.2 2x3/32" Cracked Plate

The 2x3/32" cracked plate was tested in air and in two water levels. The results are given in three subsections; these subsections give the experimental result in air and in partial/full submergence in water, respectively.

C.3.1 2x3/32" Cracked Plate in Air

In this experiment, it was found that the strain frequency response function for strain number 4 was very poor in the fourth mode (see Table C.3.1.4 in str4 row). Although the natural frequency was close to the other sensor locations in the three fits methods, the damping values were a little higher than those obtained from the other sensor locations. These damping values are excluded in the averaging process.

Table C.3.1.1   Modal parameters of the 2x3/32" cracked plate in air : 1ˢᵗ mode (broad band)

Transducer	Modal Parameters					
	Natural Frequency (Hz)			Damping (%)		
	Peak	Poly	Global	Peak	Poly	Global
Acc	16.94	16.93	16.93	-	0.27211	0.27292
Str1	16.94	16.93	16.93	-	0.27423	0.27761
Str2	16.94	16.93	16.93	-	0.28373	0.28976
Str3	16.94	16.93	16.93	-	0.28205	0.28394
Str4	16.94	16.93	16.94	-	0.26473	0.27797
Average	16.9333 (16.9333)			0.27925 (0.2725)		
Stand. Dev.	0.0047 (0.0047)			0.0071 (0.0004)		

Table C.3.1.1.1   Modal parameters of the 2x3/32" cracked plate in air : 1ˢᵗ mode (zoom)

| Transducer | Modal Parameters | | | | | |
| | Natural Frequency (Hz) | | | Damping (%) | | |
	Peak	Poly	Global	Peak	Poly	Global
Acc	17.00	16.97	16.98	-	0.21430	0.21259
Str1	16.91	16.90	16.90	-	0.22520	0.23548
Str2	16.91	16.91	16.91	-	0.21978	0.22845
Str3	16.94	16.96	16.97	-	0.22711	0.22703
Str4	16.91	16.91	16.19	-	0.23362	0.24522
Average	16.9200 (16.9833)			0.2302 (0.2134)		
Stand. Dev.	0.0224 (0.0125)			0.0073 (0.00085)		

Table C.3.1.2   Modal parameters of the 2x3/32" cracked plate in air : 2ⁿᵈ mode (broad band)

| Transducer | Modal Parameters | | | | | |
| | Natural Frequency (Hz) | | | Damping (%) | | |
	Peak	Poly	Global	Peak	Poly	Global
Acc	109.00	109.10	109.00	-	0.16973	0.17638
Str1	109.00	109.02	109.00	-	0.16639	0.17441
Str2	109.00	108.99	108.99	-	0.18117	0.17936
Str3	109.00	109.02	109.00	-	0.18146	0.18772
Str4	109.00	109.10	109.00	-	0.16885	0.17464
Average	109.0100 (109.0333)			0.17675 (0.17305)		
Stand. Dev.	0.0286 (0.0471)			0.0066 (0.0033)		

Table C.3.1.2.1 Modal parameters of the 2x3/32" cracked plate in air : 2nd mode (zoom)

Transducer	Modal Parameters					
	Natural Frequency (Hz)			Damping (%)		
	Peak	Poly	Global	Peak	Poly	Global
Acc	108.69	108.71	108.71	-	0.17407	0.17352
Str1	108.75	108.72	108.72	-	0.17120	0.17113
Str2	108.78	108.71	108.71	-	0.18017	0.18015
Str3	108.66	108.70	108.70	-	0.19036	0.19006
Str4	108.66	108.71	108.71	-	0.17872	0.17858
Average	108.7108 (108.7033)			0.18005 (0.1738)		
Stand. Dev.	0.0315 (0.0094)			0.0068 (0.0003)		

Table C.3.1.3 Modal parameters of the 2x3/32" cracked plate in air : 3rd mode (broad band)

Transducer	Modal Parameters					
	Natural Frequency (Hz)			Damping (%)		
	Peak	Poly	Global	Peak	Poly	Global
Acc	310.75	310.76	310.71	-	0.30618	0.32125
Str1	311.00	311.08	311.04	-	0.49374	0.49391
Str2	311.00	311.17	311.18	-	0.47036	0.46648
Str3	311.00	311.13	311.20	-	0.46226	0.44586
Str4	311.00	311.11	311.11	-	0.49664	0.51880
Average	311.0850 (310.74)			0.48101 (0.3137)		
Stand. Dev.	0.0729 (0.0216)			0.0221 (0.0075)		

Table C.3.1.3.1 Modal parameters of the 2x3/32" cracked plate in air : 3rd mode (zoom)

Transducer	Modal Parameters					
	Natural Frequency (Hz)			Damping (%)		
	Peak	Poly	Global	Peak	Poly	Global
Acc	310.59	310.66	310.64	-	0.44087	0.44012
Str1	310.66	310.69	310.66	-	0.43772	0.43708
Str2	310.72	310.66	310.66	-	0.42528	0.40406
Str3	310.53	310.60	310.53	-	0.41104	0.41153
Str4	310.69	310.65	310.69	-	0.43159	0.42192
Average	310.6450 (310.6300)			0.4225 (0.4405)		
Stand. Dev.	0.0585 (0.0294)			0.0119 (0.0004)		

Table C.3.1.4 Modal parameters of the 2x3/32" cracked plate in air : 4th mode (broad band)

Transducer	Modal Parameters					
	Natural Frequency (Hz)			Damping (%)		
	Peak	Poly	Global	Peak	Poly	Global
Acc	602.50	602.16	602.17	-	0.98898	0.30578
Str1	602.00	601.93	602.00	-	0.32704	0.31446
Str2	602.00	602.13	602.18	-	0.29656	0.29480
Str3	602.50	601.12	602.01	-	0.30238	0.31206
Str4	602.50*	602.11*	602.03*	-	0.26023*	0.25395*
Average	602.1258 (602.2767)			0.2952 (0.3024)		
Stand. Dev.	0.1807 (0.1580)			0.0241 (0.0034)		

245

Table C.3.1.4.1 Modal parameters of the 2x3/32" cracked plate in air : 4th mode (zoom)

Transducer	Modal Parameters					
	Natural Frequency (Hz)			Damping (%)		
	Peak	Poly	Global	Peak	Poly	Global
Acc	601.84	601.70	601.77	-	0.29476	0.28262
Str1	601.63	601.53	601.63	-	0.27882	0.27147
Str2	601.66	601.60	601.74	-	0.29088	0.28721
Str3	601.66	601.65	601.70	-	0.29070	0.28940
Str4	601.66	601.64	601.84	-	0.29448	0.29920
Average	601.6642 (601.7700)			0.2878 (0.2887)		
Stand. Dev.	0.0716 (0.05715)			0.0082 (0.0061)		

Table C.3.1.5 Modal parameters of the 2x3/32" cracked plate in air : 5th mode (broad band)

Transducer	Modal Parameters					
	Natural Frequency (Hz)			Damping (%)		
	Peak	Poly	Global	Peak	Poly	Global
Acc	967.00	966.93	966.97	-	0.46259	0.46884
Str1	967.00	967.08	967.78	-	0.46284	0.48441
Str2	966.50	967.15	967.30	-	0.50226	0.50687
Str3	967.00	967.16	967.25	-	0.44178	0.44137
Str4	967.00	967.09	967.03	-	0.62521	0.66409
Average	967.1117 (966.9667)			0.51610 (0.465715)		
Stand. Dev.	0.27760 (0.02867)			0.07829 (0.003125)		

Table C.3.1.5.1 Modal parameters of the 2x3/32" cracked plate in air : 5th mode (zoom)

Transducer	Modal Parameters					
	Natural Frequency (Hz)			Damping (%)		
	Peak	Poly	Global	Peak	Poly	Global
Acc	966.00	965.25	966.21	-	0.37550	0.36263
Str1	966.50	966.24	966.25	-	0.36132	0.36239
Str2	966.13	966.12	966.18	-	0.40277	0.40370
Str3	966.38	966.36	966.37	-	0.39478	0.38506
Str4	967.00	966.35	966.35	-	0.38144	0.37031
Average	966.3525 (966.1533)			0.38272 (0.36910)		
Stand. Dev.	0.22335 (0.10965)			0.0159 (0.0065)		

Table C.3.1.6 Peak response magnitudes of the 2x3/32" cracked plate in air : 1st mode

Mode	Sensor	Peak Magnitudes (ms^2/N) for acc; $(m/m/N \times 10^{-6})$ for str					
		Broad band			Zoom		
		Peak	Poly	Global	Peak	Poly	Global
	Acc	1.44	0.88497	0.81527	1.89	0.91928	0.84887
	Str1	31.25	20.35	19.94	52.60	24.29	24.31
1	Str2	25.80	17.58	17.27	46.45	20.91	20.59
	Str3	10.61	7.09	6.73	16.49	8.04	7.47
	Str4	41.13	25.91	25.89	64.38	31.17	30.63

Table C.3.1.7   Peak response magnitudes of the 2x3/32" cracked plate in air : 2nd mode

Mode	Sensor	Peak Magnitudes (ms⁻²/N) for acc; (m/m/N x10⁻⁶) for str					
		Broad band			Zoom		
		Peak	Poly	Global	Peak	Poly	Global
2	Acc	10.52	25.17	25.71	66.87	155.67	155.14
	Str1	24.89	55.70	56.42	150.75	342.43	341.85
	Str2	4.05	10.34	10.25	24.88	62.13	61.90
	Str3	35.34	84.71	85.06	200.32	520.03	518.65
	Str4	34.95	78.23	78.19	200.82	485.98	484.65

Table C.3.1.8   Peak response magnitudes of the 2x3/32" cracked plate in air : 3rd mode

Mode	Sensor	Peak Magnitudes (ms⁻²/N) for acc; (m/m/N x 10⁻⁶) for str					
		Broad band			Zoom		
		Peak	Poly	Global	Peak	Poly	Global
3	Acc	3.98	47.15	48.02	4.16	73.01	73.75
	Str1	0.97387	18.96	18.58	1.58	27.38	26.34
	Str2	1.40	26.09	25.76	2.14	35.61	34.31
	Str3	1.39	25.33	24.60	2.12	35.41	33.68
	Str4	1.53	29.70	30.18	2.35	40.00	39.47

Table C.3.1.9 Peak response magnitudes of the 2x3/32" cracked plate in air : 4ᵗʰ mode

Mode	Sensor	Peak Magnitudes (ms⁻²/N) for acc; (m/m/N x 10⁻⁶) for str					
		Broad band			Zoom		
		Peak	Poly	Global	Peak	Poly	Global
4	Acc	1.79	41.03	41.41	2.46	53.19	50.76
	Str1	0.06308	1.57	1.46	0.33093	6.78	6.59
	Str2	0.9870	21.74	21.51	1.39	29.96	29.34
	Str3	0.59595	13.70	13.83	1.02	21.47	21.25
	Str4	0.14956	1.31*	1.32*	0.22010	4.96	5.02

Table C.3.1.10 Peak response magnitudes of the 2x3/32" cracked plate in air : 5ᵗʰ mode

Mode	Sensor	Peak Magnitudes (ms⁻²/N) for acc; (m/m/N x 10⁻⁶) for str					
		Broad band			Zoom		
		Peak	Poly	Global	Peak	Poly	Global
5	Acc	24.12	1320	1280	120.58	4710	4470
	Str1	4.96	272.39	271.26	21.94	886.07	889.46
	Str2	7.79	458.13	438.93	32.24	1450	1450
	Str3	7.47	386.30	372.76	42.31	1780	1720
	Str4	4.50	330.14	331.27	33.54	959.54	913.22
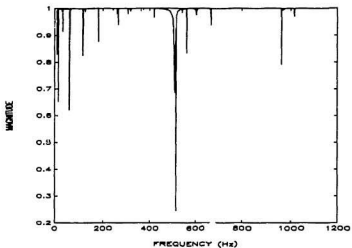
Figure C.3.1.1 Acceleration coherence function of the 2x3/32" cracked plate in air
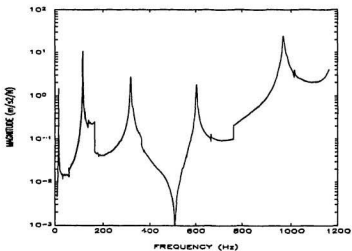
Figure C.3.1.2 Acceleration frequency response function of the 2x3/32" cracked plate in air
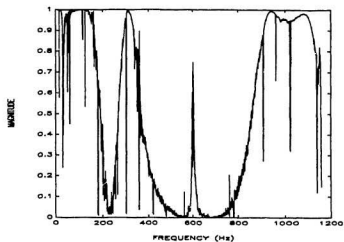
Figure C.3.1.3 Strain coherence function of the 3x3/32" cracked plate in air : strain gage no. 1
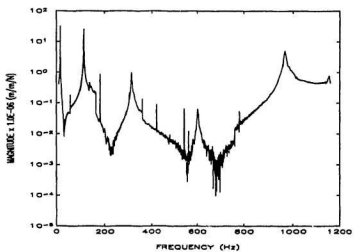
Figure C.3.1.3 Strain frequency response function of the 2x3/32" cracked plate in air : strain gage no. 1

251
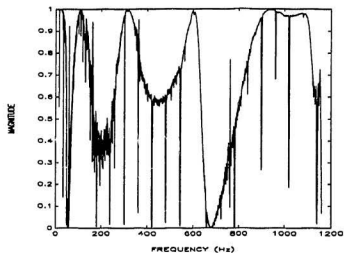
Figure C.3.1.5 Strain coherence function of the 2x3/32" cracked plate in air : strain gage no. 2
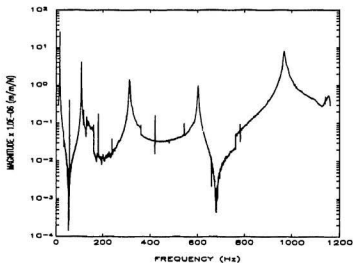
Figure C.3.1.6 Strain frequency response function of the 2x3/32" cracked plate in air : strain gage no. 2
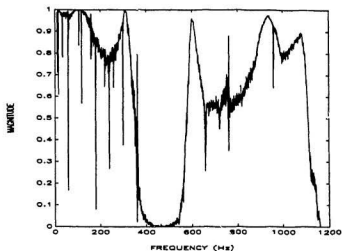
Figure C.3.1.7 Strain coherence function of the 2x3/32" cracked plate in air :
strain gage no. 3
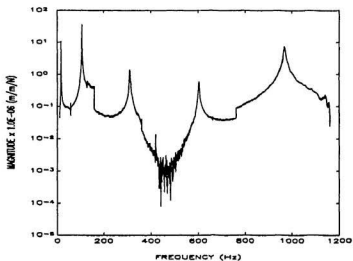
Figure C.3.1.8 Strain frequency response function of the 2x3/32" cracked plate in air :
strain gage no. 3

253
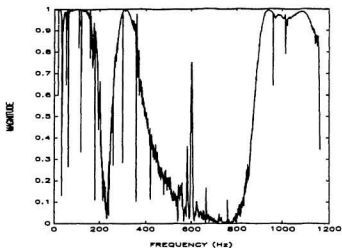
Figure C.3.1.9 Strain coherence function of the 2x3/32" cracked plate in air :
strain gage no. 4
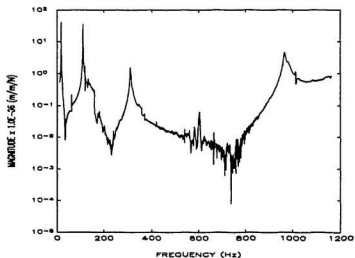
Figure C.3.1.10 Strain frequency response function of the 2x3/32" cracked plate in air :
strain gage no. 4

254

C.3.2 2x3/32"Cracked Plate Partially Submerged in Water

Values that were obtained from strain gages number one and four in the fourth mode, using zoom frequency band (see Table C.3.2.4.1), are not used since these values are too low compared with the others.

Table C.3.2.1   Modal parameters of the 2x3/32" cracked plate partially submerged in water : 1st mode (broad band)

Transducer	Modal Parameters					
	Natural Frequency (Hz)			Damping (%)		
	Peak	Poly	Global	Peak	Poly	Global
Acc	12.44	12.41	12.41	-	0.60235	0.60714
Str1	12.38	12.41	12.41	-	0.54130	0.57257
Str2	12.38	12.40	12.41	-	0.53888	0.57455
Str3	12.38	12.41	12.41	-	0.55180	0.56829
Str4	12.38	12.40	12.41	-	0.53616	0.56935
Average	12.3983 (12.4200)			0.5566 (0.60475)		
Stand. Dev.	0.0134 (0.0141)			0.0153 (0.0024)		

Table C.3.2.1.1 Modal parameters of the 2x3/32" cracked plate partially submerged in water : 1ˢᵗ mode (zoom)

Transducer	Modal Parameters					
	Natural Frequency (Hz)			Damping (%)		
	Peak	Poly	Global	Peak	Poly	Global
Acc	12.44	12.42	12.42	-	0.42162	0.42244
Str1	12.41	12.41	12.41	-	0.43258	0.46895
Str2	12.41	12.40	12.41	-	0.43260	0.46650
Str3	12.41	12.40	12.41	-	0.45578	0.48491
Str4	12.00	12.40	12.41	-	0.45162	0.47445
Average	12.3733 (12.4267)			0.4584 (0.4220)		
Stand. Dev.	0.1126 (0.0094)			0.0178 (0.0004)		

Table C.3.2.2 Modal parameters of the 2x3/32" cracked plate partially submerged in water : 2ⁿᵈ mode (broad band)

Transducer	Modal Parameters					
	Natural Frequency (Hz)			Damping (%)		
	Peak	Poly	Global	Peak	Poly	Global
Acc	81.63	81.71	81.74	-	0.80784	0.80677
Str1	81.63	81.71	81.76	-	0.80718	0.81792
Str2	81.63	81.75	81.78	-	0.82038	0.81943
Str3	81.50	81.74	81.76	-	0.82584	0.82291
Str4	81.50	81.75	81.77	-	0.82961	0.82963
Average	81.6900 (81.6933)			0.8216 (0.8073)		
Stand. Dev.	0.0974 (0.0464)			0.0069 (0.0005)		

256

Table C.3.2.2.1 Modal parameters of the 2x3/32" cracked plate partially submerged in water : 2nd mode (zoom)

Transducer	Modal Parameters					
	Natural Frequency (Hz)			Damping (%)		
	Peak	Poly	Global	Peak	Poly	Global
Acc	82.19	82.14	82.11	-	0.50456	0.55966
Str1	82.19	82.14	82.11	-	0.49492	0.55225
Str2	82.06	82.13	82.10	-	0.48132	0.52833
Str3	82.19	82.11	82.09	-	0.51259	0.56675
Str4	82.06	82.13	82.12	-	0.48600	0.53455
Average	82.1192 (82.1467)			0.5196 (0.5321)		
Stand. Dev.	0.0400 (0.0330)			0.0293 (0.02755)		

Table C.3.2.3 Modal parameters of the 2x3/32" cracked plate partially submerged in water . 3rd mode (broad band)

Transducer	Modal Parameters					
	Natural Frequency (Hz)			Damping (%)		
	Peak	Poly	Global	Peak	Poly	Global
Acc	240.75	239.33	239.65	-	0.85320	0.78750
Str1	240.75	239.71	239.73	-	0.75857	0.79330
Str2	241.00	239.26	239.28	-	0.76129	0.77131
Str3	240.75	239.30	239.29	-	0.76124	0.76326
Str4	241.00	239.66	239.66	-	0.84310	0.82734
Average	239.9575 (239.9100)			0.7849 (0.8203)		
Stand. Dev.	0.6719 (0.6082)			0.0311 (0.0328)		

Table C.3.2.3.1 Modal parameters of the 2x3/32" cracked plate partially submerged in water : 3rd mode (zoom)

Transducer	Modal Parameters					
	Natural Frequency (Hz)			Damping (%)		
	Peak	Poly	Global	Peak	Poly	Global
Acc	240.81	241.00	241.04	-	1.11665	1.12543
Str1	240.75	240.84	240.68	-	1.11580	1.11567
Str2	240.88	240.98	240.83	-	1.11578	1.11624
Str3	240.63	240.89	240.85	-	1.11561	1.11964
Str4	240.66	240.90	240.90	-	1.11606	1.12025
Average	240.8158 (240.9500)			1.1169 (1.1210)		
Stand. Dev.	0.1058 (0.1003)			0.0018 (0.0044)		

Table C.3.2.4 Modal parameters of the 2x3/32" cracked plate partially submerged in water : 4th mode (broad band)

Transducer	Modal Parameters					
	Natural Frequency (Hz)			Damping (%)		
	Peak	Poly	Global	Peak	Poly	Global
Acc	449.50	448.99	449.27	-	1.19	1.20
Str1	449.50	449.73	449.07	-	1.20	1.25
Str2	448.50	447.81	448.42	-	1.37	1.36
Str3	449.00	448.76	448.37	-	1.20	1.16
Str4	450.00	450.06	449.90	-	1.32	1.30
Average	449.0933 (449.2533)			1.2700 (1.1950)		
Stand. Dev.	0.71145 (0.2085)			0.0740 (0.0050)		

Table C.3.2.4.1 Modal parameters of the 2x3/32" cracked plate partially submerged in water : 4ᵗʰ mode (zoom)

Transducer	Modal Parameters					
	Natural Frequency (Hz)			Damping (%)		
	Peak	Poly	Global	Peak	Poly	Global
Acc	465.38	465.58	465.59	-	1.16	1.20
Str1	465.00*	464.49*	464.71*	-	0.73120*	0.72927*
Str2	464.13	464.61	464.67	-	1.06	1.04
Str3	464.19	464.14	464.08	-	1.03	1.07
Str4	465.00*	465.20*	464.98*	-	0.72919*	0.88715*
Average	464.60 (465.5167)			1.05 (1.18)		
Stand. Dev.	0.3791 (0.0967)			0.01581 (0.02)		

Table C.3.2.5 Modal parameters of the 2x3/32" cracked plate partially submerged in water : 5ᵗʰ mode (broad band)

Transducer	Modal Parameters					
	Natural Frequency (Hz)			Damping (%)		
	Peak	Poly	Global	Peak	Poly	Global
Acc	807.50	808.52	808.55	-	1.15	1.08
Str1	808.00	808.98	808.87	-	0.80356	0.80162
Str2	809.00	807.43	807.45	-	1.10	1.10
Str3	806.50	807.00	807.18	-	1.09	1.09
Str4	808.50	806.57	807.23	-	1.05	1.05
Average	807.7258 (808.1900)			1.01065 (1.1150)		
Stand. Dev.	0.8781 (0.4880)			0.1216 (0.0350)		

Table 3.2.5.1 Modal parameters of the 2x3/32" cracked plate partially submerged in water : 5ᵗʰ mode (zoom)

Transducer	Modal Parameters					
	Natural Frequency (Hz)			Damping (%)		
	Peak	Poly	Global	Peak	Poly	Global
Acc	806.50	806.50	806.49	-	1.00	1.00
Str1	806.00	805.50	806.20	-	0.96092	0.96031
Str2	805.00	804.62	805.16	-	0.99168	0.99190
Str3	803.50	803.67	803.57	-	1.07	1.08
Str4	804.50	804.93	803.42	-	0.97195	0.97744
Average	804.5058 (806.4967)			1.0005 (1.000)		
Stand. Dev.	1.0418 (0.0047)			0.0445 (0.0000)		

Table C.3.2.6 Peak response magnitudes of the 2x3/32" cracked plate partially submerged in water : 1ˢᵗ mode

Mode	Sensor	Peak Magnitudes (ms^{-2}/N) for acc; $(m/m/N \times 10^{-6})$ for str					
		Broad band			Zoom		
		Peak	Poly	Global	Peak	Poly	Global
1	Acc	0.47143	0.46154	0.46189	0.51796	0.34784	0.33979
	Str1	17.04	16.72	17.08	24.68	17.12	17.38
	Str2	14.91	14.26	14.62	21.85	14.80	15.02
	Str3	5.22	5.26	5.52	7.85	5.50	5.50
	Str4	22.21	21.40	21.89	32.56	22.48	22.46

Table C.3.2.7   Peak response magnitudes of the 2x3/32" cracked plate partially submerged in water : 2ⁿᵈ mode

Mode	Sensor	Peak Magnitudes (ms²/N) for acc; (m/m/N x 10⁻⁶) for str					
		Broad band			Zoom		
		Peak	Poly	Global	Peak	Poly	Global
2	Acc	1.07	8.78	8.76	24.87	126.33	132.22
	Str1	3.92	32.25	32.10	92.19	462.65	486.49
	Str2	0.55754	5.10	5.10	14.17	69.56	72.43
	Str3	5.42	50.55	51.03	134.76	700.73	735.09
	Str4	5.05	46.93	47.28	129.30	635.82	664.32

Table C.3.2.8   Peak response magnitudes of the 2x3/32" cracked plate partially submerged in water : 3ʳᵈ mode

Mode	Sensor	Peak Magnitudes (ms²/N) for acc; (m/m/N x 10⁻⁶) for str					
		Broad band			Zoom		
		Peak	Poly	Global	Peak	Poly	Global
3	Acc	0.48109	17.98	17.39	0.96322	13.22	13.09
	Str1	0.26002	9.25	9.23	0.58678	7.65	7.39
	Str2	0.42008	15.34	14.55	0.72989	9.26	9.64
	Str3	0.41020	14.80	14.38	0.70157	8.90	9.22
	Str4	0.44902	16.63	16.11	0.90890	12.45	12.38

Table C.3.2.9   Peak response magnitudes of the 2x3/32" cracked plate partially submerged in water : 4ᵗʰ mode

Mode	Sensor	Peak Magnitudes (ms⁻²/N) for acc; (m/m/N x 10⁻⁶) for str					
		Broad band			Zoom		
		Peak	Poly	Global	Peak	Poly	Global
4	Acc	0.25203	23.19	21.38	1.04	63.61	67.29
	Str1	0.04030	2.52	2.58	0.11035	2.18*	2.01*
	Str2	0.18614	12.28	11.75	0.73889	46.28	41.59
	Str3	0.11705	12.24	11.64	0.51032	28.24	27.51
	Str4	0.03719	3.14	2.98	0.09871	1.81*	1.62*

Table C.3.2.10   Peak response magnitudes of the 2x3/32" cracked plate partially submerged in water : 5ᵗʰ mode

Mode	Sensor	Peak Magnitudes (ms⁻²/N) for acc; (m/m/N x 10⁻⁶) for str					
		Broad band			Zoom		
		Peak	Poly	Global	Peak	Poly	Global
5	Acc	2.00	216.33	194.04	9.26	842.60	842.18
	Str1	0.58628	39.06	36.97	2.63	227.99	225.39
	Str2	0.70249	70.41	70.32	3.37	303.85	300.22
	Str3	0.93665	92.80	93.08	3.48	344.22	335.65
	Str4	0.51419	47.26	48.31	2.33	199.68	197.78
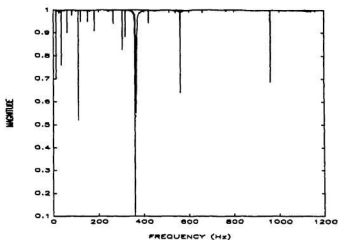
Figure C.3.2.1 Acceleration coherence function of the 2x3/32" cracked plate partially submerged in water
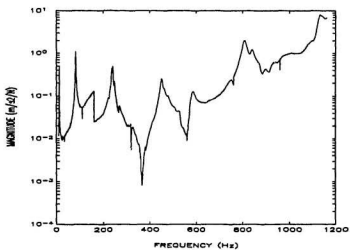
Figure C.3.2.2 Acceleration frequency response function of the 2x3/32" cracked plate partially submerged in water
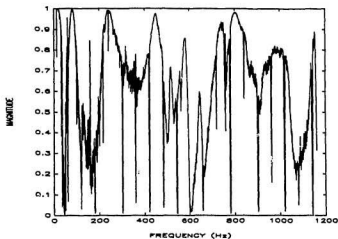
Figure C.3.2.5 Strain coherence function of the 2x3/32" cracked plate partially submerged in water : strain gage no. 2
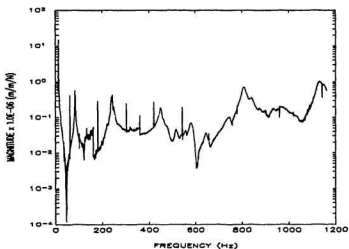
Figure C.3.2.6 Strain frequency response function of the 2x3/32" cracked plate partially submerged in water : strain gage no. 2
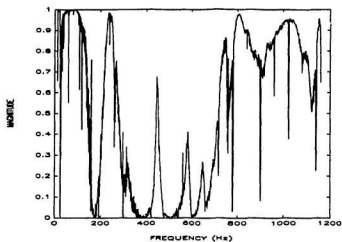
Figure C.3.2.3 Strain coherence function of the 2x3/32" cracked plate partially submerged in water : strain gage no. 1
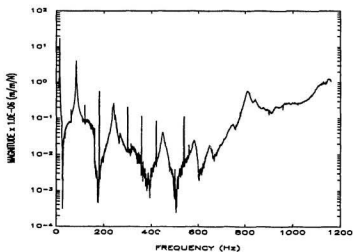
Figure C.3.2.4 Strain frequency response function of the 2x3/32" cracked plate partially submerged in water : strain gage no. 1
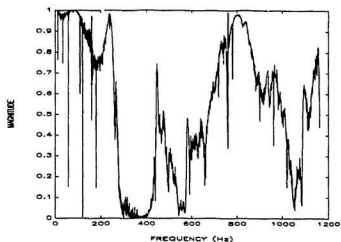
Figure C.3.2.7 Strain coherence function of the 2x3/32" cracked plate partially submerged in water : strain gage no. 3
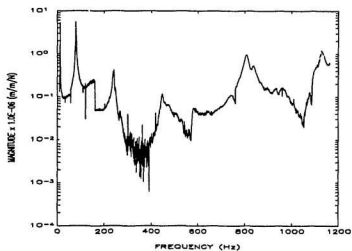
Figure C.3.2.8 Strain frequency response function of the 2x3/32" cracked plate partially submerged in water : strain gage no. 3

266
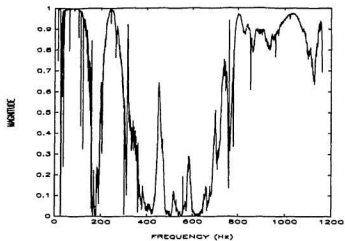
Figure C.3.2.9 Strain coherence function of the 2x3/32" cracked plate partially submerged in water : strain gage no. 4
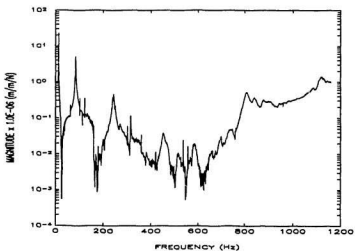
Figure C.3.2.10 Strain frequency response function of the 2x3/32" cracked plate partially submerged in water : strain gage no. 4

C.3.3 2x3/32" Crack Plate Fully Submerged in Water

The values marked by superscript * in Table C.3.3.4 are not averaged due to the same reason given earlier.

Table C.3.3.1   Modal parameters of the 2x3/32" cracked plate fully submerged in water : 1ˢᵗ mode (broad band)

Transducer	Modal Parameters					
	Natural Frequency (Hz)			Damping (%)		
	Peak	Poly	Global	Peak	Poly	Global
Acc	10.19	10.14	10.14	-	0.62957	0.61849
Str1	10.19	10.13	10.13	-	0.59259	0.59514
Str2	10.19	10.14	10.14	-	0.58548	0.58946
Str3	10.19	10.14	10.14	-	0.62756	0.64128
Str4	10.19	10.13	10.14	-	0.59671	0.58961
Average	10.1542 (10.1567)			0.6022 (0.6240)		
Stand. Dev.	0.0256 (0.0236)			0.0192 (0.0055)		

Table C.3.3.1.1 Modal parameters of the 2x3/32" cracked plate fully submerged in water : 1ˢᵗ mode (zoom)

Transducer	Modal Parameters					
	Natural Frequency (Hz)			Damping (%)		
	Peak	Poly	Global	Peak	Poly	Global
Acc	10.11	10.11	10.11	-	0.48639	0.48971
Str1	10.11	10.12	10.12	-	0.46495	0.46653
Str2	10.13	10.12	10.12	-	0.49816	0.47996
Str3	10.13	10.12	10.12	-	0.47993	0.46144
Str4	10.13	10.12	10.12	-	0.47534	0.46853
Average	10.1217 (10.1100)			0.4740 (0.4880)		
Stand. Dev.	0.0055 (0.0000)			0.0109 (0.0017)		

Table C.3.3.2 Modal parameters of the 2x3/32" cracked plate fully submerged in water : 2ⁿᵈ mode (broad band)

Transducer	Modal Parameters					
	Natural Frequency (Hz)			Damping (%)		
	Peak	Poly	Global	Peak	Poly	Global
Acc	69.13	69.08	69.07	-	0.89572	0.91385
Str1	69.13	69.07	69.08	-	0.94172	0.94341
Str2	69.13	69.07	69.06	-	0.94089	0.92124
Str3	69.06	69.05	69.06	-	0.92163	0.95178
Str4	69.13	69.06	69.07	-	0.95225	0.94259
Average	69.0808 (69.0933)			0.9394 (0.9048)		
Stand. Dev.	0.0293 (0.02625)			0.0112 (0.0091)		

Table C.3.3.2.1 Modal parameters of the 2x3/32" cracked plate fully submerged in water : 2nd mode (zoom)

Transducer	Modal Parameters					
	Natural Frequency (Hz)			Damping (%)		
	Peak	Poly	Global	Peak	Poly	Global
Acc	68.84	68.86	68.88	-	0.56317	0.56373
Str1	68.91	68.94	68.96	-	0.54289	0.54275
Str2	68.91	68.94	68.95	-	0.54059	0.54105
Str3	68.91	68.92	68.95	-	0.56505	0.55051
Str4	68.91	68.92	68.96	-	0.54107	0.54145
Average	68.9317 (68.8600)			0.4126 (0.56345)		
Stand. Dev.	0.0195 (0.0163)			0.0079 (0.0003)		

Table C.3.3.3 Modal parameters of the 2x3/32" cracked plate fully submerged in water : 3rd mode (broad band)

Transducer	Modal Parameters					
	Natural Frequency (Hz)			Damping (%)		
	Peak	Poly	Global	Peak	Poly	Global
Acc	203.00	203.32	203.38	-	1.25	1.27
Str1	203.00	203.33	203.43	-	1.29	1.26
Str2	203.00	203.42	203.47	-	1.29	1.26
Str3	203.00	203.42	203.43	-	1.27	1.27
Str4	203.00	203.44	203.48	-	1.25	1.30
Average	203.2850 (203.2333)			1.2737 (1.2600)		
Stand. Dev.	0.2045 (0.1668)			0.0165 (0.0100)		

Table C.3.3.3.1 Modal parameters of the 2x3/32" cracked plate fully submerged in water : 3rd mode (zoom)

Transducer	Modal Parameters					
	Natural Frequency (Hz)			Damping (%)		
	Peak	Poly	Global	Peak	Poly	Global
Acc	203.06	203.30	203.56	-	1.25	1.24
Str1	203.00	203.47	203.45	-	1.27	1.25
Str2	203.31	203.66	203.14	-	1.25	1.27
Str3	202.84	203.40	203.50	-	1.24	1.26
Str4	203.50	203.41	203.66	-	1.26	1.26
Average	203.3617 (203.3067)			1.2575 (1.2450)		
Stand. Dev.	0.24055 (0.2042)			0.0097 (0.0050)		

Table C.3.3.4 Modal parameters of the 2x3/32" cracked plate fully submerged in water : 4th mode (broad band)

Transducer	Modal Parameters					
	Natural Frequency (Hz)			Damping (%)		
	Peak	Poly	Global	Peak	Poly	Global
Acc	402.75	402.63	402.45	-	1.48611	1.48963
Str1	402.50	402.85	402.45	-	1.46808	1.45024
Str2	402.50	402.71	402.65	-	1.47688	1.47621
Str3	403.25	402.95	402.83	-	1.45758	1.47958
Str4	404.00*	404.47*	402.47	-	0.51379*	0.54329*
Average	402.7160 (402.6100)			1.4681 (1.4879)		
Stand. Dev.	0.2449 (0.1233)			0.0108 (0.0018)		

Table C.3.3.4.1 Modal parameters of the 2x3/32" cracked plate fully submerged in water : 4ᵗʰ mode (zoom)

Transducer	Modal Parameters					
	Natural Frequency (Hz)			Damping (%)		
	Peak	Poly	Global	Peak	Poly	Global
Acc	417.75	417.16	417.03	-	1.58594	1.56821
Str1	417.56	417.52	417.35	-	1.60078	1.59379
Str2	417.50	417.22	417.21	-	1.58325	1.58251
Str3	417.38	417.26	417.21	-	1.58522	1.58275
Str4	417.06	417.07	417.08	-	1.57818	1.58015
Average	417.2875 (417.3133)			1.5857 (1.5770)		
Stand. Dev.	0.1708 (0.3133)			0.0072 (0.0089)		

Table C.3.3.5 Modal parameters of the 2x3/32" cracked plate fully submerged in water : 5ᵗʰ mode (broad band)

Transducer	Modal Parameters					
	Natural Frequency (Hz)			Damping (%)		
	Peak	Poly	Global	Peak	Poly	Global
Acc	741.00	741.86	741.48	-	1.59	1.58
Str1	741.00	741.61	741.55	-	1.57	1.58
Str2	741.00	741.11	741.79	-	1.58	1.56
Str3	741.00	741.14	741.83	-	1.58	1.54
Str4	741.50	741.54	741.70	-	1.57	1.55
Average	741.3975 (741.4467)			1.5662 (1.5850)		
Stand. Dev.	0.3102 (0.3519)			0.0141 (0.0050)		

Table C.3.3.5.1 Modal parameters of the 2x3/32" cracked plate fully submerged in water : 5ᵗʰ mode (zoom)

Transducer	Modal Parameters					
	Natural Frequency (Hz)			Damping (%)		
	Peak	Poly	Global	Peak	Poly	Global
Acc	742.00	742.15	742.02	-	1.58	1.54
Str1	743.13	742.36	742.50	-	1.53	1.54
Str2	741.63	742.06	742.19	-	1.57	1.54
Str3	742.38	742.62	742.51	-	1.52	1.54
Str4	743.25	741.68	741.56	-	1.53	1.59
Average	742.3225 (742.0567)			1.5450 (1.5600)		
Stand. Dev.	0.5190 (0.0665)			0.0218 (0.0200)		

Table C.3.3.6 Peak response magnitudes of the 2x3/32" cracked plate fully submerged in water : 1ˢᵗ mode

Mode	Sensor	Peak Magnitudes (ms⁻²/N) for acc; (m/m/N x 10⁻⁶) for str					
		Broad band			Zoom		
		Peak	Poly	Global	Peak	Poly	Global
1	Acc	0.21461	0.18218	0.17552	0.39338	0.20242	0.20270
	Str1	17.07	14.31	11.71	28.42	14.80	14.64
	Str2	15.21	11.89	10.16	24.23	12.71	12.58
	Str3	5.39	4.31	3.77	8.59	4.48	4.44
	Str4	21.09	17.88	15.36	34.58	18.84	18.62

Table C.3.3.7   Peak response magnitudes of the 2x3/32" cracked plate fully submerged in water : 2nd mode

Mode	Sensor	Peak Magnitudes (ms⁻²/N) for acc; (m/m/N x 10⁻⁶) for str					
		Broad band			Zoom		
		Peak	Poly	Global	Peak	Poly	Global
2	Acc	13.14	38.47	38.41	1.01	3.83	3.82
	Str1	64.59	196.90	196.58	5.15	19.17	19.12
	Str2	9.45	27.96	27.88	0.3785	0.9421	0.8760
	Str3	98.61	300.39	301.64	8.23	29.27	29.18
	Str4	92.25	276.34	274.59	8.02	51.10	50.29

Table C.3.3.8   Peak response magnitudes of the 2x3/32" cracked plate fully submerged in water : 3rd mode

Mode	Sensor	Peak Magnitudes (ms⁻²/N) for acc; (m/m/N x 10⁻⁶) for str					
		Broad band			Zoom		
		Peak	Poly	Global	Peak	Poly	Global
3	Acc	0.37560	9.71	9.87	0.78546	33.82	33.27
	Str1	0.25616	6.79	6.62	0.52131	21.27	22.05
	Str2	0.44029	12.09	11.77	0.87584	38.64	36.21
	Str3	0.47298	12.41	12.49	0.99364	38.19	38.75
	Str4	0.28210	12.57	13.40	0.88674	44.12	47.81

Table C.3.3.9   Peak response magnitudes of the 2x3/32" cracked plate fully submerged in water : 4th mode

Mode	Sensor	Peak Magnitudes (ms⁻²/N) for acc; (m/m/N x 10⁻⁶) for str					
		Broad band			Zoom		
		Peak	Poly	Global	Peak	Poly	Global
4	Acc	0.26084	10.01	9.75	0.41250	18.65	18.71
	Str1	0.03013	1.03	1.04	0.03656	0.98419	0.89633
	Str2	0.24840	9.05	9.09	0.35426	16.46	15.52
	Str3	0.16403	6.02	6.05	0.26443	11.59	11.61
	Str4	0.0236*	0.2659*	0.2695*	0.03005	0.97021	1.02

Table C.3.3.10   Peak response magnitudes of the 2x3/32" cracked plate fully submerged in water : 5th mode

Mode	Sensor	Peak Magnitudes (ms⁻²/N) for acc; (m/m/N x 10⁻⁶) for str					
		Broad band			Zoom		
		Peak	Poly	Global	Peak	Poly	Global
5	Acc	0.32586	37.76	38.60	0.85233	77.51	77.81
	Str1	0.1070*	17.77*	37.58*	0.34534	31.38	31.69
	Str2	0.16834	73.08	38.76	0.44905	41.23	40.27
	Str3	0.18950	81.37	52.18	0.39698	30.70	44.27
	Str4	0.10657	24.65	22.87	0.27423	24.01	24.18
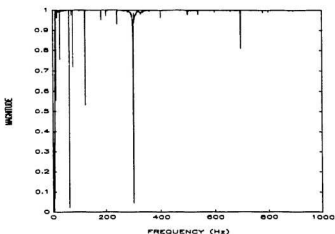
Figure C.3.3.1 Acceleration coherence function of the 2x3/32" cracked plate fully submerged in water
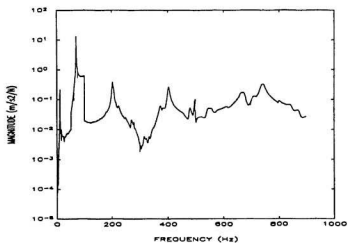
Figure C.3.3.2 Acceleration frequency response function of the 2x3/32" cracked plate fully submerged in water

Figure C.3.3.3 Strain coherence function of the 2x3/32" cracked plate fully submerged in water : strain gage no. 1

Figure C.3.3.4 Strain frequency response function of the 2x3/32" cracked plate fully submerged in water : strain gage no. 1

277
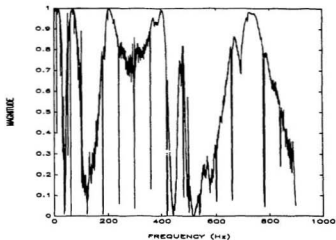
Figure C.3.3.5 Strain coherence function of the 2x3/32" cracked plate fully submerged in water : strain gage no. 2
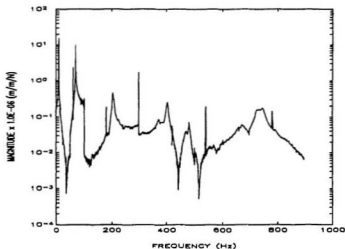
Figure C.3.3.6 Strain frequency response function of the 2x3/32" cracked plate fully submerged in water : strain gage no. 2

278
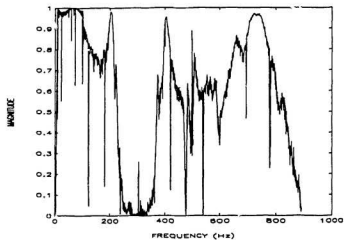
Figure C.3.3.7 Strain coherence function of the 2x3/32" cracked plate fully submerged in water : strain gage no. 3
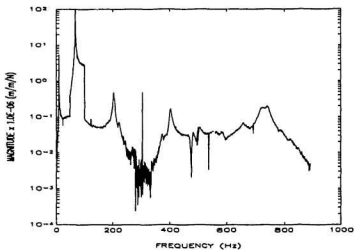
Figure C.3.3.8 Strain frequency response function of the 2x3/32" cracked plate fully submerged in water : strain gage no. 3
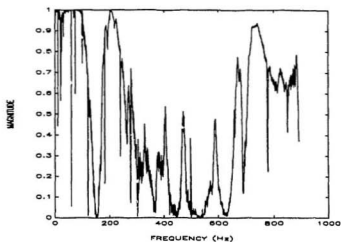
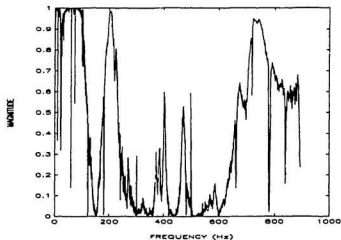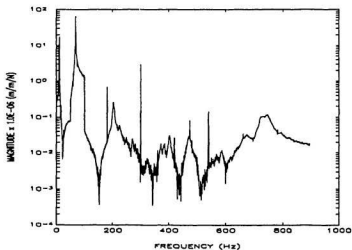**Figure C.3.3.9** Strain coherence function of the 2x3/32" cracked plate fully submerged in water : strain gage no. 4
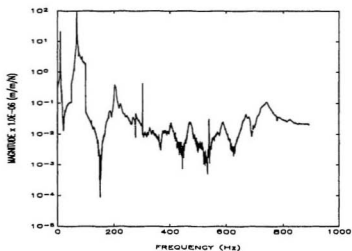
Figure C.3.3.10 Strain frequency response function of the 2x3/32" cracked plate fully submerged in water : strain gage no. 4

Appendix D

In the first part of this Appendix, the peak strain response magnitudes measured by using three strain gages, utilized in the experimental study, are normalized by the largest value of them; and the values are tabulated. In the second part, the peak response magnitudes of the uncracked plate in air computed by taking damping into consideration are given; and the bode plots of the acceleration as well as strain responses are presented.

D.1 Normalized Peak Strain Response Magnitudes

Tables D.1.1 to D.1.7 give the normalized peak strain response magnitudes of cracked and uncracked plates in air, partially submerged and fully submerged in water. The values given were measured from strain gages mounted along the middle of the plates so that the values can be compared with those obtained analytically.

Table D.1.1 Normalized peak strain response magnitudes of the uncracked plate in air

Mode	Sensor	Normalized Peak Magnitudes					
		Broad band			Zoom		
		Peak	Poly	Global	Peak	Poly	Global
1	Str1	1.0	1.0	1.0	1.0	1.0	1.0
	Str2	0.815	0.901	0.914	0.812	0.880	0.975
	Str3	0.2695	0.328	0.332	0.238	0.329	0.359
2	Str1	0.779	0.604	0.6075	0.636	0.631	0.633
	Str2	0.127	0.111	0.1095	0.122	0.116	0.116
	Str3	1.0	1.0	1.0	1.0	1.0	1.0
3	Str1	0.395	0.430	0.430	0.414	0.442	0.401
	Str2	0.924	0.931	0.964	0.920	0.927	0.914
	Str3	1.0	1.0	1.0	1.0	1.0	1.0
4	Str1	0.186	0.197	0.1965	0.238	0.226	0.226
	Str2	1.0	1.0	1.0	1.0	1.0	1.0
	Str3	0.958	0.956	0.957	0.948	0.949	0.950
5	Str1	0.639	0.658	0.653	0.582	0.557	0.536
	Str2	1.0	1.0	1.0	1.0	1.0	1.0
	Str3	0.991	0.970	0.997	0.967	0.986	0.995

Table D.1.2 Normalized peak strain response magnitudes of the uncracked plate partially submerged in water

Mode	Sensor	Normalized Peak Magnitudes					
		Broad band			Zoom		
		Peak	Poly	Global	Peak	Poly	Global
1	Str1	1.0	1.0	1.0	1.0	1.0	1.0
	Str2	0.889	0.864	0.881	0.885	0.8735	0.872
	Str3	0.295	0.315	0.305	0.296	0.?¹1	0.316
2	Str1	0.691	0.629	0.659	0.636	0.632	0.637
	Str2	0.100	0.098	0.098	0.09	0.0975	0.097
	Str3	1.0	1.0	1.0	1.0	1.0	1.0
3	Str1	0.392	0.372	0.384	0.365	0.377	0.379
	Str2	0.986	0.930	0.937	0.984	0.969	0.992
	Str3	1.0	1.0	1.0	1.0	1.0	1.0
4	Str1	0.201	0.202	0.198	0.229	0.223	0.227
	Str2	1.0	1.0	1.0	1.0	1.0	1.0
	Str3	0.917	0.864	0.9215	0.951	0.932	0.940
5	Str1	0.685	0.683	0.652	0.754	0.748	0.771
	Str2	1.0	1.0	1.0	1.0	1.0	1.0
	Str3	0.985	0.990	0.998	0.984	0.986	0.985

Table D.1.3 Normalized peak strain magnitudes of the uncracked plate fully submerged in water

| Mode | Sensor | Normalized Peak Magnitudes | | | | | |
| | | Broad band | | | Zoom | | |
		Peak	Poly	Global	Peak	Poly	Global
1	Str1	1.0	1.0	1.0	1.0	1.0	1.0
	Str2	0.907	0.971	0.875	0.884	0.882	0.872
	Str3	0.326	0.307	0.328	0.292	0.304	0.297
2	Str1	0.631	0.634	0.625	0.608	0.625	0.626
	Str2	0.084	0.084	0.085	0.080	0.081	0.078
	Str3	1.0	1.0	1.0	1.0	1.0	1.0
3	Str1	0.291	0.306	0.324	0.300	0.282	0.300
	Str2	0.928	0.909	0.859	0.904	0.905	0.911
	Str3	1.0	1.0	1.0	1.0	1.0	1.0
4	Str1	0.287	0.385	0.415	0.293	0.296	0.303
	Str2	1.0	1.0	1.0	1.0	1.0	1.0
	Str3	0.900	0.894	0.898	0.882	0.900	0.899
5	Str1	0.768	0.761	0.780	0.864	0.924	0.923
	Str2	1.0	1.0	1.0	1.0	1.0	1.0
	Str3	0.946	0.945	0.954	0.924	0.742	0.760

Table D.1.4 Normalized peak strain response magnitudes of the 2x1/32" cracked plate in air

Mode	Sensor	Normalized Peak Magnitudes					
		Broad band			Zoom		
		Peak	Poly	Global	Peak	Poly	Global
1	Str1	1.0	1.0	1.0	1.0	1.0	1.0
	Str2	0.832	0.823	0.820	0.838	0.823	0.788
	Str3	0.344	0.351	0.347	0.381	0.356	0.347
2	Str1	0.742	0.542	0.541	0.630	0.564	0.561
	Str2	0.108	0.094	0.092	0.103	0.094	0.093
	Str3	1.0	1.0	1.0	1.0	1.0	1.0
3	Str1	0.413	0.390	0.387	0.361	0.364	0.367
	Str2	0.791	0.764	0.764	0.776	0.774	0.758
	Str3	1.0	1.0	1.0	1.0	1.0	1.0
4	Str1	0.205	0.203	0.203	0.240	0.250	0.256
	Str2	1.0	1.0	1.0	1.0	1.0	1.0
	Str3	1.0	0.950	0.948	0.958	0.955	0.955
5	Str1	0.532	0.531	0.532	0.620	0.616	0.600
	Str2	0.759	0.764	0.762	0.731	0.741	0.740
	Str3	1.0	1.0	1.0	1.0	1.0	1.0

Table D.1.5 Normalized peak strain response magnitudes of the 2x3/32" cracked plate in air

Mode	Sensor	Normalized Peak Magnitudes					
		Broad band			Zoom		
		Peak	Poly	Global	Peak	Poly	Global
1	Str1	1.0	1.0	1.0	1.0	1.0	1.0
	Str2	0.826	0.864	0.866	0.883	0.861	0.847
	Str3	0.3395	0.348	0.3375	0.3135	0.331	0.307
2	Str1	0.704	0.6575	0.663	0.7525	0.6585	0.659
	Str2	0.115	0.122	0.1205	0.124	0.1195	0.119
	Str3	1.0	1.0	1.0	1.0	1.0	1.0
3	Str1	0.696	0.727	0.721	0.738	0.769	0.768
	Str2	1.0	1.0	1.0	1.0	1.0	1.0
	Str3	0.993	0.971	0.955	0.991	0.994	0.982
4	Str1	-	-	-	-	-	-
	Str2	-	-	-	-	-	-
	Str3	-	-	-	-	-	-
5	Str1	-	-	-	-	-	-
	Str2	-	-	-	-	-	-
	Str3	-	-	-	-	-	-

Table D.1.6 Normalized peak strain response magnitudes of the 2x3/32" cracked plate partially submerged in water

Mode	Sensor	Normalized Peak Magnitudes					
		Broad band			Zoom		
		Peak	Poly	Global	Peak	Poly	Global
1	Str1	1.0	1.0	1.0	1.0	1.0	1.0
	Str2	0.875	0.853	0.856	0.885	0.864	0.864
	Str3	0.306	0.315	0.323	0.318	0.321	0.316
2	Str1	0.723	0.638	0.629	0.684	0.660	0.662
	Str2	0.103	0.101	0.100	0.105	0.099	0.098
	Str3	1.0	1.0	1.0	1.0	1.0	1.0
3	Str1	0.619	0.603	0.634	0.804	0.826	0.766
	Str2	1.0	1.0	1.0	1.0	1.0	1.0
	Str3	0.976	0.965	0.988	0.961	0.961	0.956
4	Str1	-	-	-	-	-	-
	Str2	-	-	-	-	-	-
	Str3	-	-	-	-	-	-
5	Str1	-	-	-	-	-	-
	Str2	-	-	-	-	-	-
	Str3	-	-	-	-	-	-

Table D.1.7 Normalized peak strain response magnitudes of the 2x3/32" cracked plate fully submerged in water

Mode	Sensor	Normalized Peak Magnitudes					
		Broad band			Zoom		
		Peak	Poly	Global	Peak	Poly	Global
1	Str1	1.0	1.0	1.0	1.0	1.0	1.0
	Str2	0.891	0.831	0.868	0.852	0.859	0.859
	Str3	0.316	0.301	0.322	0.302	0.303	0.303
2	Str1	0.665	0.665	0.652	0.626	0.655	0.655
	Str2	0.095	0.093	0.092	0.046	0.032	0.030
	Str3	1.0	1.0	1.0	1.0	1.0	1.0
3	Str1	0.599	0.547	0.530	0.525	0.557	0.569
	Str2	0.931	0.974	0.942	0.881	1.0	0.934
	Str3	1.0	1.0	1.0	1.0	1.0	1.0
4	Str1	-	-	-	-	-	-
	Str2	-	-	-	-	-	-
	Str3	-	-	-	-	-	-
5	Str1	-	-	-	-	-	-
	Str2	-	-	-	-	-	-
	Str3	-	-	-	-	-	-

D.2 Response of the Uncracked Plate in Air with Damping

The measured damping of the uncracked plate in air are converted to Rayleigh damping and the results are included in the analysis to study the change of response due to damping. Mass and stiffness proportional damping factors, obtained using formula given by Bathe (1982), are presented in Table D.2.1. The formula is rewritten in Equation (D.1). Solving the equation for α_{ci} and β_{ci}, the factors for a mode can be obtained. The peak response magnitudes (acceleration and strain responses) are given in the Tables D.2.2 to D.2.5. The strain and acceleration response versus frequency plots are shown in Figures D.2.1 to D.2.10.

$$\alpha_{ci} + \beta_{ci}\,\omega_i^2 = 2\,\omega_i\,\xi_i$$
$$\alpha_{ci} + \beta_{ci}\,\omega_{i+1}^2 = 2\,\omega_{i+1}\,\xi_{i+1}$$

(D.1)

where :

α_{ci} is mass proportional damping factor at mode i,

β_{ci} is stiffness proportional damping factor at mode i,

ξ_i and ξ_{i+1} are damping ratio at mode i and i+1 and

ω_i and ω_{i+1} are natural frequency at mode i and i+1 respectively.

Table D.2.1   Mass and stiffness proportional damping factors

Mode	1	2	3	4	5
α_c	81.550 10^{-3}	202.511 10^{-3}	345.770 10^{-3}	722.497 10^{-3}	2528.340 10^{-3}
β_c	17.402 10^{-6}	9.265 10^{-6}	7.877 10^{-6}	6.951 10^{-6}	5.319 10^{-6}

Table D.2.2 Peak magnitudes of the uncracked plate with damping : acceleration response
(natural frequencies at mode 4 and 5 are given in brackets)

Mode	Natural frequency (Hz)	Peak magnitudes (ms⁻²/N)				
		2143	2145	2151	2155	2167
1	18.45	0.2095	0.8955	3.982	7.773	19.33
2	115.30	2.106	7.858	22.25	22.46	35.11
3	319.8	2.318	7.313	8.829	3.931	15.77
4	*	0.5561 (635.8)	1.423 (635.8)	0.3962 (640.9)	1.163 (639.5)	1.912 (638.8)
5	*	3.366 (1052)	6.290 (1051)	5.839 (1051)	3.990 (1051)	8.317 (1052)

For the header units: Peak magnitudes (ms^{-2}/N)

Table D.2.3 Peak magnitudes of the uncracked plate with damping in air : strain response
(natural frequencies at mode 4 and 5 are the same as given in Table D.2.2)

Mode	Natural Frequency (Hz)	Peak magnitudes at node $(m/m/N) \times 10^{-6}$				
		2143	2145	2151	2155	2167
1	18.45	$5.0395 \ 10^1$	$4.3419 \ 10^1$	$2.7659 \ 10^1$	$1.5710 \ 10^1$	$8.5980 \ 10^{-2}$
2	115.40	9.8603	3.1849	8.7352	$1.1620 \ 10^1$	$1.3262 \ 10^1$
3	321.30	$9.1362 \ 10^1$	$6.3231 \ 10^1$	1.3872	$7.9031 \ 10^1$	$4.9455 \ 10^2$
4	*	$2.4422 \ 10^2$	$9.7078 \ 10^{-2}$	$4.3188 \ 10^2$	$9.7656 \ 10^{-2}$	$5.2689 \ 10^{-3}$
5	*	$3.9140 \ 10^2$	$3.1550 \ 10^{-1}$	$3.1575 \ 10^{-1}$	$2.0645 \ 10^{-1}$	$1.8606 \ 10^{-2}$

Table D.2.4 Normalized peak acceleration response magnitudes of the uncracked plate with damping in air

Mode	Natural Frequency	Normalized Peak Magnitudes at nodes				
		2143	2145	2151	2155	2167
1	18.45	0.0108	0.0463	0.2060	0.4021	1.0
2	115.4	0.0600	0.2237	0.6334	0.6393	1.0
3	321.3	0.1470	0.4637	0.5599	0.2493	1.0
4	*	0.2909	0.7443	0.2072	0.6083	1.0
5	*	0.4047	0.7563	0.7021	0.4797	1.0

Table D.2.5 Normalized peak strain response magnitudes of the uncracked plate with damping in air

Mode	Natural Frequency	Normalized Peak Magnitudes at nodes		
		2143	2145	2155
1	18.45	1	0.8616	0.3120
2	115.4	0.8486	0.2741	1.0
3	321.3	1.0	0.6921	0.8650
4	*	0.2480	0.9941	1.0
5	*	0.1241	1.0	0.6544
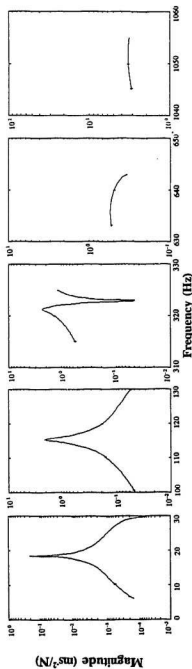
Figure D.2.1 Acceleration response of the uncracked plate in air with damping at node 2143
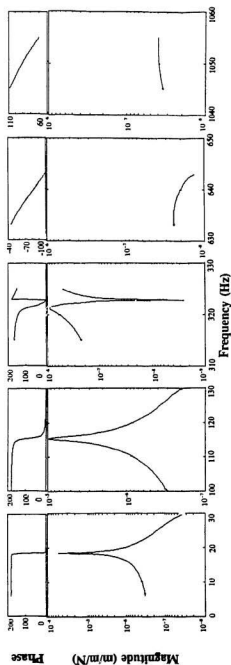
Figure D.2.2 Strain response of the uncracked plate in air with damping at node 2143
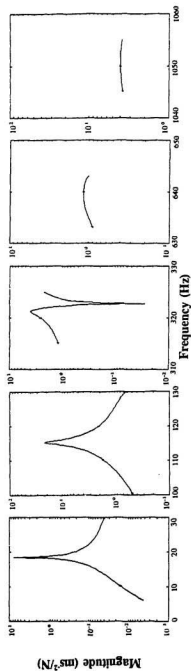
292
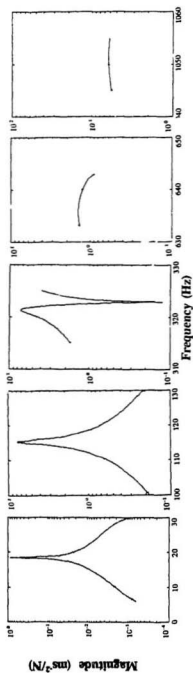
Figure D.2.3 Acceleration response of the uncracked plate in air with damping at node 2145
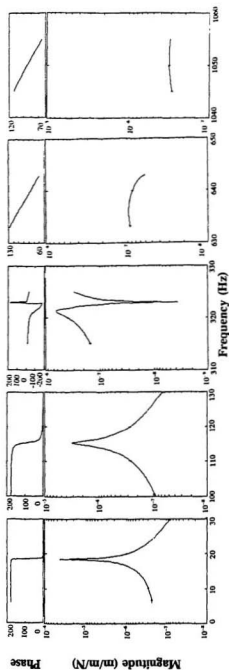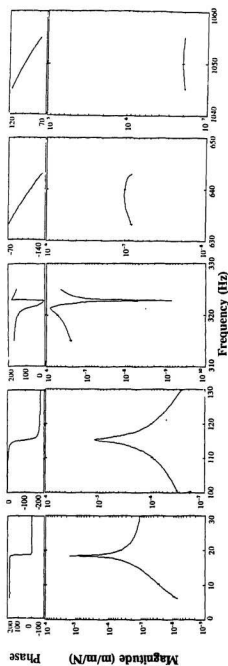

Figure D.2.4 Strain response of the uncracked plate in air with damping at node 2145
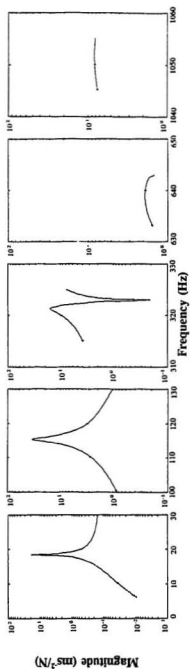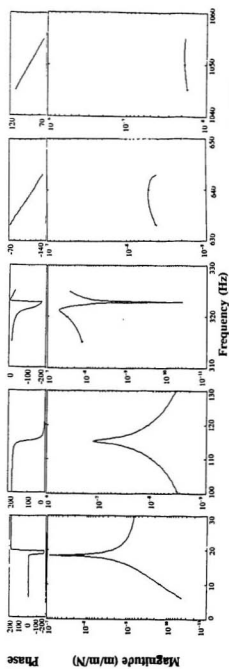
293
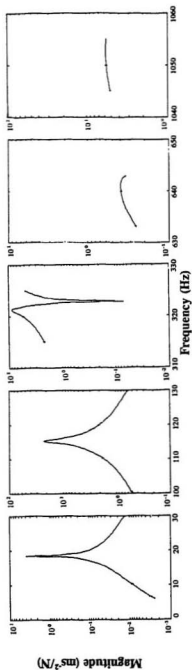
Figure D.2.5   Acceleration response of the uncracked plate in air with damping at node 2151
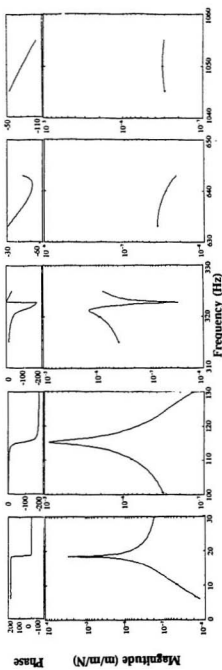
Figure D.2.6   Strain response of the uncracked plate in air with damping at node 2151

294

Figure D.2.7 Acceleration response of the uncracked plate in air with damping at node 2155

Figure D.2.8 Strain response of the uncracked plate in air with damping at node 2155

Figure D.2.9 Acceleration response of the uncracked plate in air with damping at node 2167

Figure D.2.10 Strain response of the uncracked plate in air with damping at node 2167

Appendix E

Photographs of Experimental Apparatus and Setup

Figure E.1 A force transducer and a connecting rod
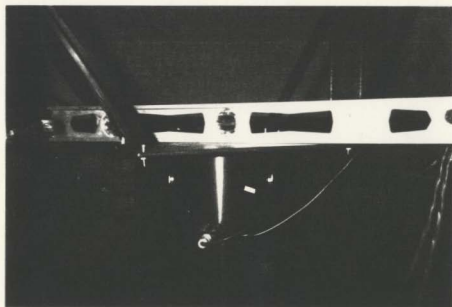
Figure E.2 An exciter hung by eight bungee cords
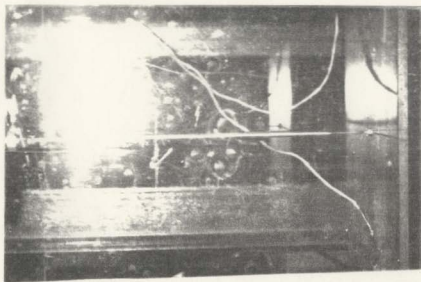
298
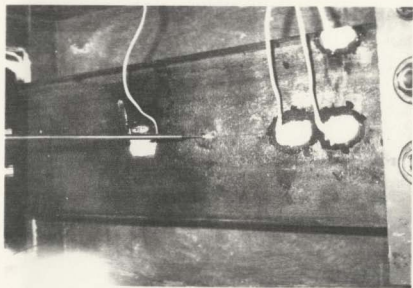
Figure E.3 Sealed strain gages

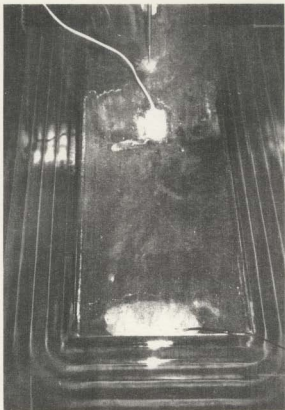**Figure E.4** Rod connecting the force transducer and driving point

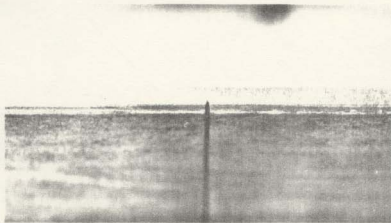**Figure E.5** Plate vibrating at water level just at the middle of the plate thickness
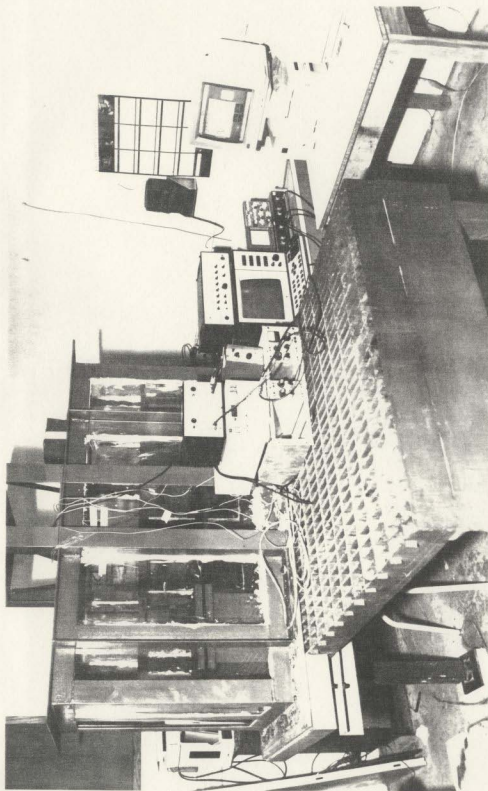

Figure E.6 Crack shape

Figure E.7 Experimental setup (plate in full submergence condition)